On the effects of non-linearities in DP systems

A.J. Quast

On the effects of non-linearities in DP systems

by

A.J. Quast

to obtain the degree of Master of Science
at the Delft University of Technology,

Student number:	4304330	
Project duration:	September 1, 2020 – April 31, 2021	
Thesis committee:	Dr. ir. S.A. Miedema,	TU Delft, chair
	Dr. ir. P. Naaijen,	TU Delft, supervisor
	Ir. M. Paalvast,	MO4, supervisor
	Ir. R. de Jong,	MO4, supervisor

This thesis is confidential and cannot be made public until July 30, 2021.

ŤUDelft **MO4**
NEXT LEVEL FORECASTING

Abstract

In offshore operations a trend is forming were vessels are more often required to do multiple short operations within a small time frame. Traditional mooring systems require execution time far beyond the operation time. Dynamic positioning systems offer great advantages for short time span operations such as crew transfer or lift operations.

Currently operations are planned based on DP capability plots and experience of captain and DPO. DP capability plots have little operational value as this is an static calculation and only provide information for average station keeping capability. During operations the displacements made by the vessel around the DP set-point, also referred to as DP offset, are of great importance to determine the operability of an operation. Currently, the only way of calculating the DP offset is by conducting extensive time domain simulations, which are hard to integrate in the operational workflow of a DP vessel involved in walk-to-work operations. Therefore, a new approach is developed which predicts the vessel's DP offset in the frequency domain, which enables a quick and robust calculation of the DP offset which is suited to merge into the on board workflow. A frequency domain model is per definition a linear model. This leads to the main challenge of this research. A vessel operating on DP is non-linear. Currently there is no insight in what the effect is of non-linear components present in a DP system, on the linear approximation of a frequency domain model.

To investigate the effect of non-linear components onto the the DP frequency domain model, a time domain model is developed that is capable of systematically enabling/disabling different non-linear components. The time domain model will serve as the 'truth' in this research as no actual vessel data is available. Furthermore, this helps identify the effects more easily, as the input for both models are identical. From the time domain model transfer functions can be derived that serve as the basis for the frequency domain model. The transfer function is a linear relation between two variables. In this case, between second order wave drift forces and displacement of the vessel in surge, sway and yaw direction. The following non-linear components are investigated in this research: Thruster ramp up, thruster turning rate, forbidden zones, saturation and thruster allocation. Thruster allocation is present in each model that will be tested, as this is an essential part of a DP system.

Using two methods of determining transfer functions the model and the effects of all non-

linear components are tested. The model is subjected to a variety sea-state, with different wave directions. Both methods offer similar results even though different approaches to determine the transfer functions are used. The selected method is capable of accurately predicting vessel offsets, although some extreme offsets are not captured.

It is concluded that the presence of non-linear components have little to no effect on the DP offset as calculated by the time domain model. Because natural frequencies characteristic to these non-linear components are expected to exist at much higher frequencies that naturally present in second order wave drift forces. Thus making a linear frequency domain model suitable for DP offset forecasting. It is advised to investigate the effect of including 2D input spectra as this is expected to improve the current model.

Preface

During strange and uncertain times I have been able to work on a very interesting and challenging research in order to obtain the degree of Master of Science at the Delft University of Technology. By taking on a difficult topic that even though very much inside my long lasting interest in the offshore industry, simultaneously was very much outside my comfort zone. I was able to develop skills and knowledge beyond what I was expecting from this last phase of my degree. I would not have been able to accomplish this all with out the help of lots of people, whom I want to thank personally here.

First of all, I want to thank Mark Paalvast and Ruben de Jong for their guidance during my research and their everlasting patience over the couple of months. Together I believe we have achieved a lot regarding insight into DP systems and forecasting models. I would also like to thank Peter Naaijen and Sape Miedema for supervising me during my research and for the freedom and trust I was granted during these past months.

During my time at MO4 & Mocean I have had the pleasure of working with some very inspiring, cleaver and dedicated colleagues. Whom I want to thank for making this last year a time to remember.

Finally, I would like to thank my parents and family for their unconditional support through out my life and during this research.

A.J. Quast
Amsterdam, July 2021

Contents

List of Figures

List of Tables

List of Symbols

α_l	commanded azimuth angle	$[deg]$
$\alpha_n l$	delivered azimuth angle	$[deg]$
$\ddot{\omega}$	angular acceleration	$[rad/s^2]$
Δ	Displacement	$[tonnes]$
ϵ	relative error TD and FD wave drift force calculation	$[\%]$
ϵ_n	Wave phase angel	$[rad]$
ϵ_p	Set-point error vector	$[m, m, deg]$
ϵ_{prop}	eccentricity propeller	$[]$
γ	Peak shape factor	$[-]$
μ	Difference frequency	$[rad/s]$
μ_n	Wave direction	$[deg]$
∇	Volume	$[m^3]$
ω	circular wave frequency	$[rad/s]$
ω_p	Peak frequency	$[rad/s]$
Φ	Velocity potential	$[rad]$
ψ	Yaw	$[deg]$
ρ	Water density	$[kg/m^3]$
σ	spectral width parameter	$[-]$
σ_ζ^2	variance	$[m^2]$
$\mathbf{x}$	Thrust vector	$[kN]$
ζ	Wave elevation	$[m]$
ζ_i	Incident wave elevation	$[m]$

ζ_r	Reflected wave elevation	$[m]$
ζ_s	Standing wave elevation	$[m]$
ζ_{a_n}	Wave amplitude component	$[m]$
A	Linear equality matrix	$[-,-,m,-$
a	Added mass	$[tonnes]$
a	acceleration	$[m/s^2]$
A	Normalizing factor	$[-]$
A_{af}	Blade area fraction	$[-]$
B	Beam	$[m]$
b	Linear equality matrix	$[kN, kN, kNm, -]$
B_{tf}	Blade thickness fraction	$[-]$
C_c	Current load coefficient	$[-]$
C_w	Wind load coefficient	$[-]$
D	Draught	$[m]$
D_p	Diameter propeller	m
eta	Displacement vessel from setpoint vector	$[m, m, deg$
F	Force matrix	$[kN]$
$F^{(2)}$	Second order wave drift force	$[kN]$
F_{env}	Environmental forces	$[kN]$
g	gravitational acceleration	$[m/s^2]$
H_s	Significant wave height	$[m]$
I_E	Polar moment of inertia entrained water	$[kg*m^2]$
I_p	Polar moment of inertia propeller	$[kg*m^2]$
$I_p S$	Polar moment of inertia propeller shaft	$[kg*m^2]$
I_x	Polar moment of inertia shaft and propeller	$[kg*m^2]$
I_z	Polar moment of inertia azimuth	$[kg*m^2]$

K	Entrained water factor	$[-]$
k_n	Wave number	$[rad/m]$
$K_{d,\alpha}$	Derivative coefficient PID turning rate	$[-]$
$K_{d,DP}$	Derivative coefficient PID DP controller	$[-]$
$K_{d,n}$	Derivative coefficient PID shaft speed	$[-]$
$K_{i,\alpha}$	Integral coefficient PID DP turning rate	$[-]$
$K_{i,DP}$	Integral coefficient PID DP controller	$[-]$
$K_{i,n}$	Integral coefficient PID DP shaft speed	$[-]$
$K_{p,\alpha}$	Proportional coefficient PID turning rate	$[-]$
$K_{p,DP}$	Proportional coefficient PID DP controller	$[-]$
$K_{p,n}$	Proportional coefficient PID shaft speed	$[-]$
$Kt,0$	Propeller torque coefficient	$[-]$
L	Length	$[m]$
L_{oa}	Length overall	$[m]$
L_{pp}	Length between perpendiculars	$[m]$
M	Mass matrix	$[kg]$
m_s	Mass shaft	$[kg]$
N	Normal unit vector	$[-]$
n_set	Commanded shaft speed	$[rad/s]$
n_{shaft}	Delivered shaft speed	$[rad/s]$
P	penalty matrix	$[-]$
p	Fluid pressure	$[Pa]$
P_{ij}	Real part Quadratic Transfer Function	$[-]$
q	penalty vector	$[-]$
Q_d	Torque azimuth driver	$[kNm]$
Q_{ij}	Imaginary part Quadratic Transfer Function	$[-]$

Q_{shaft}	Torque shaft	$[kNm]$
R	Radius blade	$[m]$
r_a	Response	$[m]$
r_s	Shaft radius	$[m]$
r_{azi}	Radius azimuth	$[m]$
S	Wetted surface	$[m^2]$
S_ζ	Energy density spectrum	$[m/s]$
S_ζ	Wave energy spectrum	$[\frac{m^2}{rad/s}]$
S_F	Low frequent energy spectrum	$[\frac{kN^2}{rad/s}]$
S_f	Wave drift force spectrum	$[\frac{kN^2}{rad/s}]$
S_r	Response spectrum	$[\frac{m^2}{rad/s}]$
$S_{x,y,\psi}$	Second order response spectrum	$[\frac{m^2}{rad/s}]$
T_p	Peak Period	$[s]$
T_{nom}	Nominal thrust	$[kN]$
T_{set}	Thruster setting vector DP controller	$[kN, kN, kNm]$
TF	Transfer function	$[\frac{m^2}{kN}]$
V	Fluid velocity vector	$[m/s]$
v_a	Inflow velocity thruster	$[m/s]$
v_c	current velocity	$[m/s]$
V_{sog}	Speed over ground	$[m/s]$
v_{stw}	Speed through water	$[m/s]$
W_p	Weight propeller	$[kg]$
x	Surge	$[m]$
Y	Specific weight blade	$[kg/m^3]$
y	Sway	$[m]$
z	Depth	$[m]$

Acronyms

2D	Two-Dimensional
4Q	Four Quadrant
CDF	Cumulative Distribution Function
DGPS	Differential Global Positioning System
DNV	Det Norske Veritas
DOF	Degree of Freedom
DP	Dynamic Positioning
DPO	Dynamic Positioning Operator
FBZ	Forbidden zone
FD	Frequency Domain
FFT	Fast Fourier Transformation
MPM	Most Probable Maximum
MRU	Motion Reference Unit
NLC	Non-Linear Components
PID	Proportional-Integral-Derivative
PM	Pierson-Moskowitz
QP	Quadratic Programming
QTF	Quadratic Transfer Function
SOV	Service Operation Vessel
TD	Time Domain
TF	Transfer Functions

1

Introduction

Offshore operations require vessels to maintain a certain position or heading for extended periods. Such operations can include drilling, pipe-laying, lifting, supplying of offshore installations and crew-transfer. Due to an increase in offshore wind farms [11] and operations at increasing water depths, traditional mooring systems are not always suitable. Dynamically positioned ships are well equipped for operations at great water depths or short span operations such as crew transfers at offshore structures. Offshore vessels are exposed to a variety of environmental forces that move the vessel around when not counteracted by either a mooring system or a Dynamic Positioning (DP) system. A DP system uses a control system that allocates thrusters to maintain position.

Figure 1.1: Acta Marine's Acta Auriga at BARD 1 preparing for crew transfer

The ability to safely perform an operation within predefined boundaries is known as the workability. A DP system is part of an operation and therefore influences the workability. For vessel operators, it is important to know what the operability of the operation is, when can it operate (Uptime) and under what conditions this is not possible (Downtime). One can image downtime leads to project costs being incurred without project progress.

Crew transfer operations are commonly executed with the use of a motion-compensated gang-way, which acts as a bridge between vessel and offshore structure. As an example, see Figure 1.1. This system can compensate vessel motions induced by first-order wave forces. However, the telescoping motion of the gangway is limited by the maximum or minimum stroke, when considering the surge and sway motion. Keeping the vessel within this range is the task of the DP system. Whether the vessel is within the operating limitations can be visualized in a DP watch circle in Figure 1.2.
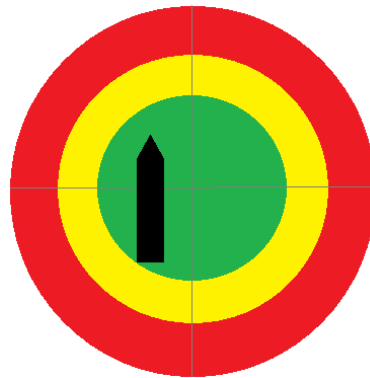
Figure 1.2: DP watch circle

A set-point lies in the centre of the green area, the distance from the set-point to the ship is called the offset. The predefined operation limits are loaded into the system and as long as the vessel remains within the green area, the operation is safe. Yellow means the operation is at its limits and direct action is needed to bring the vessel closer to the set-point. If the vessel is within the red area the operation should be aborted as the limit of the gangway, as an example, is on the verge of being exceeded. This method gives real-time feedback to the Dynamic Positioning Operator (DPO) of the distance of the vessel with respect to the set-point. A watch circle does not give any information regarding the expected motions in the near future. Furthermore, it does not provide any insight into the conditions in which the DP system can maintain position. A method widely used in the industry providing insight into the limiting conditions is a DP capability plot, see Figure 1.3.

The DP capability plot provides the DPO insight in the capability of the vessel to remain on a set-point, with environmental conditions acting from a certain direction. For this plot, a calculation has been made on the forces acting on the vessel and on the ability of the thrusters to counteract this. As this is a static calculation it can only determine if the vessel will be able to stay on set-point on average. It is not able to determine the excursion being made around this average point. This reveals a major drawback of this method. The excursions around this average point can lie beyond the operating limits. Thus, potentially creating high-

risk situations during a crew transfer, with the possibility of injury/damage to the crew and equipment.
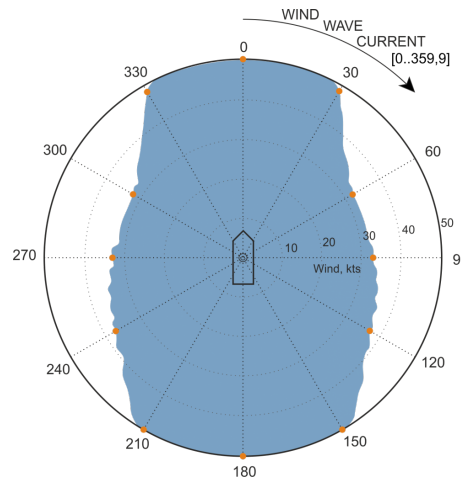
Figure 1.3: DP capability plot

Although both methods provide some insight into the operation and its limitations, critical information is missing in determining whether the operation can be conducted safely. A DP footprint forecast provides a better understanding of how the vessel will act in certain conditions as this method uses statistics to predict the vessel's behaviour. For a crew transfer operation on DP, the horizontal offset is a critical parameter. By determining the Most Probable Maximum (MPM) offset, the DPO knows what statistically the largest excursion around the set-point will be in a certain sea-state . Furthermore, the probability of larger excursions occurring can be estimated, i.e. probability of exceedance. If the statistics are known a safety level can be defined, e.g. probability of exceedance of an MPM must be smaller than 10^{-5} before an operation can be conducted.

The conventional method for determining the vessel offsets is based on Time Domain (TD) simulations. These simulations require a complex model of the whole system and therefore need a lot of computing power and time to provide the needed footprint forecast. Simulation time can easily be in the order of days, as each time step has to be calculated. Since reliable metocean data can only be provided a few days in advance, running simulations for the coming hours will become extremely hard and/or expensive. It is more common that operations are assessed based on the experience of the ship's captain or DPO, as accurate simulations are not available.

Providing a method that allows DPO's to have accurate motion forecast for the coming hours is critical for safe and smooth operations. Frequency Domain (FD) simulations are very efficient, needing very little computing power and/or time. Therefore, a method using FD simulations

to calculate the MPM offset is opted.

1.1. Problem description

Developing an FD method for motion footprint forecasting can be an outcome for operations that need forecasting during or hours in advance of an operation, as simulations can take seconds instead of days. However, some challenges arise when trying to describe a DP operation in the frequency domain.

An offshore vessel that is being held at one position and heading by a DP system, is a very complicated system that includes discontinuities and non linear phenomena such as, second-order wave drift forces, thruster saturation and the propulsion system. FD simulations can process linear input, all the non-linear effects either have to be linearized or excluded from the model. Leaving the question, which non-linear effects play a critical role in a vessel operating on DP and how can they be dealt with in an FD model? In the past, comparisons have been made between moored vessels and station keeping on DP [8] [14]. These studies model a moored vessel as a mass-spring-damper system, using FD analysis to determine the low-frequency wave drift motions. The suggestion is made that the same can be done for vessels operating on DP, where instead of mooring lines, thrusters cause a damping and stiffness term. Real conclusions on whether this method is applicable are left out.

A more recent study [23] uses Simulink and a built-in linearization tool to obtain linearized Transfer Functions (TF) from a TD model. These can then be used in an FD analysis to provide a stochastic footprint over time. The method has been proven to be effective, however, only for a 1 Degree of Freedom (DOF) system in surge direction. This simplification was made on the assumption that vessels have the ability to choose a heading into the environmental loads. This is a valid assumption, although for certain operations, like crew transfers, it does not hold. The access points to an offshore structure might be limited to one. Furthermore, this research is based on the assumption that environmental loading is unidirectional and defined by a JONSWAP spectrum, as in most other available literature. One can imagine the ocean is not best described by a unidirectional JONSWAP spectrum and therefore a 2D spectrum might offer a better understanding of the expected motions of an offshore DP vessel [10].

1.2. Goal

This research aims to create a better understanding of a 3DOF DP model as a whole and how such a model can be linearized, so the DP footprint can be estimated in the frequency domain. This will enable DPO's access to accurate and timely DP footprint forecasts, allowing them to make critical decisions regarding offshore operations. This will result in safer operations and

an increase in workability.

1.3. Scope

This research aims to increase the overall understanding of a 3DOF DP footprint forecasting model for the DP vessel 'Acta Auriga'. As a vessel has no restoring coefficients in three degrees of freedom, surge (x) sway (y) and yaw (ψ), DP systems will act against loads in these directions. Therefore, an existing model will be further developed taking into account these DOF's. Limitations of the operation based on heave, roll and pitch are not taken into account. It is assumed that the motion compensating gangway will be able to counteract these wave frequent motions. Recent research has shown the possibilities of using DP systems to increase roll damping [4]. However, this will also not be included.

This research will focus on understanding the effects of Non-Linear Components (NLC) within a 3DOF DP system. This will help to identify the importance of certain non-linear systems and how to best model these. Furthermore, this thesis will investigate the limitations of linearizing these components so that the DP offsets can be estimated in the frequency domain.

Further research into adapting the 3DOF DP model so it can utilise 2D spectra as input, would fit within the overall goal of providing accurate DP footprint estimates. As it is uncertain how long the research into the non-linearities will take, this is left out of the scope. However, if it fits within the time frame of this thesis it will be included.

1.4. Research questions

The main question of this research is formulated as followed:

> **What is the effect of non-linear components in a time domain DP model, onto the linearized DP model in the frequency domain and how does the time domain DP response compare to a frequency domain DP response?**

The sub-questions to the main question are formulated as followed:

1. Which non-linear components are included in a 3DOF DP system?

2. How are the non-linear components included in a 3DOF DP time-domain model?

3. How does a frequency domain 3DOF DP model response estimate compare to that of the time domain model?

4. What is the effect of the non-linear components on the time domain model and its response and how does this affect the frequency domain model?

5. To what extent is it possible to improve the linearization method on non-linear compo-
   nents of the DP system to obtain an improved frequency domain DP model?

2

Offshore hydromechanics

Figure 2.1: Ocean waves

Figure 2.1 shows what a typical ocean might look like. Anyone looking at this photograph would describe this as a random display of waves. It is very hard to distinguish separate waves and the direction in which they propagate, let alone trying to describe this in a mathematical form to which calculations can be performed. However, this is exactly what needs to happen in order to give a proper motion forecast. Before an estimation of the motion of an offshore vessel can be given, the forces creating those motions must be known. Before the forces acting on the ship can be calculated, the waves creating those forces must be known. This chapter will focus on describing each aspect and how it is obtained.

2.1. Ocean waves

The wave elevation at certain point in time of a single harmonic wave can be described using the following formula:

$$\zeta(t) = \zeta_a \cos(kx - \omega t) \tag{2.1}$$

Where:

ζ_a = wave amplitude $[m]$

k = circular frequency $[rad/s]$

ω = circular frequency $[rad/s]$

As discussed before the ocean is hardly represented by a single harmonic wave, rather a seemingly random mixture of different wave amplitudes, phases and directions. However, for engineering purposes a one-dimensional representation of the ocean is often used. At a later stage the two-dimensional spread will be discussed. For now the focus will lay on the one-dimensional also known as the random-phase/amplitude model. This is a mathematical representation of the wave elevation in an ocean, first used by St Dinis and Pierson Jr in 1953. Figure 2.2 illustrates the principle of the random-phase/amplitude model.
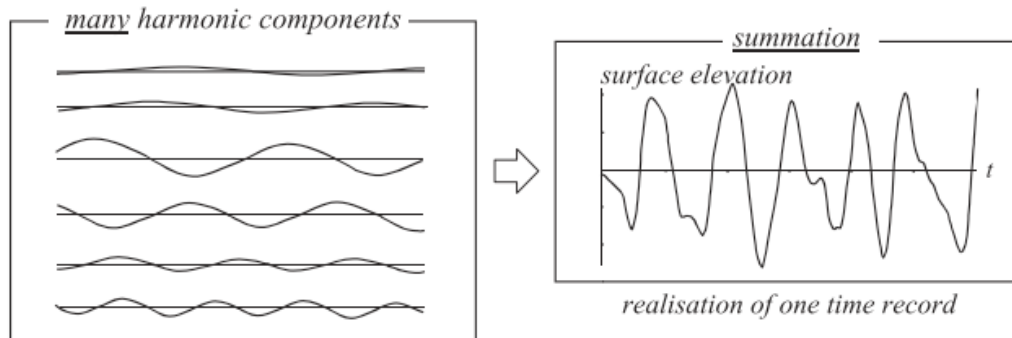
Figure 2.2: Superposition of many harmonic waves [10]

By adding (superposition) several harmonic waves over time, see Equation 2.1, the surface elevation can be created that is more similar to that of an ocean, also known as an irregular sea. This surface elevation can be mathematically formulated as followed:

$$\zeta(t) = \sum_{n=1}^{N} \zeta_{a_n} \cos(k_n x - \omega_n t + \epsilon_n) \tag{2.2}$$

Where each of the following components belong to frequency n

ζ_a = random wave amplitude $[m]$

k = wave number $[rad/m]$

ω = circular frequency $[rad/s]$

ϵ_n = random phase angle $[rad]$

In order to make the model random, wave amplitude and phase angle are respectively chosen at random from a Rayleigh distribution depending on the expected wave amplitude belonging to that frequency and a uniform distribution between 0 and 2π [10]. Random variables can be recognized by underlined symbols in Equation 2.2. Each set of random variables will create a different realisation of a time record.

2.1.1. Wave spectra

Since a vessel is moved not by the amplitude of a wave but rather by the energy that is present in that wave, a representation of energy in the waves is required. This is achieved through a spectrum, specifically a wave energy spectrum. This spectrum displays the energy per frequency, which makes it useful for frequency domain analysis. To transform a time record of the wave elevation to a spectrum, Fourier series analysis is used to create the amplitude spectrum. This is then transformed to the variance spectrum, as this is a more relevant statistic; energy of a waves is proportional to the variance [10].

$$variance = \sigma_\zeta^2 = \overline{\zeta^2} = \sum_{n=1}^{N} \frac{1}{2}\zeta_{a_n}^2 \tag{2.3}$$

Energy is proportional to variance as per linear wave theory, with the following relation [10].

$$S_\zeta = \rho g \underline{\overline{\sigma_\zeta^2}} \tag{2.4}$$

The energy spectrum is discrete, meaning it only contains values on certain frequencies. This does not give an accurate representation of the ocean, where all frequencies are present. Therefore, the spectrum needs to be transformed to the discontinuous density spectrum. This is achieved by spreading the energy over the frequency interval $\Delta\omega$, see Equation 2.5.

$$S_\zeta(\omega_n) \cdot \Delta\omega = \sum_{\omega_n}^{\omega_n+\Delta\omega} \frac{1}{2}\zeta_{a_n}^2(\omega)$$

$$S_\zeta(\omega_n) = \sum_{\omega_n}^{\omega_n+\Delta\omega} \frac{\frac{1}{2}\zeta_{a_n}^2(\omega)}{\Delta\omega} \tag{2.5}$$

Although the energy density spectrum is now distributed over the frequency intervals, it is still discontinuous between each interval. A continuous spectrum is achieved by letting $\Delta\omega$ approach zero.

$$S_\zeta(\omega_n) = \lim_{\Delta\omega\to 0} \sum_{\omega_n}^{\omega_n+\Delta\omega} \frac{\frac{1}{2}\zeta_{a_n}^2(\omega)}{\Delta\omega}$$

$$S_\zeta(\omega_n) \cdot d\omega = \frac{1}{2}\zeta_{a_n}^2$$

(2.6)

This is the continuous energy density spectrum, otherwise known as the wave spectrum. An important relation is that the area under the spectrum is equal to the variance of the surface elevation.

$$variance = \sigma_\zeta^2 = \int_0^\infty S_\zeta(\omega_n) \cdot d\omega$$

(2.7)

2.1.2. Idealized spectra

For engineering purposes, researchers have formulated idealized wave spectra in a standard form based on significant wave height H_s in meters and peak period T_p in seconds . Several different adaptations of idealized spectra are known, however, the JONSWAP spectra is the one recommended by Det Norske Veritas (DNV) for offshore operations and will be the one used in this research [7].

The JONSWAP spectrum was first presented by Hasselmann *et al.* in 1973 and is a modification of the Pierson-Moskowitz spectrum [13]. Pierson and Moskowitz first described their idealized spectrum in 1964 and assumed a fully developed sea. This concept means that the waves and wind are in equilibrium. Based on experimental data gathered during the JOINT NORTH SEA WAVES PROJECT by Hasselmann and others in 1973, it was found that a sea never fully develops. Non-linear wave-wave interaction ensures the sea keeps on developing even after very long times and distances. An extra component was added to the Pierson-Moskowitz (PM)-spectrum to ensure a better fit to the measured data. This factor generally improves the peak of the spectrum. Both spectra describe conditions during the most severe sea-states, however, do not include swell. If swell is to be included, inclusion of two peak spectra is recommended such as the Ochi-Hubble spectrum and the Torsethaugen spectrum [7]. The JONSWAP spectrum is formulated according Equation 2.8.

$$S_J(\omega) = A_\gamma \cdot \frac{5}{16} \cdot H_s^2 \cdot \omega_p^4 \cdot \omega^{-5} exp\left[-\frac{5}{4}\left(\frac{\omega_p}{\omega}\right)^4\right]\gamma^{exp\left[-\frac{(\omega-\omega_p)^2}{2\sigma^2\omega_p^2}\right]}$$

(2.8)

where

A_γ = 1 - 0.287 ln(γ), normalizing factor [$-$]

γ = non-dimensional peak shape parameter [$-$]

γ = 3.3 average value

ω_p = $\frac{2\pi}{T_p}$, peak frequency $[rad/s]$

ω = frequency [rad/s]

σ = spectral width parameter [-]

$\sigma = 0.07\ \sigma_a$ for $\omega \leq \omega_p$

$\sigma = 0.09\ \sigma_b$ for $\omega > \omega_p$

Experimental data have provided the average values for the above mentioned JONSWAP spectrum and are considered reasonable for

$3.6 < T_p/\sqrt{H_s} < 5$

If the ratio of Hs and Tp is outside these values the following values for γ can be applied:

$\gamma = 5$ for $T_p/\sqrt{H_s} \leq 3.6$

$\gamma = \exp(5.75\text{-}1.15\frac{T_p}{\sqrt{H_s}})$ for $3.6 < T_p/\sqrt{H_s} < 3.6$

$\gamma = 1$ for $5 \leq T_p/\sqrt{H_s}$

Figure 2.3 shows different JONSWAP spectra depending on the values chosen for T_P and H_s.
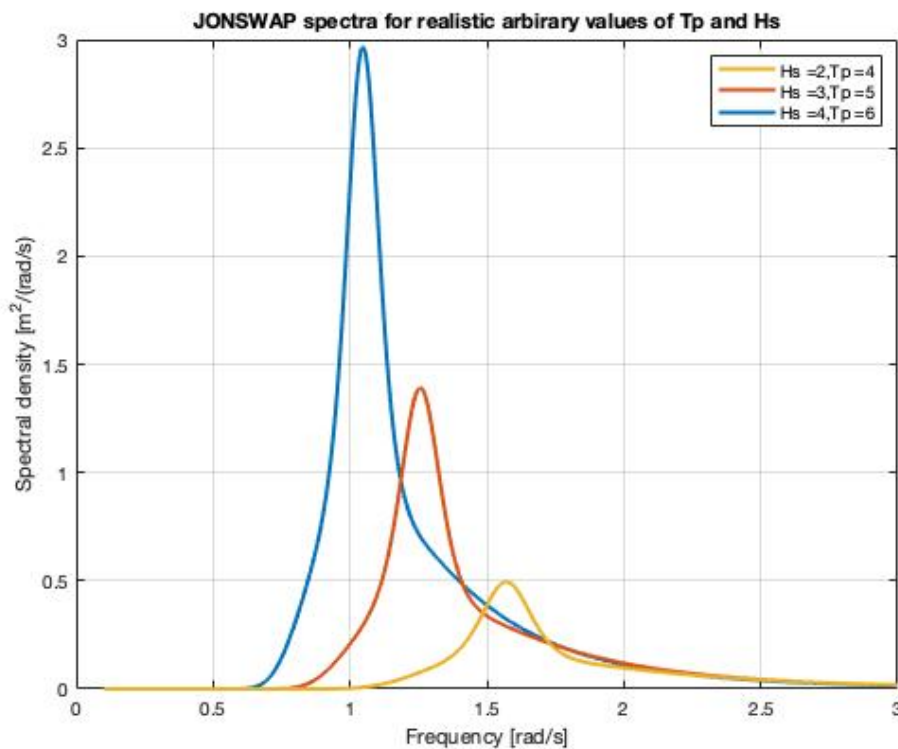
Figure 2.3: JONSWAP-spectra with realistic and arbitrary T_p and H_s

2.1.3. 2D wave spectra

In the previous sections unidirectional spectra have been discussed, meaning that the waves are assumed to propagate in one single direction. As illustrated in Figure 2.1 the ocean is hardly unidirectional, rather chaotic, suggesting waves are propagating in many different directions. In order to capture this data in a model, a Two-Dimensional (2D) wave spectra is needed.

The basic principle is applied as in the unidirectional spectra, where by means of super-positioning, a variety of waves are added to form a 'random' sea-state. Figure 2.4 is a representation of this principle.
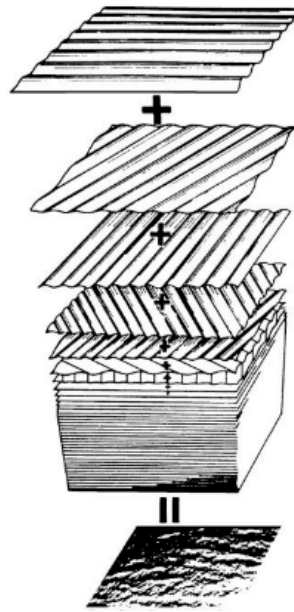
Figure 2.4: Super-positioning of waves with variable frequency f and direction μ_n

Equation 2.9 formulates super-positioning of separate components.

$$\zeta = \sum_{n=1}^{\infty} \zeta_{a_n} \cdot \cos(k_n \cdot x \cdot \cos\mu_n + k_n \cdot y \cdot sin\mu_n - \omega_n t - \epsilon_n) \tag{2.9}$$

The spectral density can be defined as followed:

$$S_\zeta(\omega_n, \mu_n)d\omega d\mu = \sum_{\substack{\omega \\ \mu}}^{\substack{\mu+d\mu \\ \omega+d\omega}} \frac{1}{2}\zeta_{a_n}^2 \tag{2.10}$$

2.2. Hydrodynamic loads

This section will discuss the hydrodynamic forces that result from the waves discussed in the previous section. As discussed in section 1.3 this research will focus on the DP footprint of offshore vessels. Therefore, second-order wave drift forces are discussed more in depth. First-order waves forces will result in first-order motions which are assumed to be counteracted by the motion compensating gangway.

2.2.1. Second-order wave drift forces

Second-order wave drift forces consist of three components. A mean component, a low frequency component and a high frequency component. The response of the vessel to this load is called wave drift and was first discovered by Suyehiro in 1924 [19]. Suyehiro found during model testing of a floating vessel in beam waves, that the waves excited a non-zero constant horizontal force in the direction of propagation. He stated that this horizontal force existed due to the ability of the model to reflect waves. This section will not discuss the entire calculation of these drift forces, as this is a very large and complex derivation. However, some simplified examples will be given which will explain the basic implication of this force and how it will be calculated in this research.

Looking at a simple example where a single wave propagates in a negative direction towards a vertical wall (the vessel). The wall reflects the wave and this wave then propagates in the positive direction. This situation can be described as followed:

$$\zeta_i = \zeta_a \cos(-kx - \omega t)$$
$$\zeta_r = \zeta_a \cos(kx - \omega t)$$

(2.11)

Adding these waves will give the formulation of the resulting standing wave

$$\zeta_s = 2\zeta_a \cos(kx)cos(\omega t)$$

(2.12)

Which has a velocity potential

$$\Phi = -2\zeta_a \cos(kx)\frac{g}{\omega} \sin(\omega t)$$

(2.13)

The wall partly submerged in the fluid is exposed to pressures acting on the wall. By integrating these pressures one obtains the forces acting on the wall. The pressures are described by the complete Bernoulli equation, see Equation 2.14

$$p = -\rho gz - \rho \frac{\partial \Phi}{\partial t} - \frac{1}{2}\rho(\nabla\Phi)^2$$
$$= -\rho gz - \rho \frac{\partial \Phi}{\partial t} - \frac{1}{2}\rho(\Phi_x^2 + \Phi_y^2 + \Phi_z^2)$$
$$= p^{(0)} + \epsilon p^{(1)} + \epsilon^2 p^{(2)}$$

(2.14)

where

$p^{(0)}$ = $-\rho g z$, hydrostatic pressure $[Pa]$

$p^{(1)}$ = $\rho \frac{\partial \Phi}{\partial t}$, first-order pressure $[Pa]$

$p^{(2)}$ = $\frac{1}{2}\rho(\nabla\Phi)^2$, second-order pressure $[Pa]$

Taking into account the boundary conditions and looking for the pressure on the wall for x=0:

$$p = -\rho g z - \rho \frac{\partial \Phi}{\partial t} - \frac{1}{2}\rho(\Phi_z^2) \tag{2.15}$$

Now the pressure is known, it can be integrated over the area of the wall leading to the formulation of the mean drift force per meter length. Then the specific situation is given and simultaneously the integration is split into the contribution from $z = -\infty$ to the z=0 (constant) and from z=0 to $z = \zeta(t)$ (time dependent). Furthermore it is averaged over one period. See Equation 2.16.

$$
\begin{aligned}
\vec{F} &= -\int\int_S p \cdot \vec{N} \cdot dS \\
\overline{F} &= -\overline{\int_{-L/2}^{L/2}\int_{-\infty}^{\zeta(t)} -\rho\left(gz + \Phi_t + \frac{1}{2}\Phi_z^2\right)n_x dS} \\
\overline{F} &= \overline{\int_{-\infty}^{\zeta(t)} -\rho\left(gz + \Phi_t + \frac{1}{2}\Phi_z^2\right)dz} \\
\overline{F} &= \overline{\int_{-\infty}^{0} -\rho\left(gz + \Phi_t + \frac{1}{2}\Phi_z^2\right)dz + \int_{0}^{\zeta(t)} -\rho\left(gz + \Phi_t + \frac{1}{2}\Phi_z^2\right)dz}
\end{aligned}
\tag{2.16}
$$

where

$\vec{N}$ = normal unit vector, $n_x = 1 [-]$

S = wetted surface area $[m^2]$

Equation 2.17 will provide the result of each separate component. The mathematics behind each derivation is left out, as these are quit elaborate.

$$
\begin{aligned}
\rho\overline{\int_{-\infty}^{0} gz dz} = 0 && \rho\overline{\int_{0}^{\zeta(t)} gz dz} = \rho g \zeta_a^2 \\
\rho\overline{\int_{-\infty}^{0} \Phi_t dz} = 0 && \rho\overline{\int_{0}^{\zeta(t)} \Phi_t dz} = -2\rho g \zeta_a^2 \\
\frac{1}{2}\rho\overline{\int_{-\infty}^{0} \Phi_z^2 dz} = +\frac{1}{2}\rho g \zeta_a^2 && \frac{1}{2}\rho\overline{\int_{0}^{\zeta(t)} \Phi_z^2 dz} = 0
\end{aligned}
\tag{2.17}
$$

The components that are equal to zero are either not part of the dynamic solution, as they are always present, averaged over time compute to zero or become a third-order and are therefore neglected. Adding the constant and time varying component results in the total second-order mean drift force, provided in Equation 2.18.

$$\begin{aligned}
\overline{F} &= \frac{1}{2}\rho g \zeta_a^2 - \rho g \zeta_a^2 \\
&= -\frac{1}{2}\rho g \zeta_a^2
\end{aligned}$$
(2.18)

The same calculation can be done for more than one wave. This will show that not only a mean wave drift force is present, but also a low and high frequency. For this example only the quadratic velocity part of the Bernoulli equation will be derived.

$$-\frac{1}{2}\rho|\nabla\Phi|^2 = -\frac{1}{2}\rho(V_1^2, V_2^2, V_3^2)$$
(2.19)

where

$\quad$ V $\;=\; (V_1, V_2, V_3)$, fluid velocity vector $[m/s]$

$\quad V_1 \;=\; \zeta_1 \cos(\omega_1 t + \epsilon_1) + \zeta_2 \cos(\omega_2 t + \epsilon_2)$, idealised two wave sea state

Through some trigonometric algebra it follows that:

$$\begin{aligned}
-\frac{1}{2}\rho(V_1^2) = -\frac{1}{2}\rho\Bigg[&\frac{1}{2}A_1^2 + \frac{1}{2}A_2^2 + \frac{1}{2}A_1^2 \cos(2\omega_1 t + 2\epsilon_1) \\
&+ \frac{1}{2}A_2^2 \cos(2\omega_2 t + 2\epsilon_2) \\
&+ A_1 A_2 \cos[(\omega_1 - \omega_2)t + \epsilon_1 - \epsilon_2] \\
&+ A_1 A_2 \cos[(\omega_1 + \omega_2)t + \epsilon_1 + \epsilon_2]\Bigg]
\end{aligned}$$
(2.20)

In Equation 2.20 three different components are clearly visible. The first component is the constant component which is similar to the outcome of Equation 2.18. The other components are time-varying and are characterised by either a difference frequency ($\omega_1 - \omega_2$) for low frequent excitation or high frequency excitation which follow from the sum frequency components $2\omega_1$, $2\omega_2$ and ($\omega_1 + \omega_2$). The low frequent components are of importance for softly moored / DP vessels as surge, sway and yaw have typical resonance periods in the order of 1 - 2 minutes. Thus resonant oscillations can occur. High frequent excitation are more important to stiffly moored vessels with much shorter resonance periods in the order of seconds [8].

In order to get a realistic force time trace, these equations need to be extended to a sea state composed of N waves. Taking all second-order components and only the difference frequencies, the second-order drift force can be formulated in the time domain as follows:

$$\begin{aligned}
F^{(2)}(t) = &\sum_{i=1}^{N}\sum_{j=1}^{N} \zeta_i \zeta_j P_{ij} \cdot \cos(\omega_i - \omega_j)t + (\epsilon_i - \epsilon_j) \\
&+ \sum_{i=1}^{N}\sum_{j=1}^{N} \zeta_i \zeta_j Q_{ij} \cdot \sin(\omega_i - \omega_j)t + (\epsilon_i - \epsilon_j)
\end{aligned}$$
(2.21)

P_{ij} and Q_{ij} are components of the time independent Quadratic Transfer Function (QTF), respectively giving the part of the wave drift force that is in-phase and out-of-phase. Both components will be determined with diffraction software which in this research will be calculated with AQWA. The QTF can also be used to calculate forces in the frequency domain.

2.2.2. Forces in frequency domain

The mean drift force in irregular waves can be found by stating that $\omega_1 = \omega_2$, this is the equivalent of integrating over the diagonal of the QTF. Equation 2.20 will be simplified to the following equation:

$$F_{1_{mean}}^{(2)} = \sum_{i=1}^{N} \zeta_i^{(1)^2} \cdot P_j j \qquad (2.22)$$

Which can be rewritten to

$$F_{1_{mean}}^{(2)} = 2 \int_0^\infty S_\zeta(\omega) \cdot P(\omega, \omega) \cdot d\omega \qquad (2.23)$$

$P(\omega, \omega)$ is the mean drift force coefficient for regular waves. The low frequency spectral density can be found in a similar manner.

$$\begin{aligned} S_F(\mu) &= 8 \int_0^\infty S_\zeta(\omega_1) \cdot S_\zeta(\omega_2) \cdot |T(\omega_1, \omega_2)|^2 \cdot d\omega \\ &= 8 \int_0^\infty S_\zeta(\omega + \mu) \cdot S_\zeta(\omega) \cdot |T(\omega + \mu, \omega)|^2 \cdot d\omega \end{aligned} \qquad (2.24)$$

2.3. Motion

This section will discuss the motion the vessel experienced due to the loads discussed the previous section, often referred to as the vessel response. The vessel response can be calculated both in the time domain as well as in the frequency domain. As both methods are used in this research, both will be addressed in this section.

2.3.1. Motion response - Time Domain

Determining the offset of the vessel through a time domain calculation is straight forward and is based on one of the most important relations known in physics.

$$F = M \cdot a \qquad (2.25)$$

where

  F = 3x3 force matrix, main diagonal filled $[kN]$

    M = 3x3 mass matrix, main diagonal composed of mass of the vessel + added mass corresponding to DOF $[kg]$

    a = acceleration of vessel in surge, sway and yaw direction $[m/s^2]$

For each time step the acceleration can be determined by dividing the force matrix F by mass matrix M. A double integration over time of the acceleration leads to the displacement and rotation of the vessel. An overview of this principle, the variables that can be deducted from this calculation and how it is incorporated in the model is provided in Section 4.1.2.

2.3.2. Transformation response

The principle of transformation of time domain to frequency domain is shown in Figure 2.5. It also displays the transformation from wave height to response. Both important principles that form the foundation of this research. This particular representation is that of heave motion due to irregular first-order waves. The linear theory holds for all six DOFs and for higher-order wave loads [12] [23].
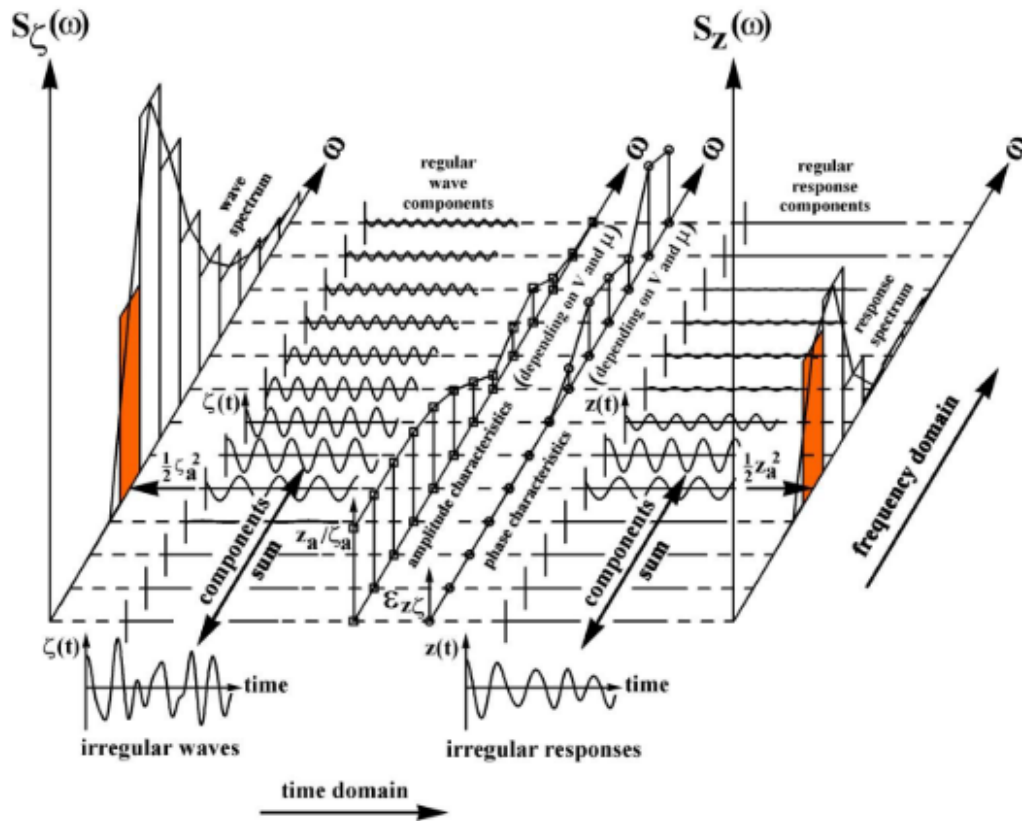
Figure 2.5: Visual representation of interaction between TD and FD

Starting at the bottom left corner, a irregular wave time trace, $\zeta(t)$, is provided. This time trace consists of a series of regular wave components, each with its own frequency, amplitude and phase shift (Time Domain). Which are shown on the left hand side of the figure. Each regular wave component can be transformed to the frequency domain through $\frac{1}{2}\zeta_a^2(\omega)$.

Transforming the wave height to wave energy for each $\delta\omega$, forming the wave energy spectrum (Frequency Domain). A second transformation can be executed with the regular wave components, through a transfer function, the regular response component is obtained. It this example the heave component is obtained through TF $\frac{z_a}{\zeta_a(\omega)}$. The irregular response of the vessel is obtained through superposition of each regular response component, see bottom right corner of Figure 2.5. Each regular response component can be transformed to FD through a similar relation as for wave components, $\frac{1}{2}z_a^2(\omega)$. By adding regular response components, the response spectrum is formed, i.e. right-hand side of the figure.

2.3.3. Motion response - Frequency Domain

As described in Section 2.3.2 and Equation 2.9 the wave energy spectrum for first-order waves can be described as

$$S_\zeta(\omega_n) \cdot d\omega = \frac{1}{2}\zeta_{a_n}^2 \tag{2.26}$$

The response spectra can be described as

$$
\begin{aligned}
S_r(\omega) &= \frac{1}{2}r_a^2(\omega) \\
&= \left|\frac{r_a}{\zeta_a}(\omega)\right|^2 \cdot \zeta_{a_n}^2 \\
&= \left|\frac{r_a}{\zeta_a}(\omega)\right|^2 \cdot S_\zeta(\omega)
\end{aligned}
\tag{2.27}
$$

Using this same relation from the linear wave theory. However, using a second-order force spectrum instead of a first-order force spectrum, results in the response spectrum corresponding to wave drift forces spectrum exiting the vessel. This results in the following relation:

$$S_r(\mu) = |TF|^2 \cdot S_f(\mu) \tag{2.28}$$

where

S_r = second-order response spectrum $[\frac{m^2}{rad/s}]$ or $[\frac{deg^2}{rad/s}]$

TF = transfer function F_{env} to x, y or ψ $[\frac{m}{kN}]$ or $[\frac{deg}{kN}]$

S_f = wave drift force spectrum $[\frac{kN^2}{rad/s}]$

2.4. Sea-states and statistics

This research aims to analyze the effects of non-linearities on a model-based forecasting method. However effects of the input for this model, in this case a random wave train, can be of great importance. It is not yet clear what the effect of certain sea-states is. In order to have a true relation with the actual physical conditions a SOV operates in, a statistical study will determine

which three sea-states will be tested during this research.
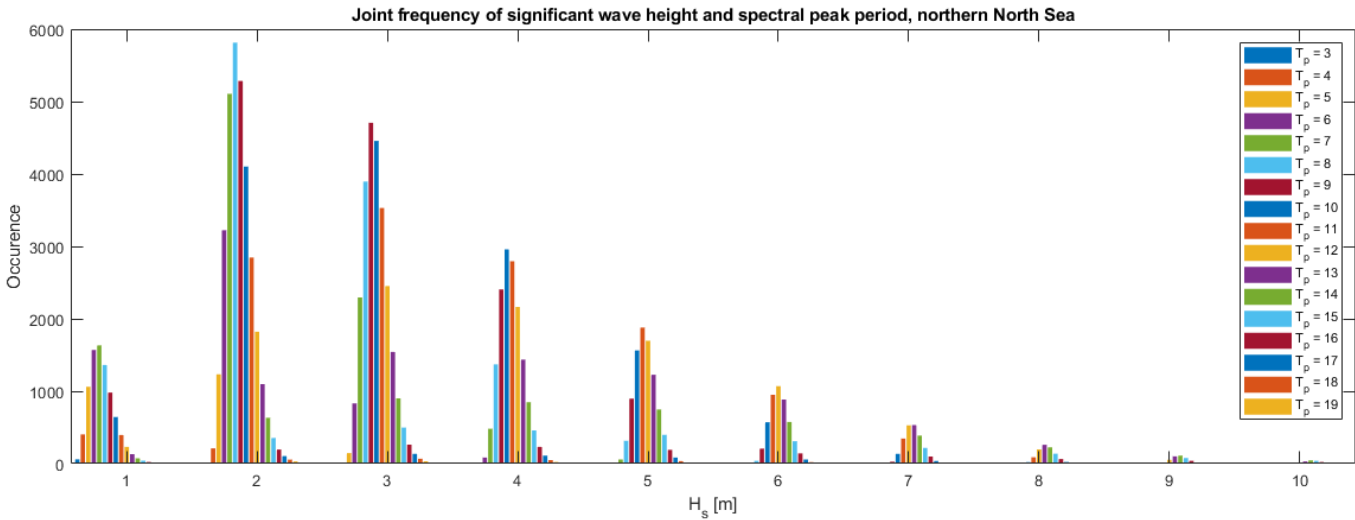
Figure 2.6: Statistical overview of waves occurring in the northern north sea

Figure 2.6 shows the relationship between peak period T_p and significant wave height H_s in the northern north sea [8], from now referred to as sea-state. From this overview it can be determined which sea-sates are most likely to be encountered by the vessel during an operation. From this diagram the following sea-states have been selected:

Sea-State	H_s [m]	T_p [s]
Low	1	5
Medium	2	7
High	3	8

Table 2.1: Sea-sates selected based on expected occurrence

Important to notice is that only operable sea-states have been included in the scope. Even though sea-states with a H_s of 4-5m are more likely to be encountered, the sea-state with H_s = 1m is selected. This because operations are generally not executed in seas above H_s = 3m. Although the vessel might be able to remain within the watch circle based on DP performance. Crew well-being and other mechanical limitations need to be factored in. Also notice that the peak periods have been selected shorter that the most likely to occur based on the statistics. This has been done to account for less swell. The SOV in this research operates in the southern regions of the north sea, shielded by the Great-Britain landmass. Therefore shorter wave periods are to be expected here.

3

Vessel characteristics

For this research a typical Service Operation Vessel (SOV) is used and replicated in the model. This vessel is used for service operations in offshore wind-parks, for which crew transfer and lifting operations are a daily activity. Vessel characteristics are known by MO4 or can be provided by partner companies from within the industry.

3.1. General characteristics

The general characteristics are provided in Table 3.1. The characteristics relate to the condition of vessel when the deck load is at a maximum. These values have been averaged between departure and arrival to compensate for fuel use. However, it must be mentioned that the differences are small.

Designation	Symbol	Unit	Quantity
Length between perpendiculars	L_{pp}	[m]	89.6
Length overall	L_{oa}	[m]	93.0
Beam	B	[m]	18.0
Draught	D	[m]	5.6
Displacement	Δ	tonnes	6436.0

Table 3.1: General characteristics SOV

3.2. Hydrodynamic characteristics

The hydrodynamic are obtained from available literature or calculated in-house using AQWA.

3.2.1. Wind coefficients

The wind load coefficients have been based on the vessel displayed in Figure 3.1 [2] with a frontal surface area of 132 m^2 and longitudinal surface area of 702 m^2. The data was interpolated to construct a complete data set needed for the model. The numerical data is provided in Appendix A Table A.1.
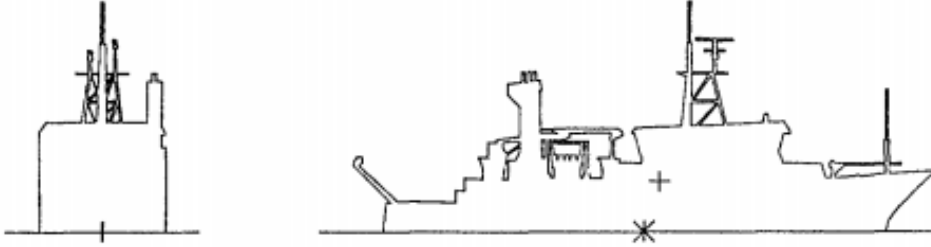
Figure 3.1: front and side view vessel [2]

3.2.2. Current coefficients

The current coefficients are based on standardized coefficient from the MARIN database. In this case, a DP drill vessel. [9]. The numerical data which is used in the model is provided in Appendix A Table A.2. Appendix A Table A.2 contains the interpolated graph of this data.

3.2.3. Added mass

Appendix A Figure A.3 provides an overview of the added mass at each excitation frequency for each DOF. The data has been provided by MARIN and calculated with DIFFRAC / DRIFTP software. As this research focuses on second order wave drift forces, a value will be determined representing the low frequent wave motions. By taking the limit $\omega \to 0$, the added mass value for each DOF is found. See Appendix A Table A.3.

3.2.4. Resistance

The resistance experienced by the vessel due to the hull moving through water is calculated for each DOF using the following equations [24], this is slight variation from the method provided by DNV [7]:

$$
\begin{aligned}
F_x &= \frac{1}{2}\rho \cdot v_{stw}^2 \cdot T \cdot B \cdot Cc_{surge} \\
F_y &= \frac{1}{2}\rho \cdot v_{stw}^2 \cdot T \cdot L_{pp} \cdot Cc_{sway} \\
M_z &= \frac{1}{2}\rho \cdot v_{stw}^2 \cdot T \cdot L_{pp}^2 \cdot Cc_{yaw}
\end{aligned}
\tag{3.1}
$$

where

Fx = Force in surge direction $[kN]$

Fy = Force in sway direction $[kN]$

Mz = Moment about z-axis $[kNm]$

v_{stw} = speed through water $[m/s]$

T = Draught $[m]$

B = Beam $[m]$

L_{pp} = Length between perpendiculars $[m]$

Cc = Dimensionless current coefficient $[-]$

Resistance loads can be induced by a non-zero velocity of the vessel, current or a combination.

3.2.5. Quadratic Transfer Functions

In order to determine the wave drift forces the vessel is exposed to, the Quadratic Transfer Function (QTF) is needed. For the first stage of this research a 2D QTF will be used to calculate the wave drift forces. This QTF has two variables, difference frequency in rad/s. For each direction of the incoming waves and the DOF of the vessel a specific QTF will be calculated. This has been done with the use of diffraction software AQWA. The frequency range is chosen from 0 to 4 rad/s, in increments of 0.025 rad/s, as this is the range in which waves naturally occur. This leads to a QTF with the size 160-by-160 for each wave direction and DOF. In order to keep computation time to a workable amount, only the diagonal and ten off diagonals to either side are calculated, all other data points are set to zero. This can be done as very little energy is present in these regions. A representation of this is shown in Appendix A.5, it can be seen that only the diagonal region has non zero values. The rest of the matrix is equal to zero.

At a later stage a 4D QTF will be used. This QTF will also include directionality of the waves. This will give a more realistic simulation, as in reality vessels are not exposed to waves from only one single direction.

3.3. Thruster layout and propulsion
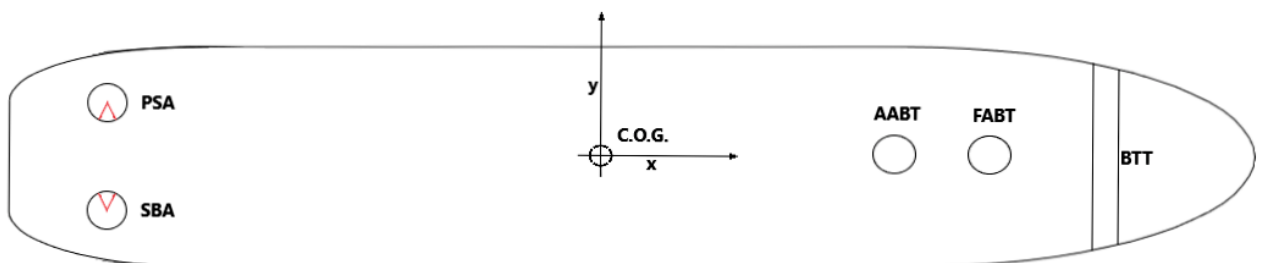
Figure 3.2: Thruster arrangement SOV

The vessel has a propulsion system consisting of 5 thrusters in total, in a layout that is schema-

tized in Figure 3.2. For the four azimuth thrusters and one tunnel bow thruster, specifics are provided in Table A.4.

3.3.1. Moments of inertia

For this research two moments of inertia of the propulsion system will be considered, as they are expected to characterize the station keeping ability of the vessel. The first moment of inertia is due to the rotating of the shaft and propeller to generate thrust, the second is due to the rotating of the azimuths in the direction assigned by the DP system. In this research the moments of inertia will respectively be referred to as I_x and I_z, the values of which can be found in table A.4.

The polar moments of inertia are defined as followed:

$$I_x = I_p + I_{ps} + I_E \tag{3.2}$$

The total polar moment of inertia is a summation of the moment of inertia of the propeller I_p, the shaft I_{ps} and the entrained water I_E. This estimation is referred to I_x, as the default rotation of the propeller is around the x-axis. Because it is an azimuth, this is not always true and the shaft is actually partly orientated in the z-direction. The different components are defined as [17]:

$$I_p = 0.2745 \cdot W_p \cdot R_p^2 \tag{3.3}$$

With the estimation of the propeller weight:

$$W_p = 1.982 \cdot B_{tf} \cdot A_{af} \cdot Y \cdot R^3 \tag{3.4}$$

B_{tf} = blade thickness fraction $[-]$
A_{af} = blade area fraction $[-]$
Y = specific weight blade $[kg/M^3]$
R = blade radius $[m]$

The entrained water moment of inertia can be approximated using the Equation 3.5. The value for K should be between 0.25 and 0.50 [3] and according to Saunders [16] a value of 0.25 is widely used in the industry.

$$I_E = K \cdot I_p \tag{3.5}$$

The moment of inertia for the shaft is calculated using the following approximations:

$$I_{ps} = \frac{1}{2} \cdot m_s \cdot r_s^2 \tag{3.6}$$

where

m_s = mass shaft, calculated for 3m steel shaft $[kg]$

r_s = radius shaft, estimated at $0.075D_p$ $[m]$

The inertia that is present due to the azimuths being orientated in a certain direction are modelled as a point mass (propeller) at the end of a shaft (azimuth shaft housing). The point mass is situated outside of the axis about which the housing and the propeller rotate. The weight of the housing is estimated by subtracting the weight of the propeller from the total azimuth weight [15]. The weight of the propeller is calculated using Equation 3.4.

$$
\begin{aligned}
I_z &= I_{housing} + I_{prop} \\
&= W_p \cdot \epsilon_{prop}^2 + \frac{1}{2} \cdot (W_{azimuth} - W_{prop}) \cdot r_{azi}^2
\end{aligned} \tag{3.7}
$$

where

r_{azi} = radius housing azimuth $[m]$

ϵ_{prop} = eccentricity propeller $[m]$

<div align="right">

4

</div>

Dynamic Positioning

During a DP operation the vessel needs to maintain position on a certain set-point, this set-point is initiated by the DPO at the beginning of the operation. As soon as the vessel deviates from this set position, the DP system brings back the vessel to the original position. In order to achieve this, the system utilises several systems to do this as efficient as possible, see Figure 4.1 for an overview. The function of each component of the DP system and how they operate will be discussed in this chapter and how this is incorporated in the model.
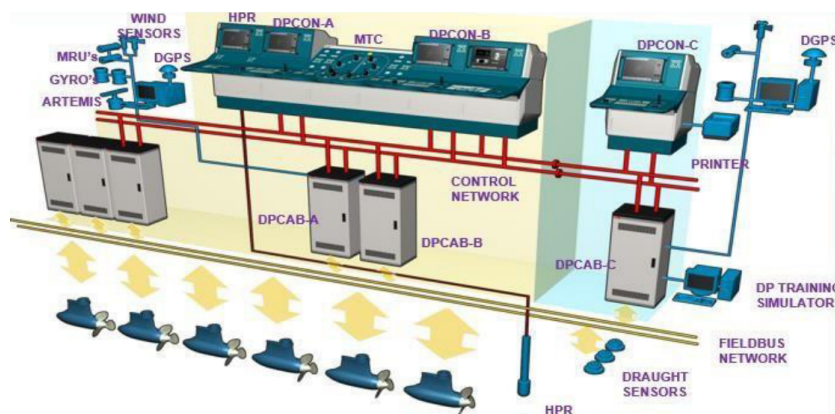
Figure 4.1: Overview of Class 3 DP system [6]

4.1. Position

A wide variety of sensors aboard the vessel constantly monitor the position of the vessel, that can be relative to a reference point or the position on earth. The vessel used for this research has three reference systems: Differential Global Positioning System (DGPS), satellite based positioning system, Fanbeam/Cyscan, radar system that uses reflective panels on the offshore

structures and when conducting a crew transfer the gangway is used as a reference system, this is done by measuring the extension and rotations of the gangway. Motion Reference Unit (MRU) are also widely used aboard vessels to measure roll, yaw, pitch and heave.

Combining all systems allows for an accurate position indication for the crew of the SOV. However, this is not the only reason several systems are installed that can perform similar tasks through different techniques. Redundancy is very important in the offshore industry. Should one of the systems malfunction or a technique not work under certain conditions, for any reason, the SOV has back-up systems.

4.1.1. Set-point

During an operation the crew will choose a position and heading according the operational requirements. Depending on the offshore structure, options can be limited. Once the vessel is in position the DPO will activate the set-point. From this time on until the set-point is deactivated or altered the vessel will measure the distance from this point and the deviation from the heading. This is known as the set-point error. This research will only focus on the horizontal movements of the vessel. Therefore, data is stored in the horizontal plane (x, y and ψ). Section 4.2 will elaborate on how this data is used.

4.1.2. Model

This section of the model translates the forces acting on the vessel into motion. The schematics can be seen in Figure 4.2, where green is input and red is output. An entire overview of the model is included in Appendix B.1.
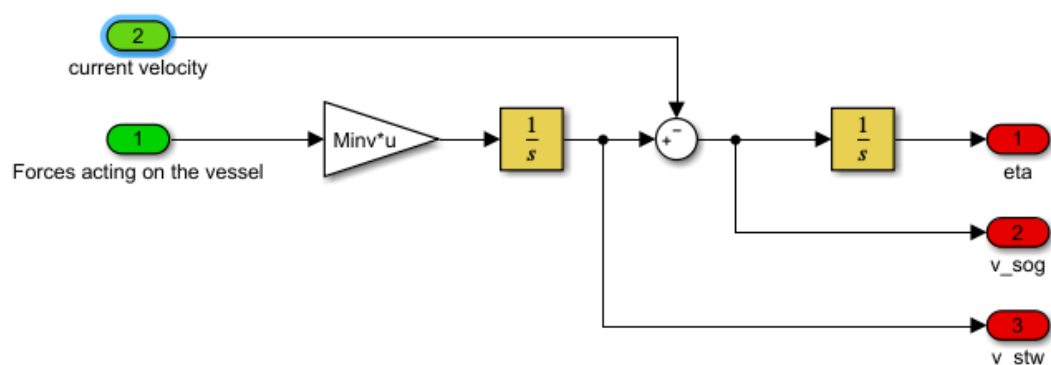
Figure 4.2: Schematic overview of Vessel in Simulink model

Input:

tau = forces and moment acting on the vessel, is a summation of wave drift forces, wind, thrust delivered by propulsion system and resistance of the vessel moving through wa-

ter.

v_c = Current velocity, in x- and y-direction.

By multiplying the forces acting on the vessel with the inverse of the mass matrix, the acceleration of the vessel is obtained. Following basic physics of Equation 4.1.

$$F = M \cdot a \Longrightarrow a = \frac{F}{M} \tag{4.1}$$

Integrating the acceleration of the vessel delivers the speed of the vessel through the water (v_{stw}). The velocity of the water itself (v_c) can be subtracted to obtain the speed over ground of the vessel (v_{sog}). If this is integrated the displacement is obtained, in this research referred to as eta. Each of these outputs will be used in different parts of the model.

Output:

eta = displacement of the vessel, will be used to calculate set-point error.

v_{sog} = speed over ground of vessel, will be used for propeller efficiency.

v_{stw} = speed through water of vessel, used to determine the resistance experienced by the vessel.

4.2. DP controller

A Proportional-Integral-Derivative (PID) controller is a typical control unit used in a variety of industries. It measures the difference between what the output is of a system and what it should be, also known as the aforementioned set-point error. This error is treated in three different ways simultaneously in order to minimize the value. As a PID controller is 'unaware' of what it is controlling, the only aim is to minimize the error. The settings determine how stiff the response is.

In this particular case the PID controller will control the thrust set-point T_{set}. This is the thrust that is needed to get the vessel back to its intended position. An overview of this controller can be seen in Figure 4.3 This information will be used by the thruster allocation algorithm to find the most optimal combination of thruster settings to achieve this in the most economic way possible.
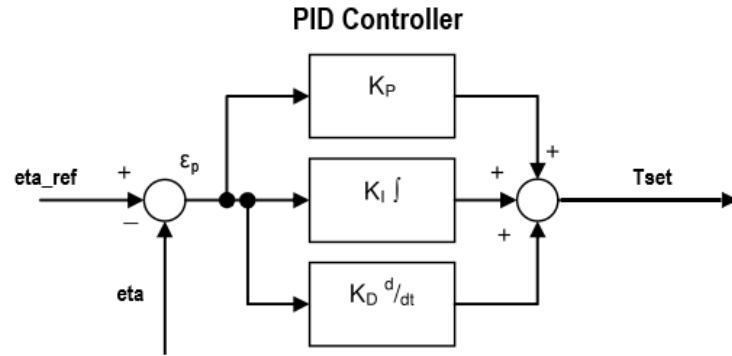
Figure 4.3: Schematic overview of PID controller

A PID controller can be described in mathematical form as:

$$T_{set} = K_{p,DP} \cdot \epsilon_p + K_{i,DP} \cdot \int_{\Delta t} \epsilon_p + K_{d,DP} \frac{\delta}{\delta t} \epsilon_p \qquad (4.2)$$

where

$K_{p,DP}$ = Proportional coefficient $[-]$

$K_{i,DP}$ = Integral coefficient $[-]$

$K_{d,DP}$ = Derivative coefficient $[-]$

ϵ_p = Set-point error $[-]$

4.2.1. Settings

The settings of a PID controller determines how the system responds and is highly sensitive. Wrong settings can easily cause a controller to become unstable and useless. Following a method described by Faltinsen in 1990 [8] leads to a rough estimate for the different coefficients. However, he also states that the controller should be tuned in order to get a proper response. According to Willemse (et al.) [25], "The best PID loop tuning usually overshoots slightly to reach the set- point more quickly, however some systems cannot accept overshoot.". This same method has been followed. The coefficients that have been chosen in order to get this type of response can be found in Table 4.1.

Coefficient	x	y	ψ
$K_{p,DP}$	$57.9 \cdot 10^2$	$57.9 \cdot 10^2$	$26.9 \cdot 10^6$
$K_{i,DP}$	17.4	17.4	$80.6 \cdot 10^3$
$K_{d,DP}$	$19.3 \cdot 10^4$	$19.3 \cdot 10^4$	$89.6 \cdot 10$

Table 4.1: PID settings for thrust control

4.2.2. Auto tune PID

Through out the model, multiple PID controllers will be used, for example to control the shaft speed or the turning rate of an azimuth. PID controller blocks, available in Simulink, provide great control over dynamic systems. The settings can be done manually, in case these are known. In other cases the function includes 'Auto tune' software, in which case the dynamic model is linearized in order to create a very well tuned transfer function. The software allows for manual adjustments to be made, as the 'Response Time' and 'Transient Behaviour' can be altered. The function automatically displays the 'new' transfer function with respect to the initial signal. This function will be used to set all other PID controllers.

4.3. Thruster allocation

The PID controller delivers a thrust setting that is needed to navigate the vessel back to its intended position. However, the thruster system is not able to perform this action, as only a total thrust in x- and y-direction and a total yaw-moment are provided. In order to effectively use the entire thruster system, a thruster allocation algorithm needs to be used. This algorithm calculates the settings of all thrusters in order to deliver the T_{set} in the most economical way, meaning the least amount of thrust. The differential equations that come with these types of convex optimization problems, lie well outside of what the human brain is possibly capable of. Therefore, computational solvers will be used.

Let us consider a very simple example to explain the necessity of using a thruster allocation algorithm. Imagine a vessel that has two thrusters that can either produce thrust forward or backward. The vessel can only displace forward or backward. The vessel needs to move forward with a force of 10 kN. Two solutions are given in Figure 4.4, of the infinite amount of combinations possible. Although generally only one results in the most economic outcome. In this example, the first option.
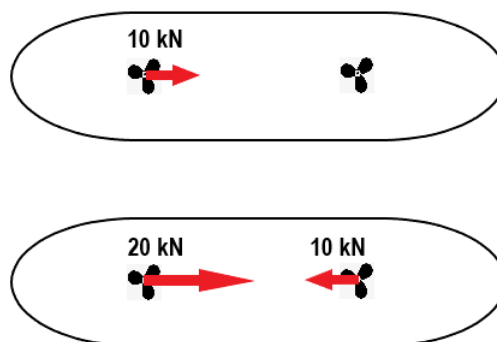
Figure 4.4: Thrust allocation example: Two possible settings for thrusters

The balance of forces and moments is not the only consideration that needs to be taken into

account. The simple example shows that the second option could in principle be considered correct. Except that over 3x more thrust is utilized for an identical outcome. This results in an unnecessary use of resources (fuel and lubrication) and wear on thruster components. The first option also has its downsides. Using a single thruster will result in extensive use and this thruster might be operating near its limits, all undesired effects. The next section will discuss how such problems can be solved and how the aforementioned considerations can be taken into account.

4.3.1. Quadratic Programming

The vessel considered in this thesis, has four azimuth thrusters capable of delivering thrust in a 360°region. Furthermore it has a bow thruster that can only deliver thrust in 90°or 270°in the local reference system. Figure 4.5 displays the different thrust regions that the SOV has.

(a) Thrust region of a tunnel thruster   (b) Thrust region of a azimuth thruster
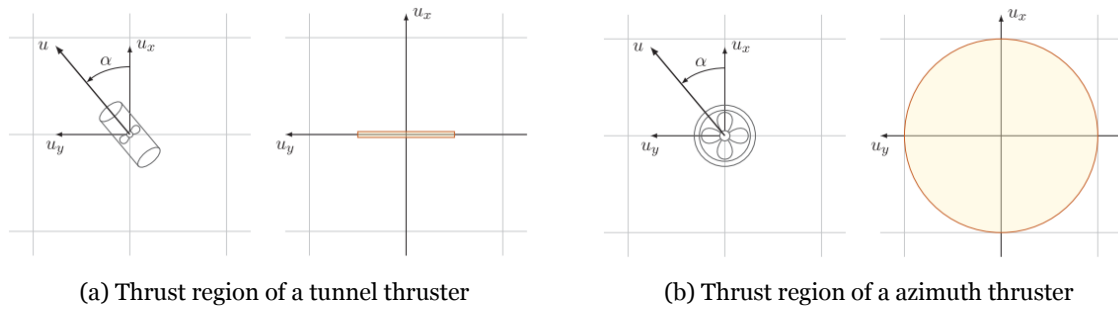
Figure 4.5: Thrust regions SOV [5]

As described by De Wit in 2009, Quadratic Programming (QP) offers great results, compared to e.g. a Lagrange thrust allocator, for vessels that operate on DP [5]. QP is an economic optimization algorithm that can be applied to a wide variety of quadratic problems. The method uses equality and inequality constraints to solve the optimization problem. The thrust allocation problem is defined as:

$$x = minimize \ \frac{1}{2}\mathbf{x}^T P \mathbf{x} + q^T \mathbf{x}$$
$$s.t. \ A\mathbf{x} = b$$
$$G\mathbf{x} \leq h$$

(4.3)

where

A**x**=b = Linear equality constraints

G**x**≤h = Linear inequality constraints

x $= [x_{PSA} \ \ y_{PSA} \ \ x_{SBA} \ \ y_{SBA} \ \ x_{AABT} \ \ y_{AABT} \ \ x_{FABT} \ \ y_{FABT} \ \ x_{BBT} \ \ y_{BBT}]^T$

The problem is subject to linear equality constraints, these solve the force/moment equilibrium part of the problem. In other words this part equals all forces in the x- and y- direc-

tion and the yaw-moment as requested by the PID controller (T_{set}). An additional equality constraint is added, stating that the BTT thrust in x-direction is equal to zero, to ensure the thruster is only able to deliver thrust in y-direction. Furthermore, the problem is subject to linear inequality constraints, these ensure that the thrusters are not able to deliver more thrust than physically possible. Matrix A and vector b are formulated as:

$$
A = \begin{bmatrix}
1 & 0 & 1 & 0 & 1 & 0 & 1 & 0 & 1 & 0 \\
0 & 1 & 0 & 1 & 0 & 1 & 0 & 1 & 0 & 1 \\
-3.900 & -36.285 & 3.900 & -36.285 & 0 & 24.065 & 0 & 30.505 & 0 & 36.615 \\
0 & 0 & 0 & 0 & 0 & 0 & 0 & 0 & 1 & 0
\end{bmatrix}
\tag{4.4}
$$

$$
b = \begin{bmatrix}
T_{set,x} \\
T_{set,y} \\
T_{set,\psi} \\
0
\end{bmatrix}
\tag{4.5}
$$

See Appendix C for P and q. The P matrix can be used to give preference to certain thrusters. For this research each thruster will be utilized equally. The q vector contains only zeros as this represents the linear contribution of the problem.

The linear inequality constraints ($G\mathbf{x} \leq h$) ensure that the optimized solution lies within the physical capabilities of each thruster, the thrust region. Figure 4.5 shows that for azimuth thrusters the thrust region is non-linear and convex. For each thruster, a set of inequality constraints is created, to form the thrust region. By intersecting a large number of hyperplanes, a convex polygon is created that approximates the convex shape of the actual thrust region. The convex polygon is the linearized thrust region. See Figure 4.6 for the linearized thrust region of the PSA. Tunnel thrusters are defined by a T_{max} and $-T_{max}$ as the direction was already defined by the extra equality constraint (see row four of A and b matrix).

This formulation can be solved by different solvers compatible with MATLAB. Different solvers will be tested to see if results are consistent, from which the most suitable will be selected. MATLAB offers an integrated solver Quadprog. However, this requires expensive packages and therefore this might not be a pragmatic option. Different open-source solvers are available like QPIP and CVX, which are free to use and therefore highly recommended by different experts on QP.

The QP solver aims to find a solution for $\mathbf{x}$ that satisfies all constraints at each time step. The solution is given as a matrix with an x- and y-vector representing the thrust component for each thruster, see Equation 4.3. From this result, the absolute thrust and direction can be derived
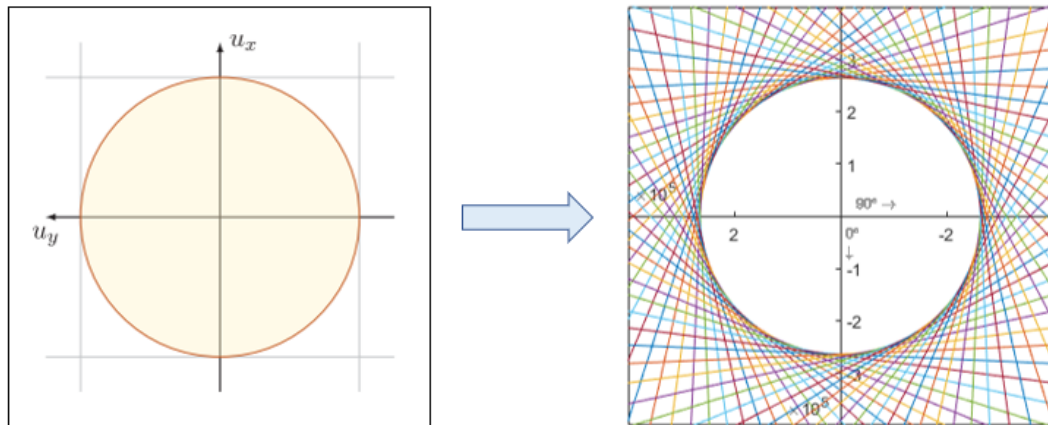
Figure 4.6: Linearized PSA thrust region in terms of force [N]

through basic geometry. Essentially the QP solver is aiming to find the minimal combination of thrust that needs to be delivered (and thus direction) by five thrusters to bring back the vessel to the set-point. Depending on the solver, different settings can be applied to increase accuracy and sensitivity. Besides the outcome of **x**, the solver can deliver other information regarding the results. The most important being the appreciation of the result. Depending on the solver, a value is returned stating whether an ideal solution has been found or not.

4.3.2. Solver selection and verification

As mentioned in Section 4.3.1 different solvers are tested to find out which is best suited for this research. The selection is made through the following criteria:

- Compatibility with model and other software

- Capability of QP solver and documentation available

- Source and accessibility

Table 4.2 shows how each solver performers relative to each other. The CVX solver is not compatible with Simulink in the way the model is designed at this moment. The CVX software is provided with elaborate documentation and a wide variety of data can be extruded from the solver in comparison to the other solvers. The software is open source, allowing insight in the way the solver is designed. However, for it to be used in this research, extensive redesign of the model is necessary, therefore it is not deemed a viable solver. The software is updated yearly and used extensively by optimization engineers.

Quadprog is a QP solver provided by MATLAB, through aquisition of the optimization toolbox. Use of the tool is well documented, therefore the ease of use is high. Furthermore, the software is easily integrated in the model and compatible with Simulink. As the function is a MATLAB

product no insight in the design of the solver is possible. In future use this might become problematic as engineers tend to stay away from black-box software.

Qpip is an open source QP solver written by Adrian Wills [1]. The capability is limited compared to the other two solvers, however, sufficient for the extent of this research. Full insight in the solver is possible, C++ is required to open certain drivers. The Software was last updated in 2010, compatibly problems regarding future MATLAB versions are plausible. Integration into the model is very similar to Quadprog. Limited data can be extracted compared to the other solvers.

QP Solver	Criteria 1	Criteria 2	Criteria 3
CVX	Not compatible - Simulink	Extensive	Open source
Quadprog	Compatible	Extensive	Matlab package
Qpip	Compatible	Limited	Open source

Table 4.2: Performance of QP solvers compared

In order to verify that the solvers are performing as expected and are capable of solving the problem at hand, a simple cost optimization problem is solved for which the solution can be verified. Quadprog and Qpip are compared, as CVX is not deemed viable. The following cost function is to be optimized:

$$cost = minimize\ 0.4x_1^2 - 5x_1 + x_2^2 - 6x_2 + 50 \tag{4.6}$$

Figures 4.7a and 4.7b are subject to the following limits:

$$\begin{aligned} s.t. \quad & 0 \leqslant x_1 \leqslant 10 \\ & 0 \leqslant x_2 \leqslant 10 \end{aligned} \tag{4.7}$$

Both Quadprog and Qpip have run successfully and found the same optimal value, indicated by the red star. The cost function is plotted with a contour function. The limits ensure a solution can only be found in the top right segment. Figures 4.7c and 4.7d are subject to the following inequality constraints in addition to the limits:

$$\begin{aligned} s.t. \quad & x_2 - x_1 \geqslant 2 \\ & 0.3x_1 + x_2 \geqslant 8 \end{aligned} \tag{4.8}$$

(a) Quadprog: no constraints

(b) Qpip: no constraints

(c) Quadprog: > green, > purple

(d) Qpip: > green, > purple
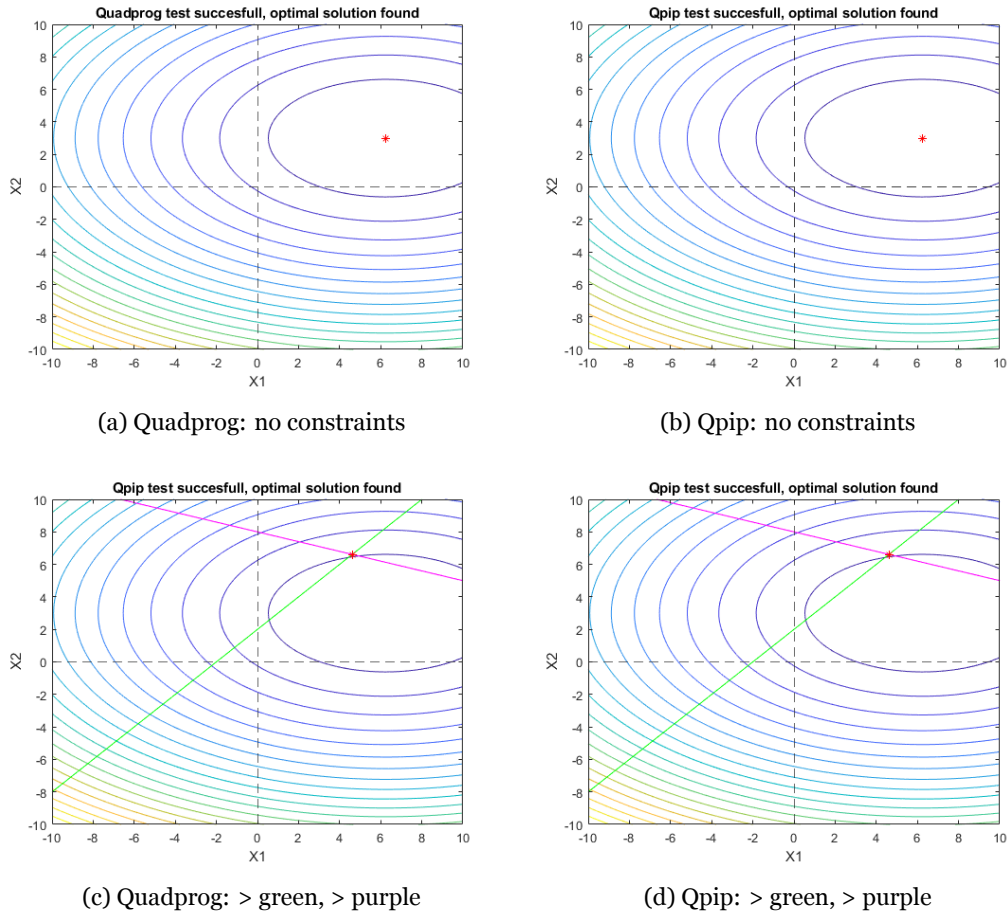
Figure 4.7: verification QP solvers

The constraints prevent the solver from finding the optimal solution as found in the previous step. A solution should be found in the top right segment and should be equal or higher than the green and magenta line. Both solvers find the same optimal solution within constraints enforced. Figures 4.8a and 4.8b are subject to a set of constraints that do not have a solution within the defined limits. This will provide insight in how the software reacts to contradicting settings. The following constraints are used in addition to the limits used before:

$$s.t. \quad x_2 - x_1 \geqslant 8$$
$$0.1x_1 - x_2 \geqslant -2 \tag{4.9}$$

In this example the solution should still be found in the top right segment, however, the solution should also satisfy the inequality constraints. The solution should be in the region that is both below the magenta line and above the green line. Both solvers give a different solution. Notice that the optimization in both cases has failed and the solves indicate that no optimal solution is found. It can be argued that both solvers prioritize the limits above the inequality constraints. As otherwise each solver would have given the solution provided in Figures 4.8c and 4.8d. Here the optimization problem is not subject to limits. Both solvers find the same

optimal solution after a successful test. To fully understand how each solver chooses to find a solution after a failed test, the source code of each solver should be examined. This however lies outside of the scope of this research. If this is deemed necessary in future research, this would only be possible for the Qpip solver.

(a) Quadprog: > green, < purple

(b) Qpip: > green, < purple

(c) Quadprog: > green, < purple, no limits

(d) Qpip: > green, < purple, no limits
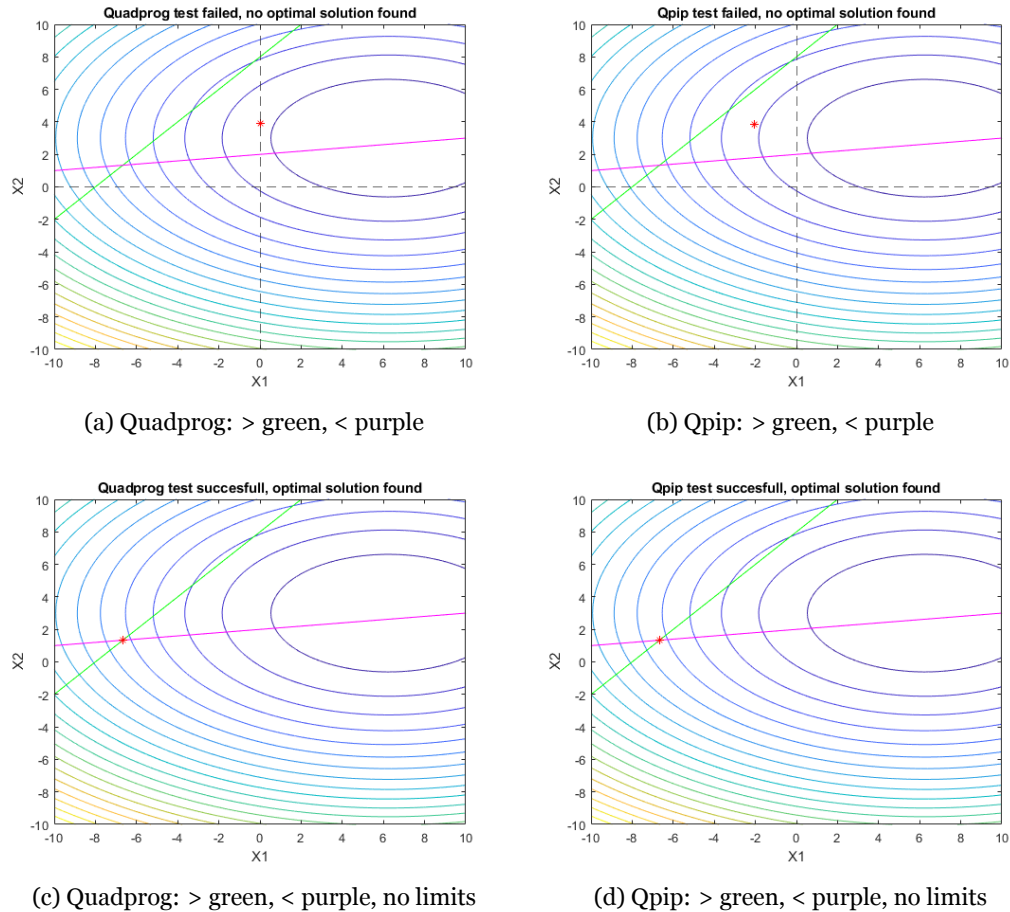
Figure 4.8: verification QP solvers

The optimization problem as described at the start of this paragraph serves both as testing method as well as verification of the solvers capability of minimizing a quadratic function. As the thruster allocation problem is not subject to limits, only to equality and inequality constraints, both solvers are considered equal in performance. An additional test is run to see if it can be determined if either solver outperforms the other. In this case both solvers are incorporated into the time domain model of the Acta Auriga. The vessel is loaded by 30°stern waves. The thrust commanded by the DP controller (PID) and the thrust allocated to each thruster are compared for both solvers in Figure 4.9.
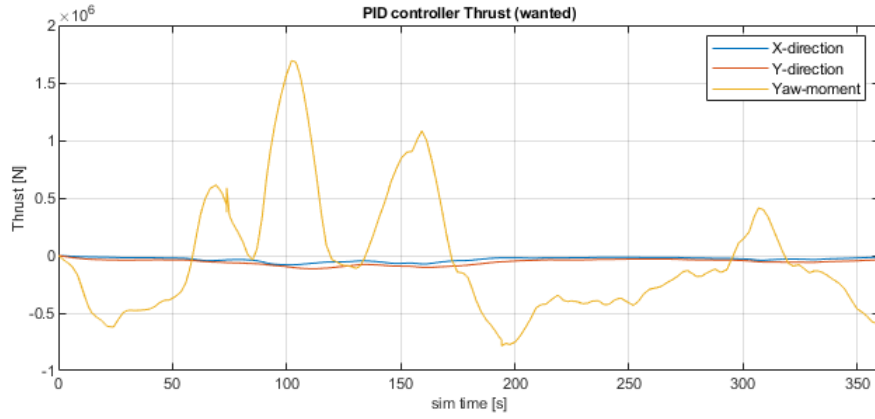
(a) DP controller thrust commanded
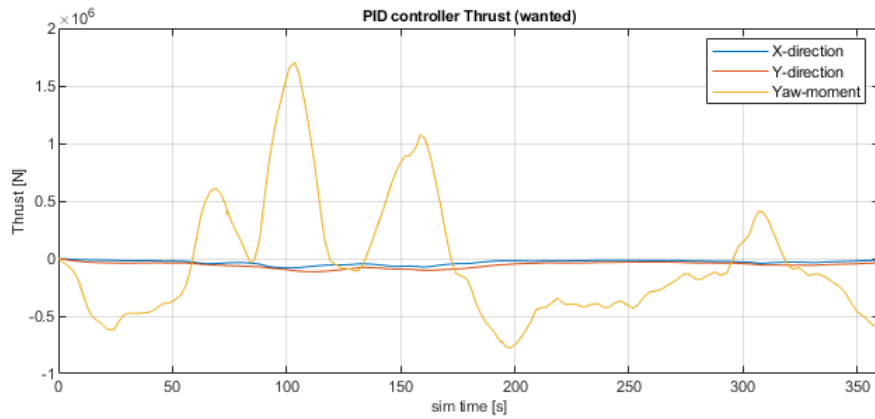
(b) DP controller thrust commanded
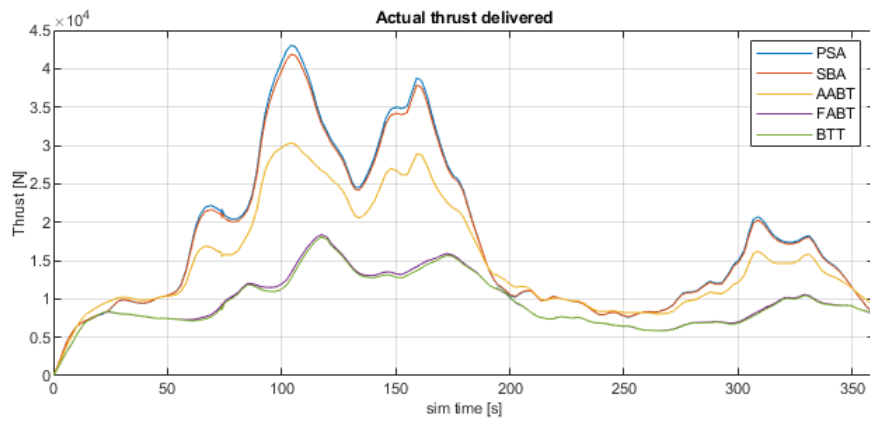
(c) Thrust allocated by Quadprog
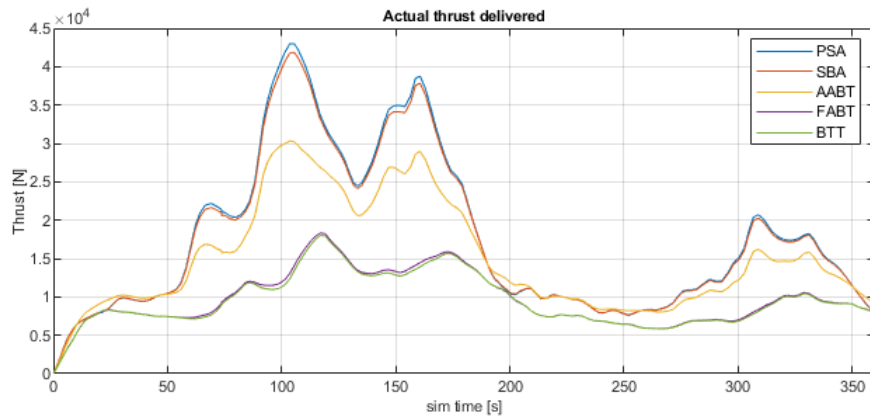
(d) Thrust allocated by Qpip

Figure 4.9: Comparison of QP solver integrated into time domain model Acta Auriga

From Figure 4.9 it can be concluded that both QP solvers perform highly similar when considering the allocation of thrust over five thrusters. The complexity of the problem has increased to such an extent that manually checking the solution is no longer possible, this is what the verification in the previous paragraphs serves for. This comparison merely serves as an extra check. As both solvers clearly perform identical except when confronted with an unsolvable problem, the decision for which solver to use is based on availability and accessibility. The QP solver Qpip is open-source and allows insight in the source code. For these reasons, Qpip is the selected QP solver for this research.

5

Non-linear components

This section will discuss the various non-linear or discontinuous components that have been studied in this research. The goal is to get an understanding of the effects of each component on the frequency domain approach. In order to achieve this, the components need to be modeled in the time domain model and resemble realistic behaviour of the vessel. For each non-linear component it will be discussed how they are incorporated in the model.

To understand the effect of each component on the behaviour of the vessel it is important to test all components separately. This is done in order to prevent influences from other non-linear components affecting the results. In some cases this will lead to unrealistic responses from the dynamic systems. Should such events occur, it will be mentioned with the results.

5.1. Forbidden zones

The vessel has four azimuth and a tunnel thruster available for station-keeping and manoeuvring. Depending on the configuration of the azimuths and the shape of the vessel, thrusters might interact with each other or with the vessel's hull. These effects are known as thrust degradation effects [25]. In order to prevent these effects from occurring during an operation, which might lead to unexpected situations like drift-off, a Forbidden zone (FBZ) is introduced to the thruster. A thruster subject to a FBZ will not be allowed to deliver thrust in a certain range, this prevents thruster wash from interacting with other thrusters or the hull in the opposite direction.

Figure 5.1 (a) shows the thrust region of a thruster not subject to a forbidden zone, thrust can be delivered in all directions. Whereas, Figure 5.1 (b) represents the thrust region of thruster

(a) Thrust region without forbidden zone

(b) Thrust region with forbidden zone
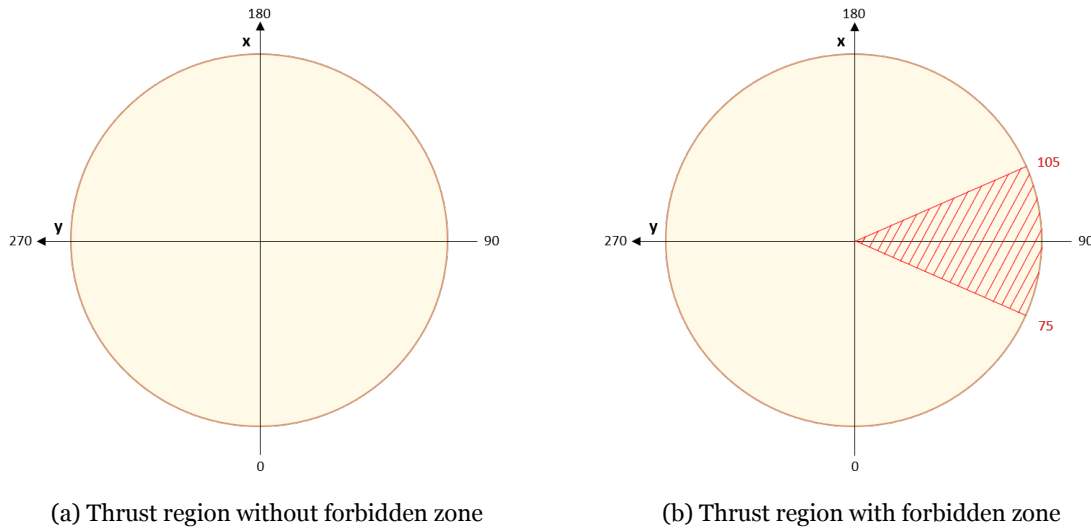
Figure 5.1: Schematic thrust region that can be delivered by an azimuth

with a forbidden zone of 30°, ranging from 75°to 105°. This will prevent the thruster wash from interacting with a thruster or part of the hull situated in the range between 255°and 285°. This is a typical FBZ for a azimuth situated on the starboard side of a vessel, with an other thruster at the same distance from mid-ship on port-side of the vessel. An overview of the FBZ's for each thruster of the vessel used in this research is given in Table 5.1.

Thruster	FBZ	Lower boundary	Upper boundary	Size
PSA	Yes	75°	105°	30°
SBA	Yes	255°	285°	30°
AAFT	No	-	-	-
FABT	No	-	-	-
BBT	No	-	-	-

Table 5.1: Forbidden zones overview

Solving the thrust allocation problem through QP requires the inequality constraints to be of a strictly convex shape. However, by introducing FBZs, the polygon ceases to be of convex shape. The definition of a convex polygon is that each vertex should turn only right (clockwise) or left (counter-clockwise) and the intersection between two points on the polygon remains within the polygon [18]. Which results in all internal angles being less than 180°.

When closely inspecting Figure 4.6 it is clear that all internal angles are indeed less than 180°. When analysing Figure 5.1 (b), notice not all vertices are less than 180°, see the vertex located at the origin. The thrust region is no longer convex and cannot be solved using QP. By splitting the 'Pac-Man' shape into two disjunct segments, the polygons return to a convex shape and

therefore creates a solvable problem at the cost of computation time. The split is created by introducing an extra inequality constraint that lies exactly in the middle of the FBZ (in case of Figure 5.1 a constraint that lies on the y-axis). A plot of the disjunct segments bounded by linear constraints is given in Figure 5.2. A full overview of the thrust regions used by the model in this research can be found in Appendix D.1.
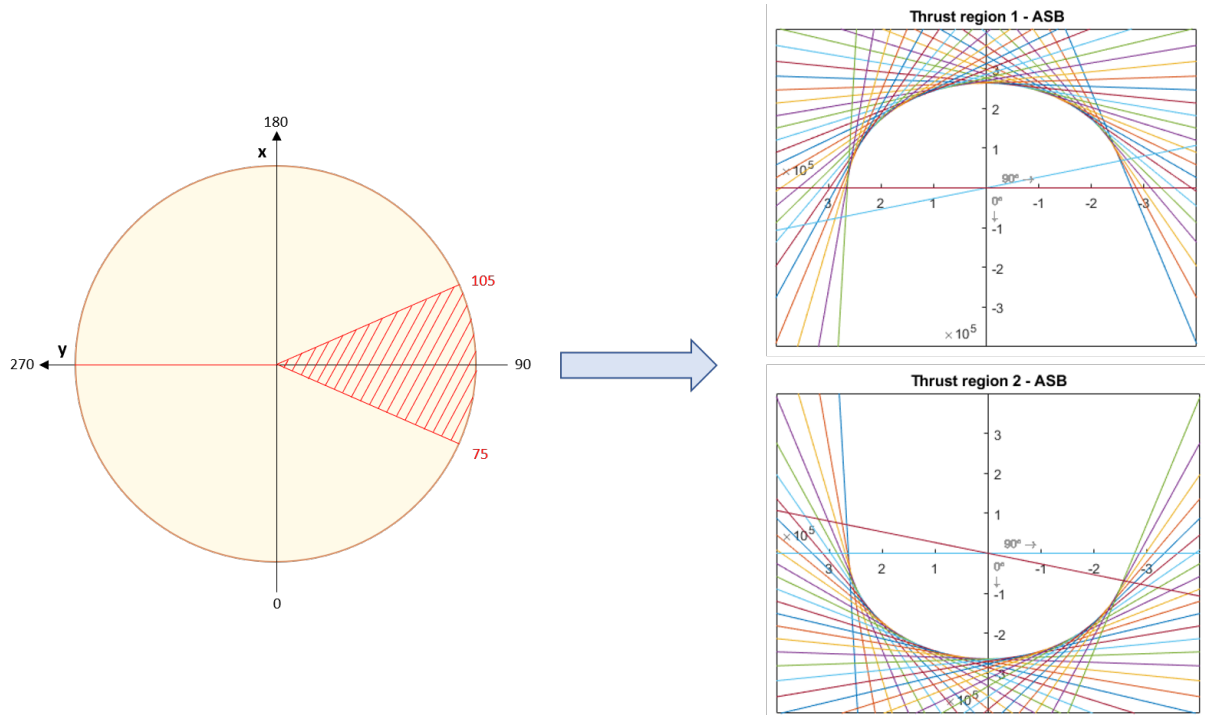
Figure 5.2: Thruster region split in disjunct thrust segments

Splitting the thrust region in two disjunct segments creates a different challenge. The convex optimization problem is set up so that for each thruster a setting will be delivered. This setting, in combination with the other thrusters will be the best possible solution. Best in this case being the least amount of total thrust. For one thruster the optimal solution can only lie within one of the segments. As the thrusters have effect on each other, the optimization algorithm can only test one segment in combination with the other thrusters in one calculation. Thus, for each time step both combinations have to be tested. The combination with the least amount of thrust is the most optimal for that time step. As the vessel in this research has five thrusters, of which two have a FBZ, each time step will require four different calculations. The lowest value of these four solutions will be selected as the settings used for thruster allocation.
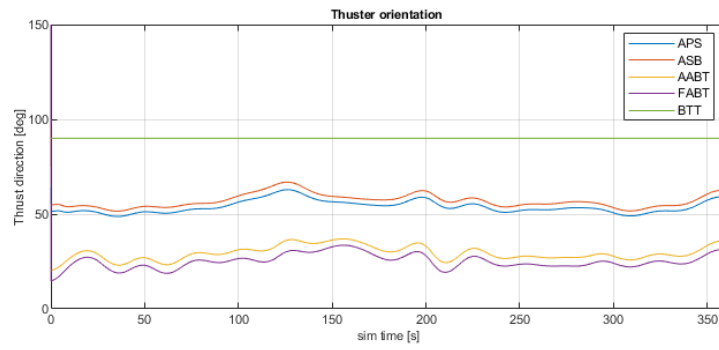
(a) No FBZ, F_{env} coming from 15°
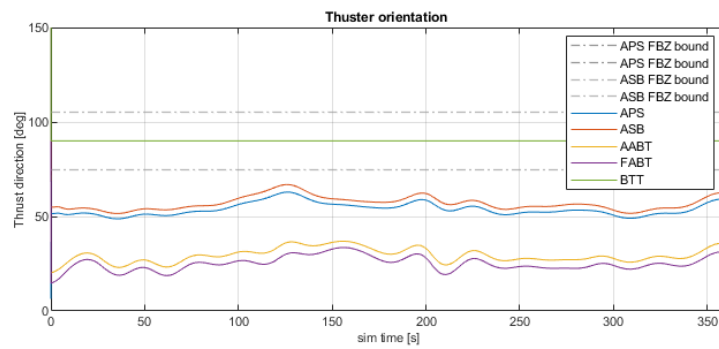
(b) FBZ, F_{env} coming from 15°
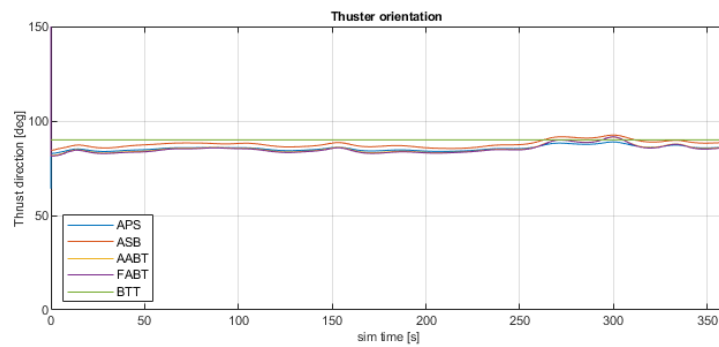
(c) No FBZ, F_{env} coming from 75°
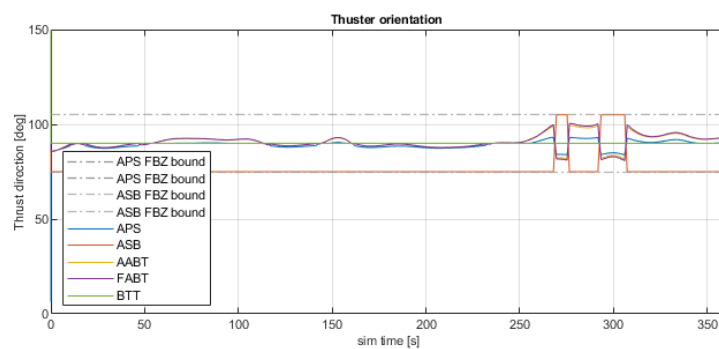
(d) FBZ, F_{env} coming from 75°

Figure 5.3: Same simulation with and without FBZ and F_{env} inside and outside FBZ

Figure 5.3 includes four graphs depicting the orientation of all thrusters under different circumstances. These figures show the effectiveness of including the FBZ function in the TD model. Two tests have been conducted. Figures 7.1a and 7.1b are simulations done with the same seed and act as the control test. F_{env} coming from 15°, with Figure 7.1a representing a vessel without FBZ. Figure 7.1b represents a vessel with thruster PSA and SBA subject to a FBZ. The second test, represented by Figures 7.1c and 5.3d, has been conducted in the same manner. However for these simulations, F_{env} is coming from 75°. Notice the dashed grey lines representing the boundaries of the FBZ. Also notice that F_{env} is defined as 'coming from', this means that vessel is loaded from this direction by wind, waves and current, displacing the vessel in the opposite direction.

When comparing the top two simulations the results are exactly the same. This is as expected. The direction of thrust of each thruster is generally in the direction from where F_{env} originates. This is a logic response. By including an FBZ to the SBA thruster the results should not be affected. This is the case, meaning the control test is successful.

The second test has been done to determine if the thruster that is subject to a FBZ does not deliver thrust in the FBZ, when the optimal solution lies in that range. Figure 7.1c displays the optimal solution. F_{env} is coming from 75°and all thrusters deliver thrust in that general direction. Figure 5.3d clearly shows that the SBA thruster does not deliver thrust in the range from 75-105°. This behaviour is what is to be expected. As the thruster is not permitted to deliver thrust in the optimal direction (FBZ), the algorithm seeks the most optimal solution within the allowed thrust region. This is most likely on the boundary of the FBZ, in Figure 5.3d it can be seen that SBA indeed follows the boundary of the FBZ. After about 270 seconds there is a jump in direction, the algorithm has found a more optimal solution in the second thrust region of SBA. This shows that the algorithm is working correctly.

5.2. Turning rate azimuth

By taking a closer look at segment 250s-350s of Figure 5.3d, unrealistic behaviour is demanded by the thruster allocation algorithm. The optimal solution requires the azimuth thrusters to instantly deliver thrust in a direction that can differ up to 30°in this case. This is unrealistic behaviour. Due to inertia the turning response of azimuth thrusters will be non-linear. The polar moments of inertia as calculated in Section 3.3.1 will be used for this. Furthermore, the azimuth thrusters maximum turning rate is limited to 12 deg/s [24]. Figure 5.4 gives an overview of how the optimal azimuth angle α_l (wanted by the DP controller) is translated to a realistic response α_{nl}.
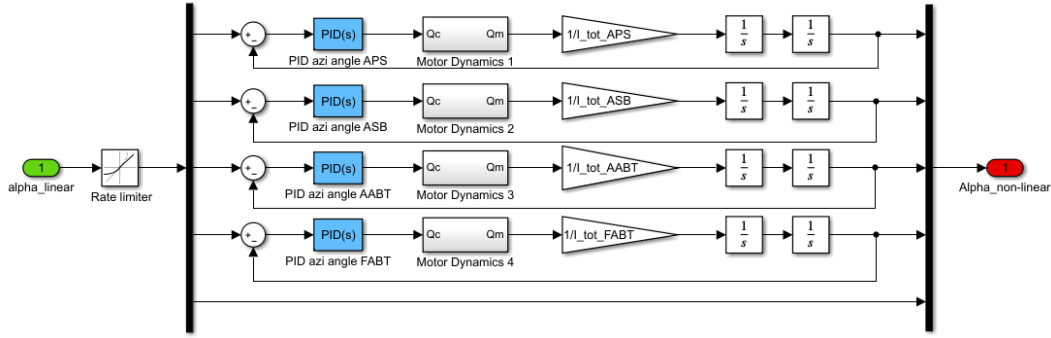
Figure 5.4: Simulink block modeling non-linear turning rate behaviour azimuth thrusters

On the left side of the Simulink block the commanded azimuth angle α_l is input. This signal is limited by a rate limiter set to 0.2095 rad/s (12 deg/s), as α_l is in radians. The signal is then split into five separate signals, one for each thruster. BTT is a tunnel thruster and thus not subject to any turning, the signal is directed towards output. The signals for azimuths angles are of interest in this section. These are fed into a feedback loop controlled by a PID-controller. The azimuth angle set-point is fed into the PID-controller which returns a torque set-point. The azimuth angle is not directly imposed onto the vessel by the DP controller, the torque provided by the driver turning the azimuth is actually controlled. The driver motor, turning the azimuth housing, is modeled through a simple driver gain block, translating the torque set-point to actual torque Q_d. After which the torque is divided by the polar moment of inertia I_z and integrated twice to acquire the actual azimuth angle, see Equation 5.1. This is then fed back to find the azimuth angle set-point error.

$$\ddot{\omega} = \frac{Q_d}{I_z} \rightarrow \omega = \iint \frac{Q}{I_z} \tag{5.1}$$

The actual azimuth angles of all thrusters are used to find the actual thrust delivered by the vessel in combination with the efficiency of the thrusters depending on the Four Quadrant (4Q) method. The next section will discuss how the 4Q diagram is used to determine propeller torque and thrust.

PID	$K_{p,\alpha}$	$K_{i,\alpha}$	$K_{d,\alpha}$
PSA	1.351	0.063	7.089
SBA	1.351	0.063	7.089
AABT	0.394	0.018	2.068
FABT	0.394	0.018	2.068

Table 5.2: Azimuth angle PID-controller settings

In Figure 5.5 the same simulation has been run twice, once with limitations as described in Figure 5.4 and once without. Even though the first part of a simulation is not very interesting

for actual data, as simulations need time to 'settle', these segments are discarded from the actual data. The effects of introducing the control system and limiting the rate of change are clearly visible. Also notice the expanded section, the rate of change of the direction demanded by the allocation algorithm is not realistic. By including the control block a more realistic response is achieved.
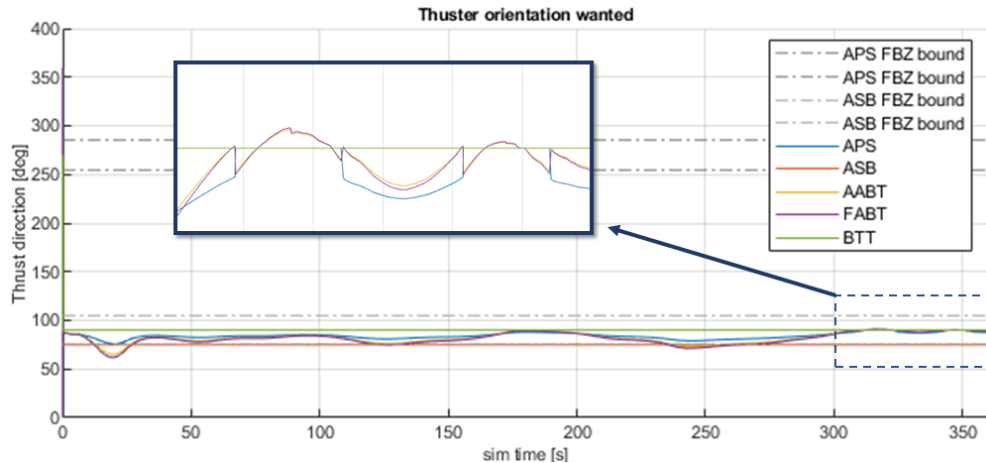
(a) Unlimited linear turning behaviour thrusters
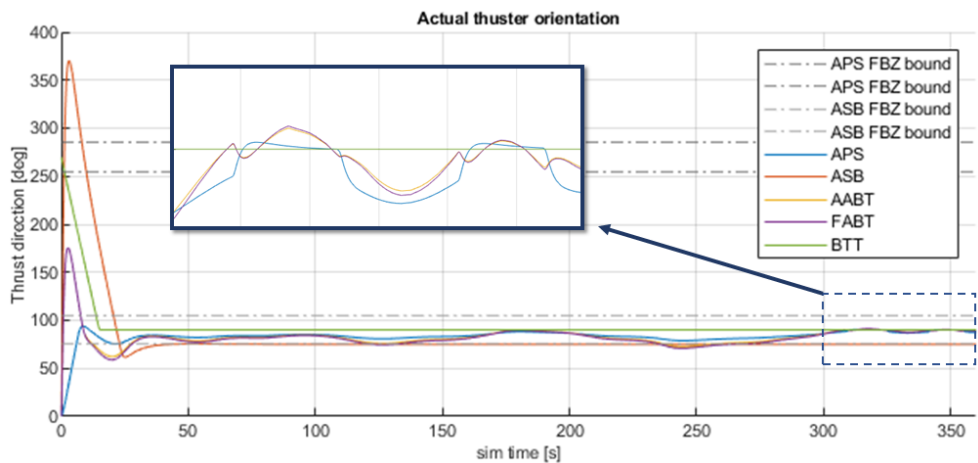
(b) Limited non-linear turning rate behaviour

Figure 5.5: comparison between thrusters with and without inertia effects.

5.3. Propeller ramp up speed

In a similar manner as azimuth turning rate, the thrusters cannot instantaneously deliver the requested thrust. Due to inertia, the propellers need time the fully deliver the commanded thrust. This system will also be controlled by a PID controller.

Through the set-point error the DP controller has determined how much thrust is required to get the vessel back in position. The allocation algorithm has determined the most optimal

distribution of thrust. It is vital to understand that the thrust required by the vessel is however not directly controllable. Thrust is the result of a propeller rotating through water. The angular velocity of the propeller creating thrust can be controlled by the vessel's machinery, through the shaft speed n_{shaft}. Therefore, T_{set} must be translated to n_{set}, using the following equation:

$$n_{set}^2 = \frac{T_{set}}{\rho \cdot D_p^4 \cdot K_{t,0}} \tag{5.2}$$

where

D_p = diameter propeller $[m]$
$K_{t,0}$ = propeller torque coefficient at $v = 0$ m/s $[-]$
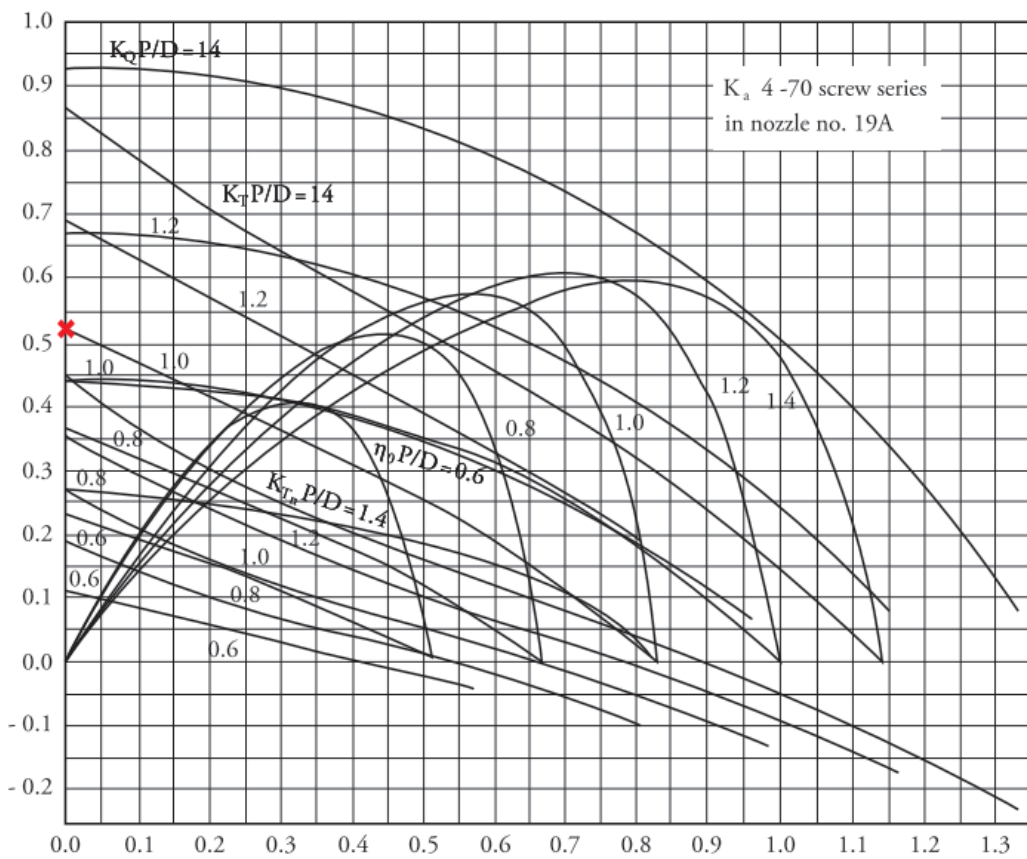
Figure 5.6: Open-water diagram Ka4-70 propeller in 19A Duct

$K_{t,0}$ is used in this instance as the vessel speed is not known at this stage. The estimated shaft speed is fed into a control loop to determine the actual shaft speed. The actual shaft speed is fed back to estimate the shaft speed set-point error. The shaft speed is also used to determine the actual torque through the 4Q diagram, which is then also fed into the control loop to determine the shaft speed. Figure 5.7 displays an overview of the control loop including the side 4Q loop for one thruster. Table 5.3 provides the control loop settings for all thrusters.
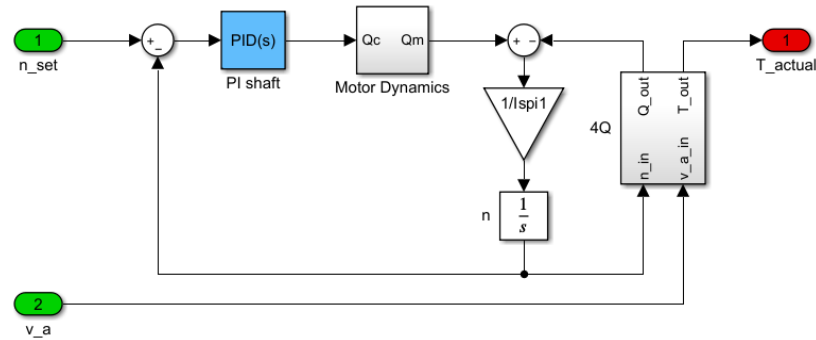
Figure 5.7: Control loop and 4Q diagram

Thruster	$K_{p,n}$	$K_{i,n}$	$K_{d,n}$	$K_{t,0}$	I_x
PSA	1.1	1.1	0	0.25	5665
SBA	1.1	1.1	0	0.25	5665
AABT	1.1	1.1	0	0.25	1371
FABT	1.1	1.1	0	0.25	1371
BTT	1.1	1.1	0	0.25	3956

Table 5.3: Control loop settings for each thruster

5.3.1. Four Quadrant Diagram

The shaft speed is found through Equation 5.3, the polar moment of inertia of the propeller and shaft have been discussed in Section 3.3.1.

$$n_{shaft} = \int \frac{Q_{shaft}}{I_x \cdot 2\pi} \tag{5.3}$$

As mentioned before the shaft speed is relevant for determining the torque and thrust delivered by each thrusters. The 4Q diagram is used to calculated the torque and thrust of a propeller based on rotational speed and flow velocity of the water. As the vessel motions are limited and environmental loads can come from any direction, propellers can be subjected to a negative inflow velocity during DP operations. The four quadrant diagram determines whether a propeller has negative/positive flow velocity and negative/positive rotational velocity, creating four quadrants. For this research the 4Q diagram of a Ka4-70 in 19A duct is used, this diagram is provided in Appendix D.2.

Besides the vessel encountering negative forward speeds, each thruster can rotate 360°independently from each other. Taking into account that thruster are located at different locations, each thruster will encounter unique inflow velocities and directions. Translating the ship velocity and direction is achieved through rotation matrices and the rotation of each thruster

relative to that of the vessel. The unique inflow velocities are used as input v_a for the control loop, visualized in Figure 5.7.

5.4. Saturation

Saturation is the effect that occurs when a thruster is operating at its physical limit and fails to produce the requested thrust. Such an event is highly unlikely to occur as several safety measures are in place. However, in case a event like this does occur it is important to understand what the effects are and how it is captured in the frequency domain forecasting model. Furthermore this addition to the model can be used to investigate the effects of malfunctions to one or more engines.

The thruster allocation algorithm is designed to select a distribution of thrust over the five thrusters that stays within the predetermined limit of each thruster. However, when this is not possible, the algorithm is also capable of giving a setting that does not comply with all constraints. This is because the thruster allocation algorithm is limited by a variety of safety factors. Common practice in the offshore industry is to operate each thruster at a maximum of 50% of its physical capability for DP2 operations. The excess power is available to cope with engine failure or extreme conditions.

Figure 5.8 shows the effect of introducing saturation to the Simulink model. The saturation level of APS has been set to 10% (2670 N) for demonstration purposes. Under normal conditions the thrust commanded by the DP controller will not reach the actual saturation level. The effect of introducing saturation to APS thruster is clearly visible. Once the saturation level is reached, no more thrust is allocated to this thruster.
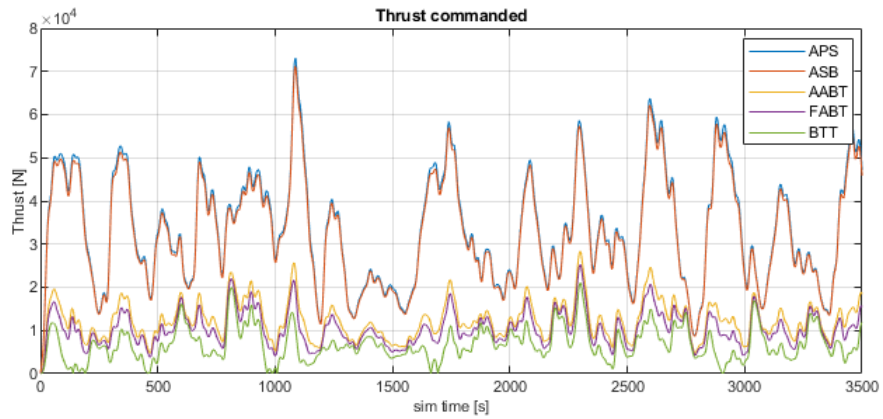
(a) Saturation off
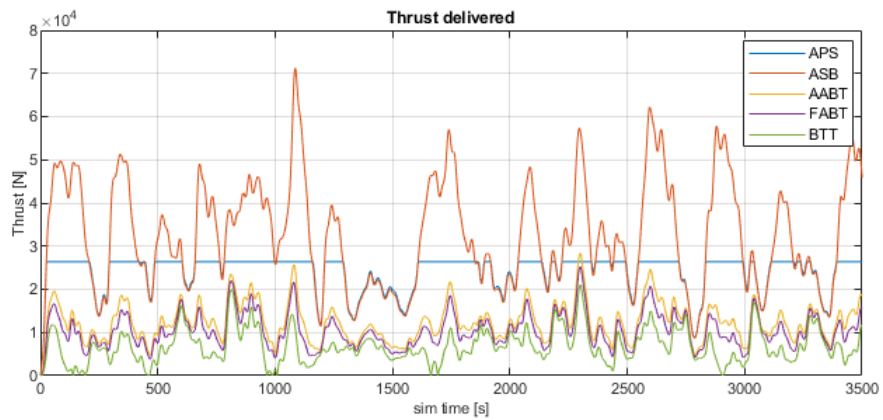
(b) Saturation on

Figure 5.8: Effect of including saturation to model

6

Methodology

This chapter presents the methodology used in this research to investigate the effects of non-linearities on the transfer function used to forecast vessel motions in the frequency domain. First, a general overview will be discussed of the different models used to capture the physics behind motion forecasting of offshore vessels in this research. After which the most important components will be discussed in depth. The methodology of verifying components of this research will also be discussed in this chapter. Finally the simulation set-up regarding testing the effects of each non-linear component is presented in this chapter.

6.1. Model description

Figure 6.1 displays an overview of the global model used in this research. This diagram also provides insight in the data-stream within this model, from a sea-state to a vessel response spectrum in surge, sway and yaw. Each plane represents a deliverable in either the TD or the FD, the orange plain represents the MATLAB/Simulink model of the SOV Acta Auriga. The steps in between each plain is a chronological process that will be explained in this section. Double plains represent moments in the process where comparisons can be made between the TD and FD results. Notice the dashed line, this represents information being translated between time and frequency domain.

Frequency Domain

Time Domain
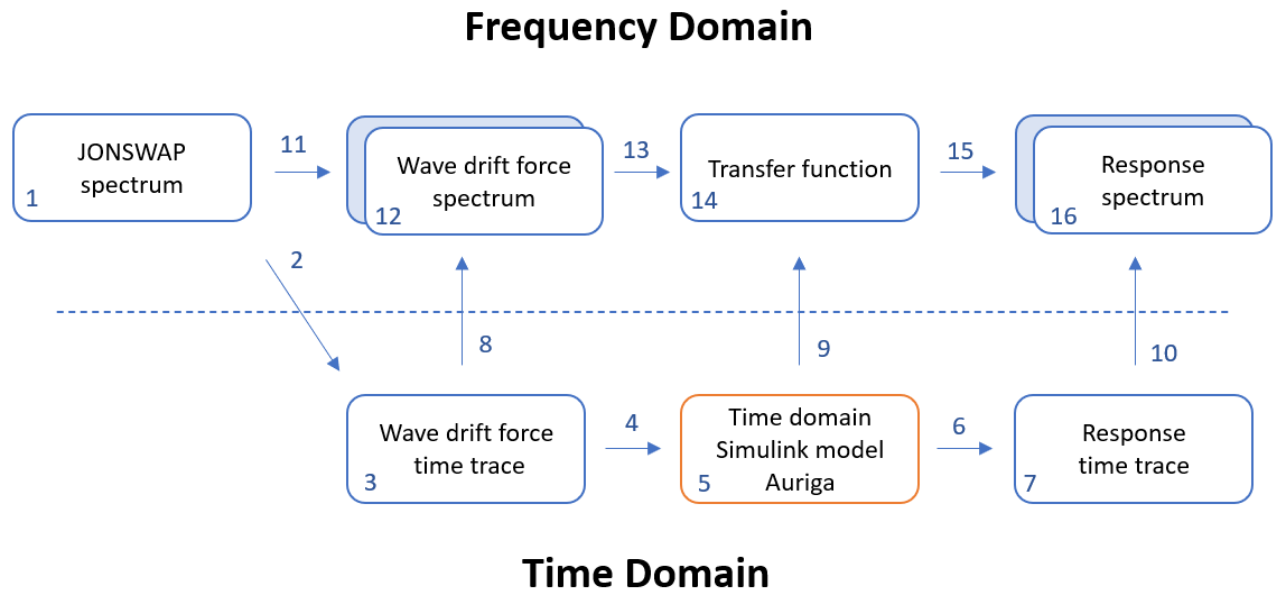
Figure 6.1: Global overview of approach, information stream and models used

1. A JONSWAP spectrum is generated with corresponding H_s and T_p from each sea-state selected in Section 2.4, through Equation 2.8.

2. The QTF's ($d\mu$=0.025 rad/s) as obtained from MARIN's DIFFRAC software are interpolated to a difference frequency ($d\mu$) of 0.001 rad/s, this creates accuracy in the lower frequency range. Random frequencies and phases ensure a time signal that does not repeat itself. Amplitudes are determined through relation 2.6.

3. A time signal of the wave drift force is generated from the JONSWAP spectrum and interpolated QTF diagonals, amplitudes, difference frequencies and phases. See Equation 2.21, specifically the low frequent part.

4. Low frequency wave drift forces are used as input for the MATLAB/Simulink time domain model of the Acta Auriga.

5. The time domain model simulates how the vessel reacts to forces acting on it via the time signals. Non-linearities can be enabled/disabled in this model to study the effects it has on the vessel's capability to maintain position.

6. All data regarding the performance of the vessel is stored and can be accessed. Commands from the vessel's DP controller are stored and compared to actual performance.

7. The motion response time trace is the most important output of the time domain model. This provides insight in how well the vessel is able to maintain position around a certain set-point.

8. Wave drift force time trace is transformed to the density spectrum of the low frequent wave drift force.

9. Time domain model is linearized using two methods that include a build-in Simulink function and the MATLAB function 'tfestimate'. This function captures a non-linear system in a transfer function. The TFs can be from and to any selected parameter, in this case from wave drift force (kN) to displacement/rotation from the set-point (m or rad).

10. The motion response time trace is transformed to a displacement density spectrum. (See 8)

11. From the JONSWAP spectrum a low frequent wave drift force spectrum is calculated through Equation 2.24.

12. The wave drift force spectrum obtained from the time domain realisation and the spectral representation are compared and should correspond. A 100% match is not feasible, as an infinite long time trace should be generated for this.

13. The wave drift force spectrum is multiplied by the square of the absolute TF. The TF is the representation of the DP system in the frequency domain

14. A transfer function is derived for every degree of freedom based on the time domain model output.

15. The FD model results in a motion response spectrum for every degree of freedom.

16. The response spectra derived from the time domain model are compared to those as calculated based on the FD model. A 100% match is not expected, because the input spectra have slight differences and non-linear behavior is not captured when using a linearized FD DP model

6.2. Test approach

This research aims to gain insight in the effect of NLCs in a DP system and to investigate the possibility of predicting the DP offset based on a linearized DP model in the frequency domain. Each non-linear component has been discussed in depth in Chapter 5. The different test approaches will be explained in this section including the goal of each test.

In order to fully comprehend the effect of each NLC, each component needs to be tested individually. This prevents results being influenced by other NLCs. A general model is developed that includes each NLC with the possibility to enable/disable each component by activating a switch in Simulink, creating model variations. Ensuring changes to the model are applied to each NLC. The transfer functions obtained from each model variation are compared. A control

test is implemented, from now on referred to as the benchmark model, to which the effects of implementing a NLC can be compared. A variation of the model with all NLCs engaged will be compared to the benchmark model. This model is the most realistic to the actual SOV. Furthermore, the possibility of NLCs interacting is of interest and will be investigated during the research. An overview of each model is presented in the list below, title representing the NLC that is tested and compared to the benchmark.

1. Benchmark

2. Forbidden zones

3. Ramp up

4. Turning rate

5. All NLCs

Each model is loaded by the exact same conditions, specifically the three different sea-states as discussed in Section 2.4 in seven directions: 0, 15, 45, 90, 136, 165 and 180°wave heading. A single seed for each combination is taken to prevent interference in results caused by different time traces.

TFs obtained from each variation of the model are compared to the benchmark TFs. Furthermore, the TFs from each model variation can be compared across different environmental directions, this is to test if the TFs are direction depended. It is expected that this is not the case as each DOF has a unique TF. Compare this to a mass-spring system, the spring does not determine the excitation, the force with which the spring is loaded does this. Same goes for a vessel, which can arguably be simplified to a mass-spring system [8] [23]. The force spectra differentiates for each direction as the QTFs differentiate over direction, causing a unique response of the vessel for each direction. However, it is unclear to what extent a NLC like a forbidden zone influences TFs in the forbidden zone direction. The FBZ can cause the 'stiffness' to decrease as certain thrusters are not allowed to deliver thrust in this direction.

By comparing TFs across sea-states it helps to understand for which conditions the model is valid. Again it is expected that the TF will not be influenced by this as predominantly the magnitude of the loads change. However the effect of change in the T_p on the TF is to be investigated.

Besides testing the aforementioned effects, tests will also be conducted to see what the effect of simulation time is on transfer functions. The effect of changing the operation point will be tested. This effect was first noted by De Wet [23]. The TFs are affected by the time at which the actual linearization takes place in the simulation.

6.3. Model verification

The results obtained from the simulations described in Section 6.1 and 6.2 are only of scientific value if the model captures what it intends to represent. The model can only be expected to perform as it is intended if the input and intermediate steps calculated or implemented correctly. This is known as verification, determining whether the math behind a model are implemented correctly. This section will discuss how the verification of components of the model in this research is done. Reference to other sections will be made were results are presented [20] [22].

6.3.1. Input - Wave drift forces

The input for the time domain model is a time trace of second-order wave drift forces. This time trace has been calculated based on a JONSWAP spectrum, see Section 2.2.1. By comparing the mean wave drift force calculated in the TD and the FD the mathematical implementation can be verified, as the frequency domain calculation is based on a different method. Table 6.1 provides an example of the error found between the time domain and frequency domain approach. A full overview of each time trace use in this research is provided in Appendix E.

	Surge [kN]	Sway [kN]	Yaw [kNm]
TD	5.1049	2.80E-06	5.20E-04
FD	5.0345	2.86E-06	-5.07E-04
ϵ	1%	2%	2%

Table 6.1: Mean wave drift force error TD and FD calculation - 0°stern waves, low sea-state

6.3.2. Non-linear components

All non-linear components that are discussed in Chapter 5 have been verified using the same method. A time domain simulation is run two times, once with the non-linear components disabled and once enabled. The specific test for each NLC is discussed in the respective sections of Chapter 5. For thruster orientation, verified based on vessel data from the Acta Auriga during DP operation. The lag between thruster orientation commanded and delivered is provided in Appendix E.1 for the different types of azimuths aboard Acta Auriga.

6.3.3. Thruster allocation

The verification of the thruster allocation algorithm, solved using a quadratic programming method, and the solver used have been discussed at length in Section 4.3.2.

6.3.4. Frequency domain model

The Frequency Domain model as described in Section 6.1 is verified in two steps. First a wave drift force spectrum is created from the time trace of the wave drift force. Simultaneously the spectrum is calculated by using the frequency domain method (See Chapter 2.3.2). Both spectra are compared and should in theory match completely, this is not likely as a infinite long time trace would be required. However both spectra should match very closely. A similar approach is used to verify the response spectrum. One spectrum is obtained through the FD model, this is then compared to that derived from the response time trace calculated with he TD model. If both comparisons match it implies that the transfer function, generated by linearization of the TD model, is correct. An example for one simulation is provided in Appendix E.2, belonging to the Benchmark model in a low sea-state loaded by 165°head waves.

7

Results

In this chapter the results from the experiments discussed in Chapter 6 are presented and discussed. Furthermore the different methods of linearization and spectral calculations are discussed, providing advantages and disadvantages of each method.

7.1. Time domain analysis

The most straightforward method of comparing the effects of non-linear components on to DP systems, is to compare the effects on the DP offset in time domain. The standard deviation of the displacement signal is a good indication weather the introduction of a non-linear component to the model has any effect on the DP offset. This is because the entire signal is captured in one single value. Standard deviation is the measure of the dispersion of set of values, where a low standard deviation indicates a narrow spread around a certain mean. A high standard deviation is an indication for a more dispersed signal. The absolute value of the standard deviation found at each experiment is a measure of how well the vessel is able maintain position during certain environmental conditions. However, for this research the relative change in standard deviation to the different models under the same environmental condition is more of interest. A different standard deviation suggests the model is affected by the introduction of a certain non-linear component. Figure 7.1 shows an overview of the standard deviation of the different simulations sorted per sea-state and environmental loading direction.
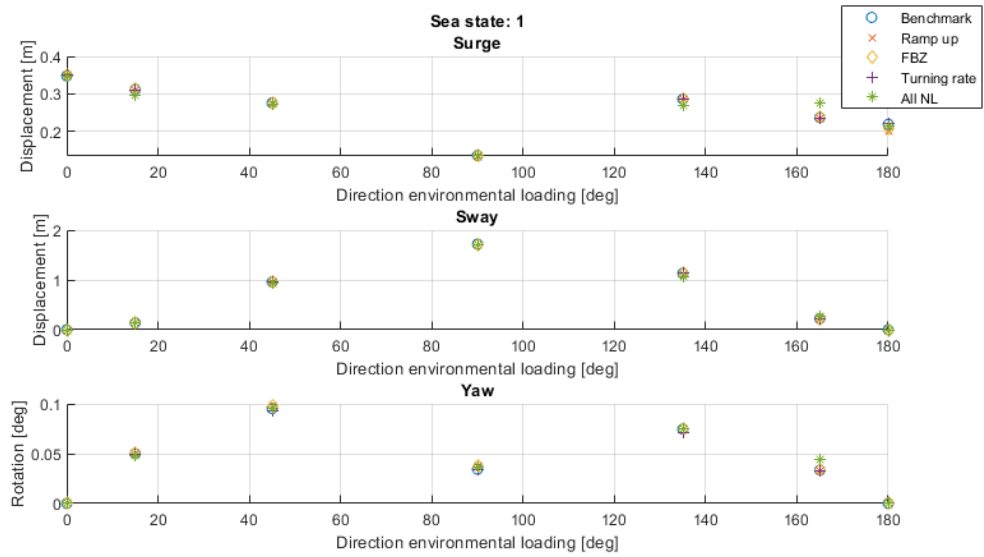
(a) Sea-state low
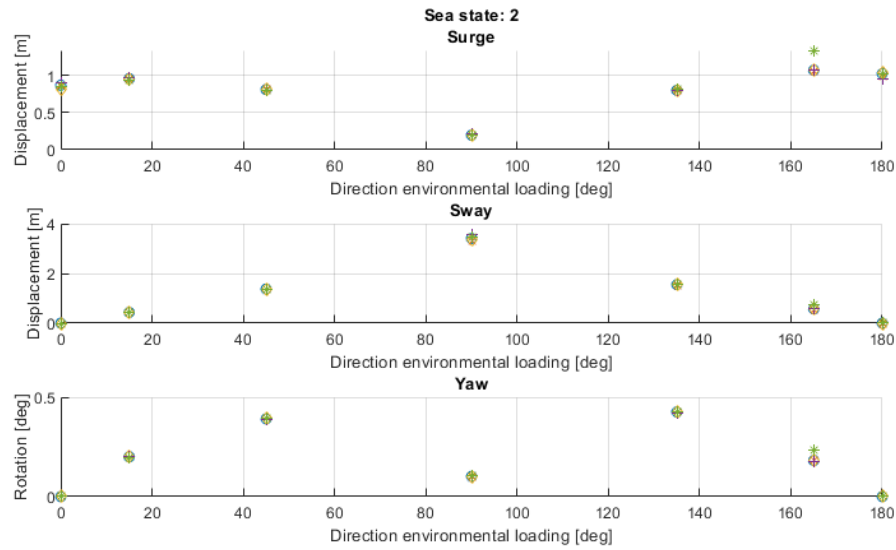
(b) Sea-state medium
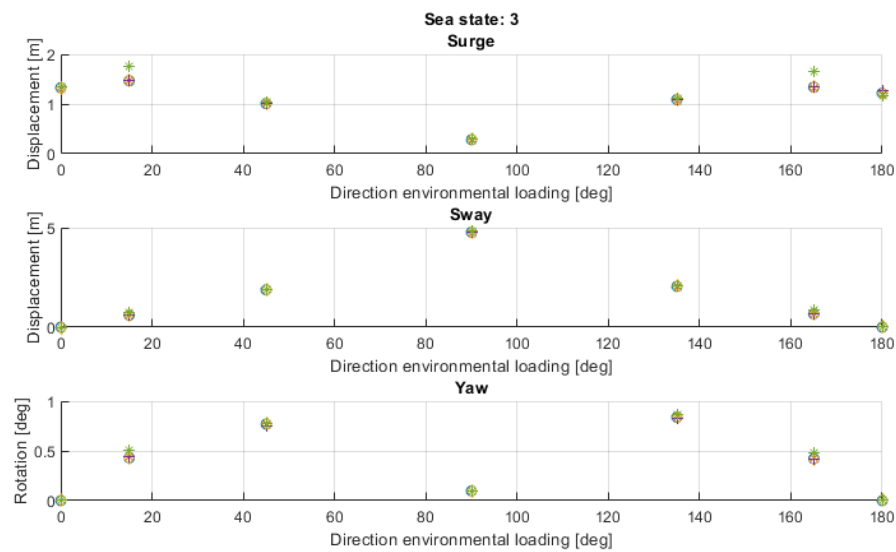
(c) Sea-state high

Figure 7.1: Standard deviation of displacement from the setpoint per model, per direction and per sea-state

In the time domain model, the simulations that have been done with the exact same input can only be compared to each other. Each model can only be compared to different non-linear models loaded by the same sea-state and environmental direction. Any directional or sea-state dependence can not be found through this analyses. Figure 7.1 provide an overview of all simulations used in this research through a scatter diagram. By scanning through this overview some clear conclusions can be drawn. First of all, the displacement from the setpoint *eta* does not seem to be affected much by any of the implemented non-linear components, based on the standard deviations of each of the time traces. However, for the simulations 15°and 165°, the difference of the standard deviation of the model that contains all non-linear components to that of the other models, suggests that a combination of the different non-linear components does affect the vessel offset. That this effect is only noticeable at the mentioned directions, does not mean this effect only occurs at these directions. It could be possible that resonance occurs at these directions and the effect is more distinct. The results will be analysed more in depth.
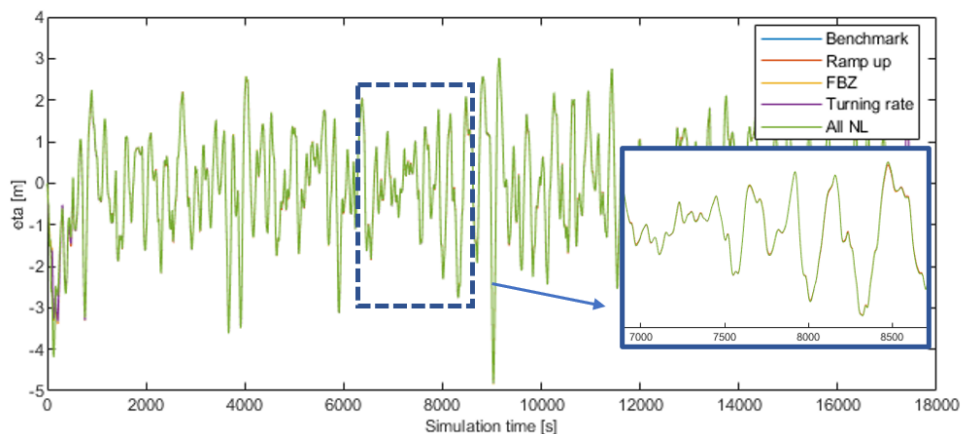

Figure 7.2: Sway displacement of vessel loaded from 135°by high sea-state
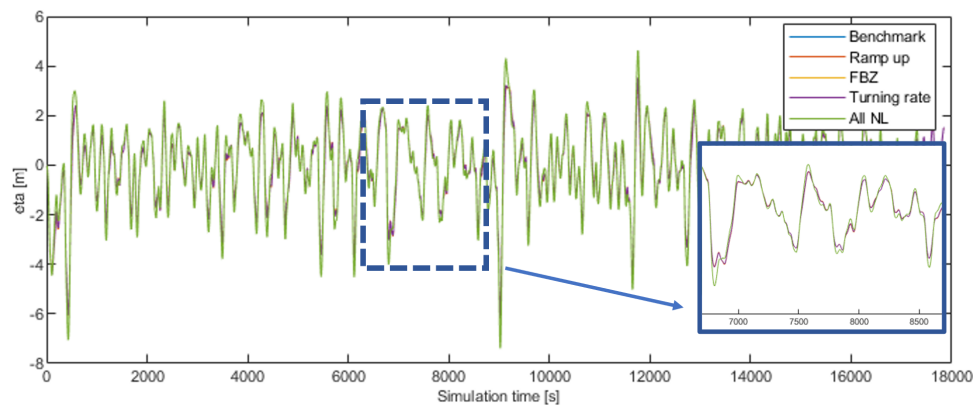
Figure 7.3: Surge displacement of vessel loaded from 165°by high sea-state

Figures 7.2 and 7.3 show the time signals of each model for the same simulation. These can be used to check whether the conclusions made from the standard deviation graphs are correct. Figure 7.2 provides the sway offset from the 135°loading case. According to Figure 7.1 the time traces should be almost equal. An enlarged segment shows the behaviour of the model is hardly affected by the introduction of a non-linear component, a combination off all NLCs does not result in a significant deviation between the signals. Figure 7.3 shows similar behaviour except for the model that includes all NLCs. The standard deviation of this model is slightly off, this is in correspondence with the behaviour that can be seen through out the time signal and more clearly in the enlarged segment. The green signal, corresponding to the all NLCs combined model, displays larger offsets in the peaks. In this case the offset in surge direction is displayed. It is not possible to assign this effect to that of a single NLC, as the models that are only introduced to a single NLC display very similar behaviour. This would suggest that the different NLCs have an affect on each other. Note that for any calculation the first 4000 seconds of each time trace have been discarded, this is to discard any transient behaviour that occurs during the start-up phase of the Simulink simulations.
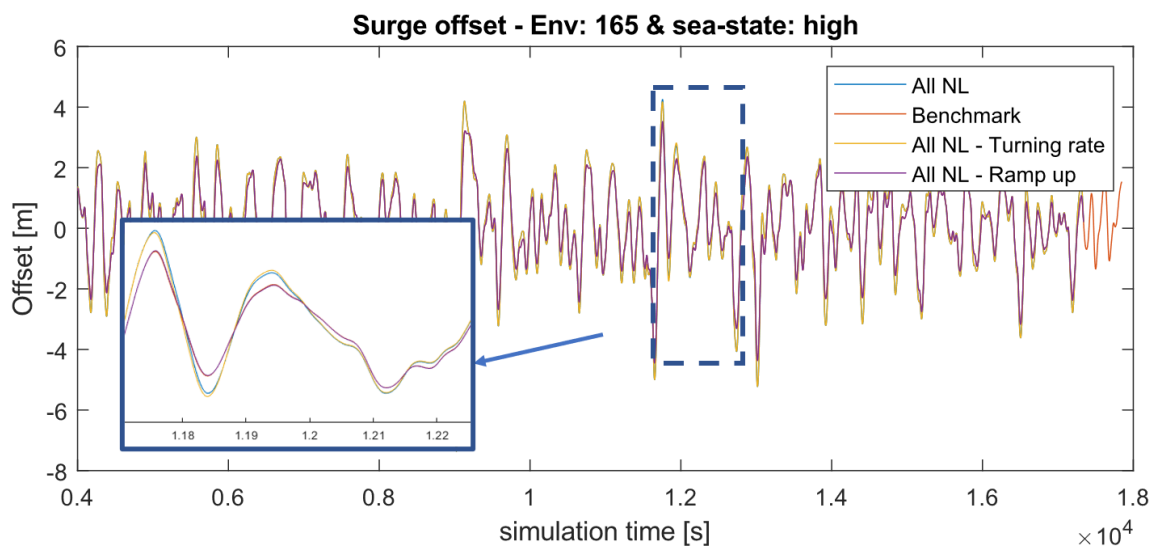
Figure 7.4: Surge displacement variations for all non-linear models minus thruster ramp-up or turning rate

In order to find out if the larger offsets are predominantly caused by one NLC or by the combination of NLCs, the following model variations are simulated. All NLCs but one are engaged. The results are provided in Figure 7.4. Because the FBZs are not in this direction only the thruster ramp-up and turning-rate needed to be tested. The simulation with all NLCs engaged serves as comparison in this case. It is evident that thruster ramp-up is the non-linearity that has the biggest effect. The simulation with all NLC engaged and ramp-up disengaged is almost identical to the benchmark simulation. Whereas the simulation with turning rate disengaged displays the same behaviour as the model containing all NLCs. From this the conclusion can be drawn that thruster ramp-up the dominant NLC causing this behaviour. However, the ef-

fect is only found in combination with the other NLCs.

A variety of analysis have been conducted in order to better understand how this effect originates, without conclusive results. The relation between the standard deviation of the vessel speed and environmental loading directions has been investigated. Where no clear relation has been found. A high standard deviation of the vessel velocity at 15 °and 165°could explain the large offsets. This would mean the DP controller is constantly varying the commanded rpm, causing the thruster to constantly ramp up or down and not being able to match commanded and provided rpm. However, this is not the case, as higher standard deviations are found for directions other then 15°and 165°. Furthermore, the standard deviation is expected to become greater for higher sea-states for the same hypothesis. This is not the case. Because the effect is found at all tested sea-states, does not increase for an increasing sea-sate and is only found at 15°and 165°, it is suspected that it might be caused by a control system anomaly that occurs only at specific model settings. In order to verify this presumption and rule out other causes, further research is necessary.

7.2. Frequency domain analysis

Now that the effect of introducing non-linearities to a time domain DP model is known, it is essential to determine the effect it has on the frequency domain model. This section will also include different methods of determining the transfer function necessary for FD model.

7.2.1. Second-order Wave drift force

In order to determine the performance of the frequency domain model, the input into the time domain and frequency domain model must be similar. A wave drift force spectrum has been calculated directly from the JONSWAP spectrum, see Section 2.2.2. The time traces, one for each DOF, used in the TD model are transformed using the MATLAB function dat2spec from the WAFO toolbox [21], based on Fast Fourier Transformation (FFT).
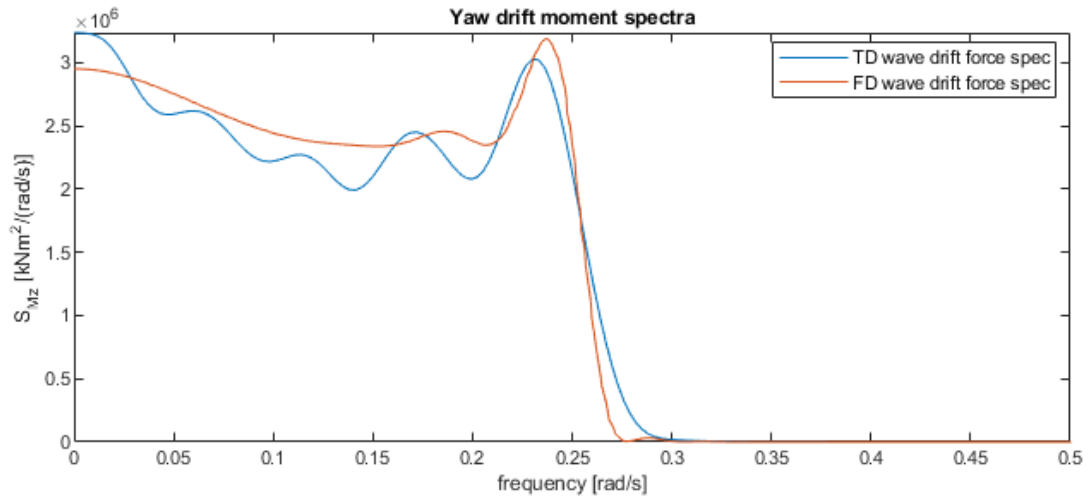
Figure 7.5: Comparison wave drift force TD and FD spectra, high sea-state from 135°

Figure 7.5 shows the difference between the spectra obtained through a spectral calculation, explained in Section 2.2.2, and a spectrum derived from the time trace used in the TD model. It can be seen that a close relation is achieved. However, a perfect fit is not realized. This is to be expected as a infinite long time signal should be used to achieve this. Furthermore, it is worth mentioning that the TD spectra are not used for any further calculations. This comparison only serves as a check. The TD spectra should approach the FD spectra. The FD spectra will be used for further calculations, as this is a spectral calculation it can be assumed to be correct.

In order to quantify the differences between the spectra from both the time and frequency domain model, the m_0 is calculated. This statistical value is also known as the area under the spectrum. m_0 is also an indication for the variance of the spectra, through the following relation:

$$var = \sigma^2 = m_0 \tag{7.1}$$

An example of the overview for the entire wave drift force data base is given in Table 7.1. Appendix F includes the entire database overview.

	Surge [kN]	Sway [kN]	Yaw [kNm]
TD	227.84	1881.00	647140.52
FD	234.81	1897.11	670291.89
ϵ	3%	1%	3%

Table 7.1: m_0 wave drift force error TD and FD calculation - 135°bow waves, high sea-state

7.2.2. Transfer function calculation

The transfer functions needed for the FD model can be calculated through different methods. In this research two methods are used and compared. The first method is based on a linearization function build into Simulink. The second method is the MATLAB function *tf estimate*, this function uses an input and output time signal and determines a TF between those parameters.

Simulink linearization

By setting an operating point at an arbitrary time within the simulation time, Simulink performs a linearization of the entire model at this point in time. The input and output parameters can be selected anywhere within the Simulink model, this means a TF can be derived between any two parameters. The downside to this method is that the TF is only valid for a small period before and after the set operating point. No specifics is given in the documentation of this function as to how large this period is.
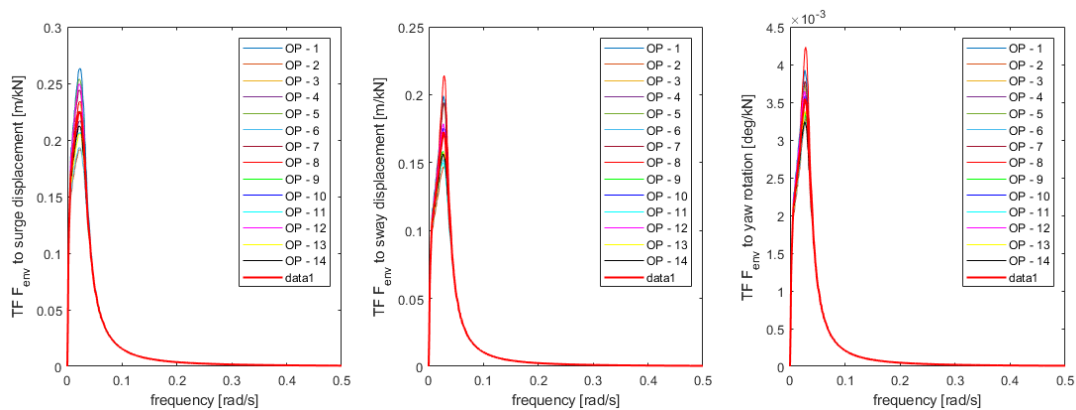
Figure 7.6: Effect of selecting different operating points for one simulation

Figure 7.6 shows the effect of selecting a range of operating points for the same simulation. large variations are visible, specifically in the peak of the TF, a difference between up to 25% is present between the largest and smallest TF. This will lead to a large variation the peaks of the offsets. The solution is also present in Figure 7.6, in the form of a mean TF. The downfall to this method is that a large amount of simulations needs to be run before a mean transfer function can be determined. The upside to this method is that the approach is very straightforward and little to non tweaking of the linearization method is possible, preventing faulty TFs due to misuse of function.

MATLAB function

The MATLAB function tfestimate does take into account the entire time signal from the input and output, respectively the wave drift force time traces and offset time traces. By including the entire time signals, no information is lost at this step of determining the transfer function.

Different to method 1, is that this method allows for derivation of a transfer function between any variable in the Simulink/MATLAB model. The TF is determined after the simulation and allows for pre-processing of any signal before being used to determine the TF.

A downside to this method is that the use of this function is highly complex and requires specific knowledge regarding signal analysis. Furthermore the function can be tweaked in a variety of different ways, some of which are very sensitive. It is difficult to determine whether good settings have been selected. First of all a window setting can be selected, this divides both signals into segments and performs windowing. The amount of overlap between each segment can also be selected. Furthermore the sampling frequency has to be selected corresponding with both time signals. As the Simulink model uses a variable time-step, the input (wave drift force time trace) and output (DP offset time trace) signal have different time steps. The input signals has a constant time step set to $1\ s$, where the output signal has a variable time step. Therefore, pre-processing of the signals is necessary. Both signals need to have a equidistant time-step and in order to increase accuracy both signals are interpolated to $0.05s$. Finally, a amount of frequencies returned is selected. The following settings are used in the research:

Setting	value	unit
Window	hann(60000)	[-]
Noverlap	no overlap	[-]
f	495200	[-]
fs	20	Hz

Table 7.2: Settings for MATLAB function tfestimate

7.2.3. Transfer function comparison

By comparing transfer functions of different models, sea-states and directions, insight is created into the effect non-linear components have on the transfer function calculations. The findings from this paragraph can be compared to those of the time domain analysis. In order to simplify the analysis and drastically decrease simulation time, TFs are generated at a single operating point. Even though the found TF is not representative for an entire simulation, it does provide insight in the effect of non-linear components on TFs. The high sea-state transfer functions will be provided in this report, the effects are expected to be most visible in the high sea-state simulations.
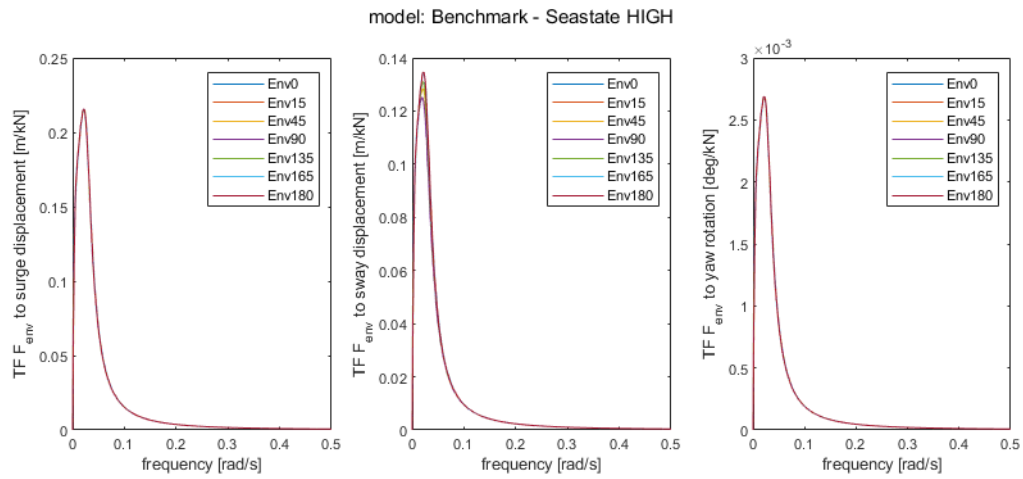
Figure 7.7: TF method 1: Benchmark loaded by high sea-state

Figure 7.7 represents the TFs of the most basic model (Benchmark) used in this research for different environmental directions. It can be clearly seen that the TFs are not effected by different environmental directions. This is as expected, since the environmental direction will have an effect on the input wave force spectrum, the TF should remain unchanged. Furthermore, the results from the Benchmark simulations are in line with the results obtained from the time domain simulations.
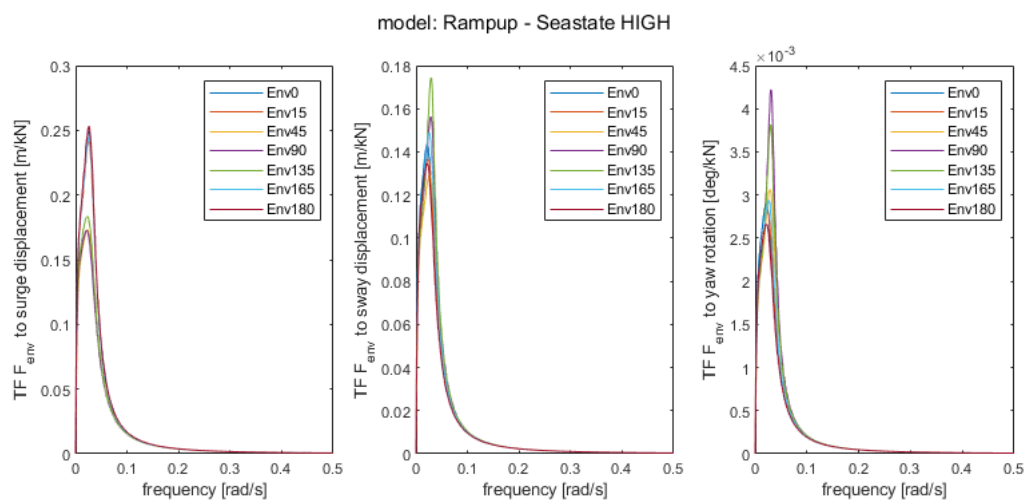
Figure 7.8: TF method 1: Thruster ramp up loaded by high sea-state
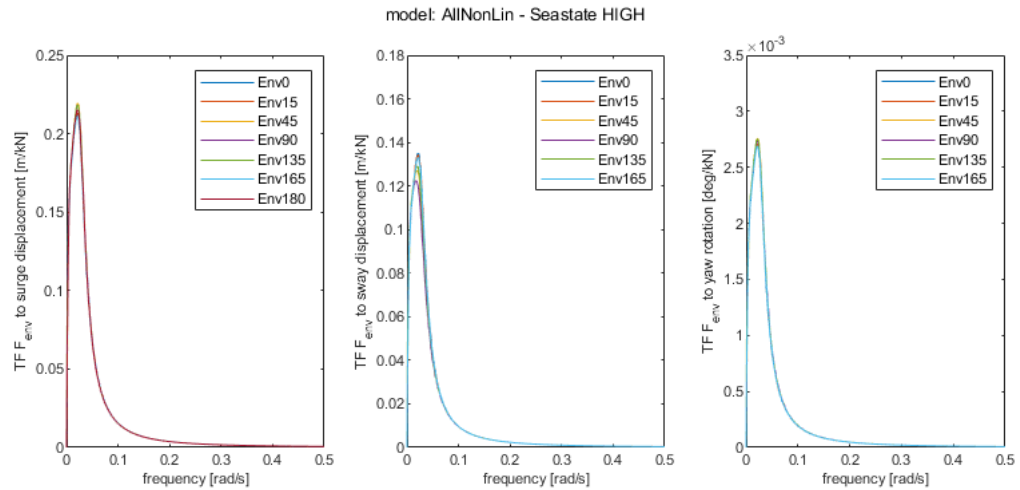
Figure 7.9: TF method 1: All NLC loaded by high sea-state

Figure 7.8 suggests that the hypothesis stated in this section is not valid, as the transfer functions from the model that includes thruster ramp-up are clearly affected by different environmental directions. Thus suggesting the introduced NLC has an unexpected effect on the TFs that does not match with the time domain results. Furthermore, this effect is not found when analysing the results from the model that includes all NLCs, see Figure 7.9. The TFs found through the first method are not effected by the direction of the load. Figure 7.10 includes the TFs from the benchmark and most complex model. The TFs are not effected by either direction or the presence of non-linear components.
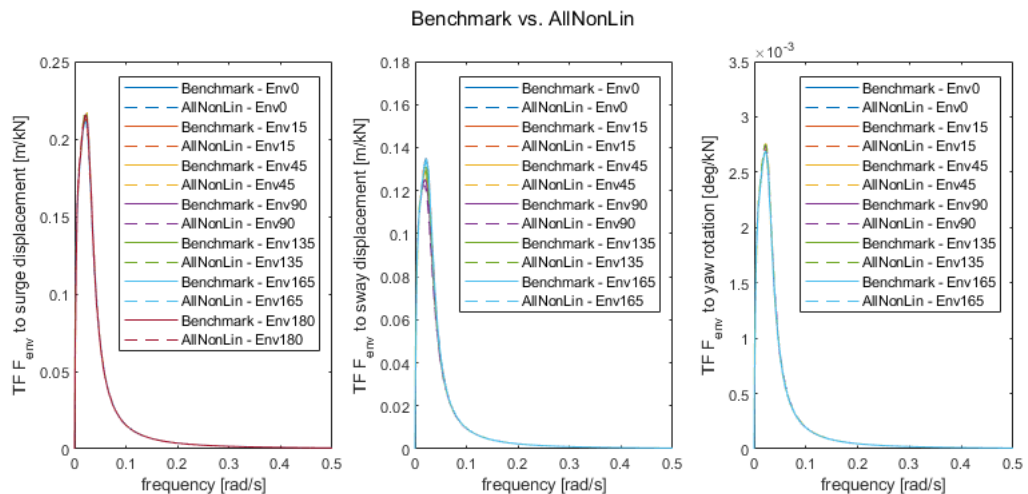
Figure 7.10: TF method 1: Benchmark vs All NLC loaded by high sea-state

Besides direction, the sea-state or the magnitude of the load on the vessel could have an effect on the transfer functions. Similar to the hypothesis of independence of direction, the magnitude should have no effect. The offset spectrum should increase as an effect of extra energy present in the wave drift force spectrum and not because of an increase of the transfer func-

tion, since the system characteristics are unchanged. In order to verify this hypothesis transfer functions of three models are compared in Figures 7.11, 7.12 and 7.13. For each model the TFs found for every direction and sea-state are plotted on top of each other. Note that for sway and yaw the 0°and 180°TFs have been removed from the data sets. Because the vessel is not loaded by any force/moment in these simulations, input spectra are nearly zero. Simulink has difficulty dealing with this problem and gives a random arbitrary transfer function. The spectrum found, in this case does not matter as it is multiplied by zero.
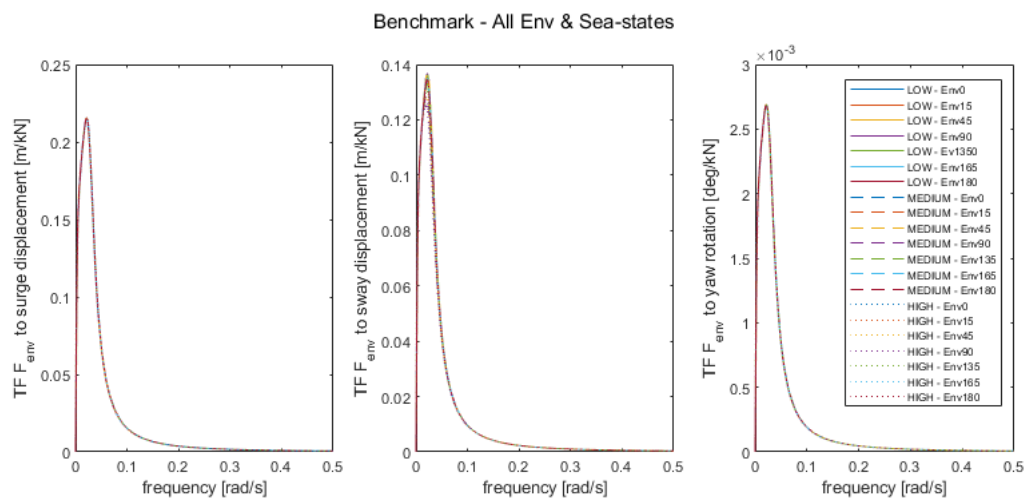
Figure 7.11: TF method 1: Benchmark - loaded from all direction and by all sea-states
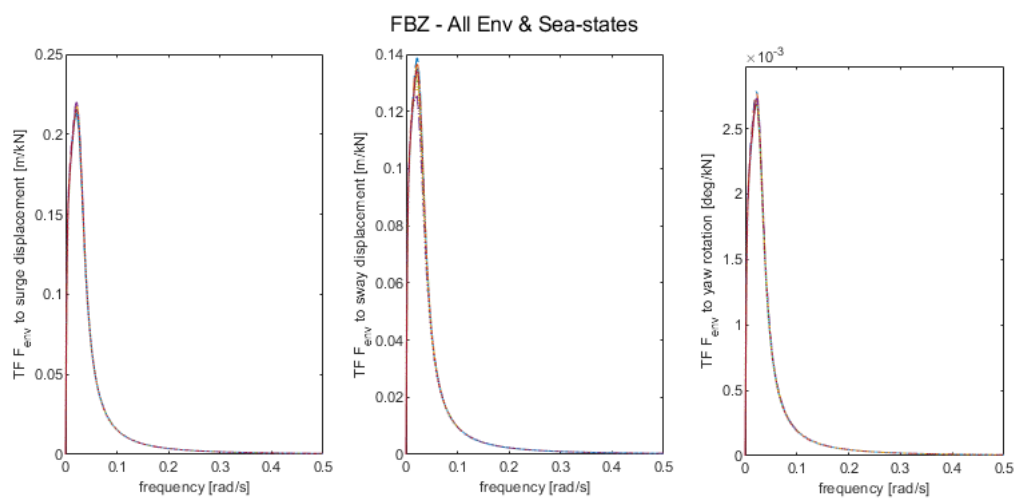
Figure 7.12: TF method 1: Forbidden zones - loaded from all direction and by all sea-states
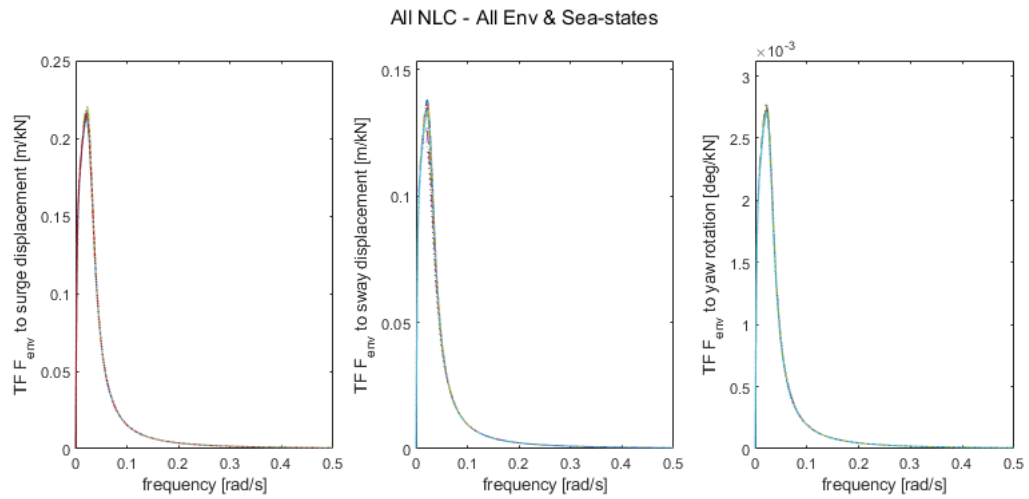
Figure 7.13: TF method 1: All NLC - loaded from all direction and by all sea-states

Now that the introduction on NLCs or variation in load cases and direction do not seem to effect the derived transfer functions, specifically not for TFs that are the result of a single operating point. A comparison of the transfer functions obtained through the second method can be made. It will be interesting to see whether TFs representative for an entire simulation are also not affected by NLCs, direction or force magnitude. Figure 7.14, 7.15 and 7.16 show the transfer functions for the different models, each for a different environmental direction, at a high sea-state.
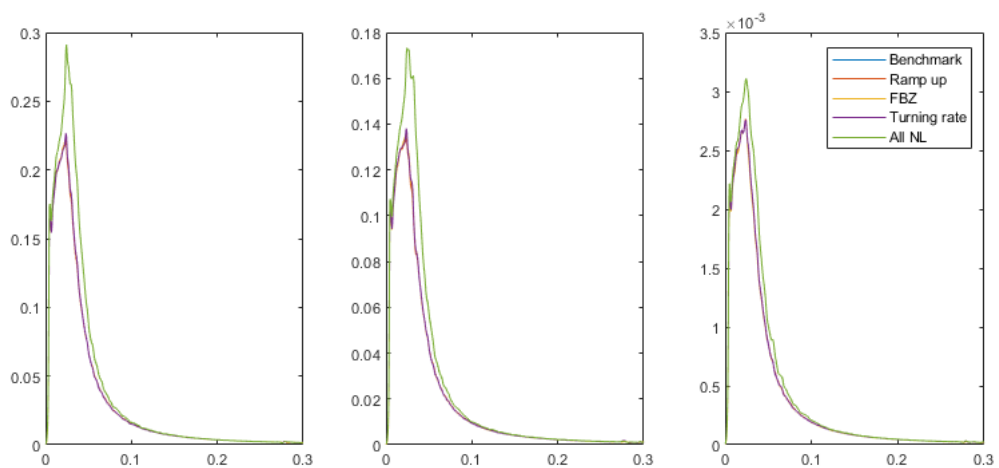
Figure 7.14: TF method 2: All models loaded from 15°
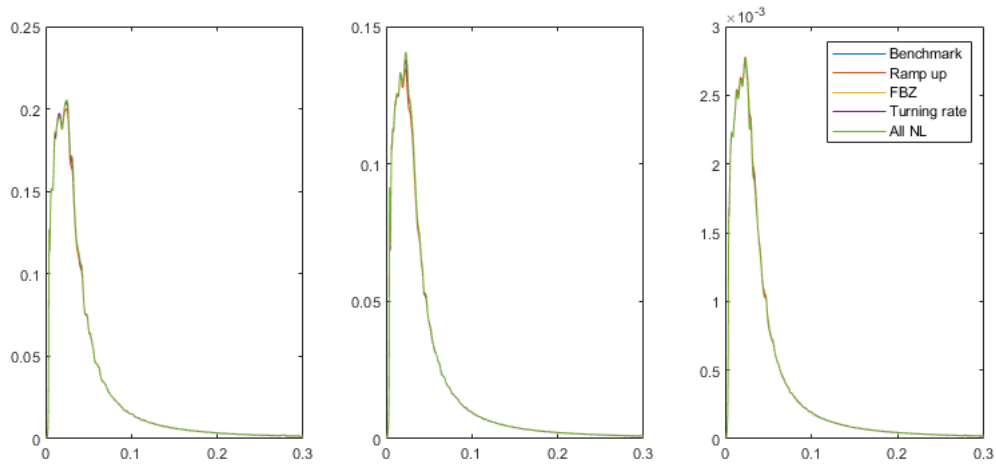
Figure 7.15: TF method 2: All models loaded from 135°
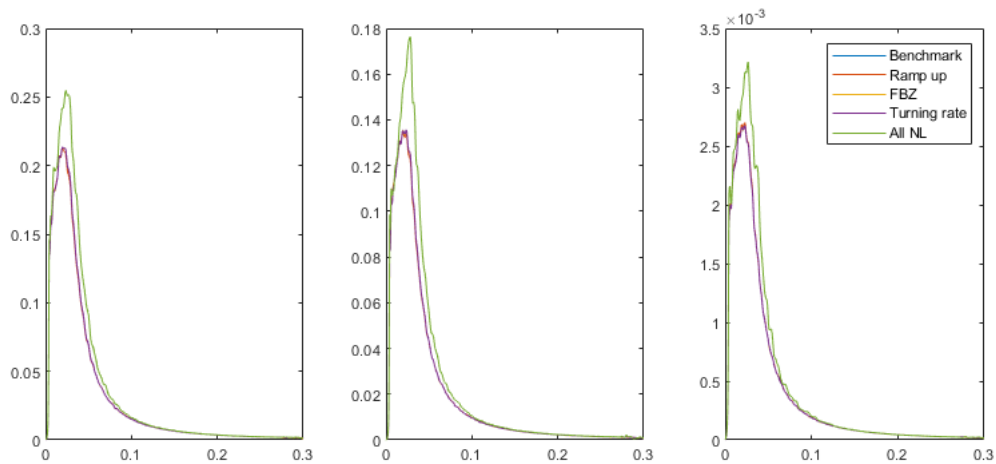
Figure 7.16: TF method 2: All models loaded from 165°

Interesting is to see that again the introduction of the different NLCs hardly have an effect on the transfer functions. However, for the model that includes all NLCs and is loaded from either 15°or 165°the TF is different from the rest. If this is compared to the results from Figure 7.1, a clear agreement is found. The most complex model has a higher standard deviation when loaded from the same directions. Although mostly visible in the surge direction, it was not determined that the effect does not occur in the other DOFs. Furthermore, these environmental directions predominantly excite the vessel in surge direction. Thus a larger standard deviation in this DOF is expected. All other directions have similar results to that of 135°simulation.

7.3. Response

The vessel response is the most important comparison that needs to be made. This will determine whether the frequency domain approach using the found transfer functions is representative, it will also determine which TF method best describes the behaviour of the vessel. A comparison of the results is made in the FD and the TD. The FD comparison is straightforward, where spectra derived from time domain can be compared to spectra found with both methods of deriving TFs.

By transforming the response spectra found in the frequency domain to a time trace it can be compared to the time trace obtained from the Simulink model. The time signal obtained from a FD spectrum is a stochastic process, therefore, the time signal will never be equal to that obtained from the time domain model. The time signal is calculated through Equation 7.2. The force amplitudes are found through Equation 2.6. A visual check can be performed on both signals, which will determine if the general shape is similar. However, a footprint of the time signal is needed in order to make a real comparison. In this research, the footprint will come in the form of the distributed displacement. The footprint is a representation of the expected offsets away from the setpoint experienced by the vessel in a set time frame. From the footprint the probability of occurrence of a DP offset can be derived, which is equal to the area of the corresponding bin (see Figure 7.19).

$$F(t) = \sum_{i=1}^{N} a_i \cdot cos(\omega_i t + \epsilon_i) \tag{7.2}$$

where

$F(t)$ = Wave drift force time trace [kN]

a_i = force amplitude [kN]

ω_i = difference frequency [rad/s]

ϵ = random phase shift [rad/s]

Analysing each individual simulation is not efficient and for sake of clarity, a pre-selection is made based upon m_0 of the response spectra. A benchmark simulation is first selected and analysed, so findings can be compared to this case. Appendix F.1 & F.2 contain m_0 values of the response spectra for the Benchmark model, each direction and spectra made with both TF methods. Furthermore the difference compared to the TD response spectra for each method is given. Based on these difference, a selection is made on which simulations will be discussed in this section. The least performing simulation is selected. This is the simulation at a high sea-state and loaded from 15°. Appendix F.4 & F.5 contain the area under the spectra for the model containing all non-linear components. From which a simulation will be selected that

has a high performance and one that performs low, based on the aforementioned criteria.
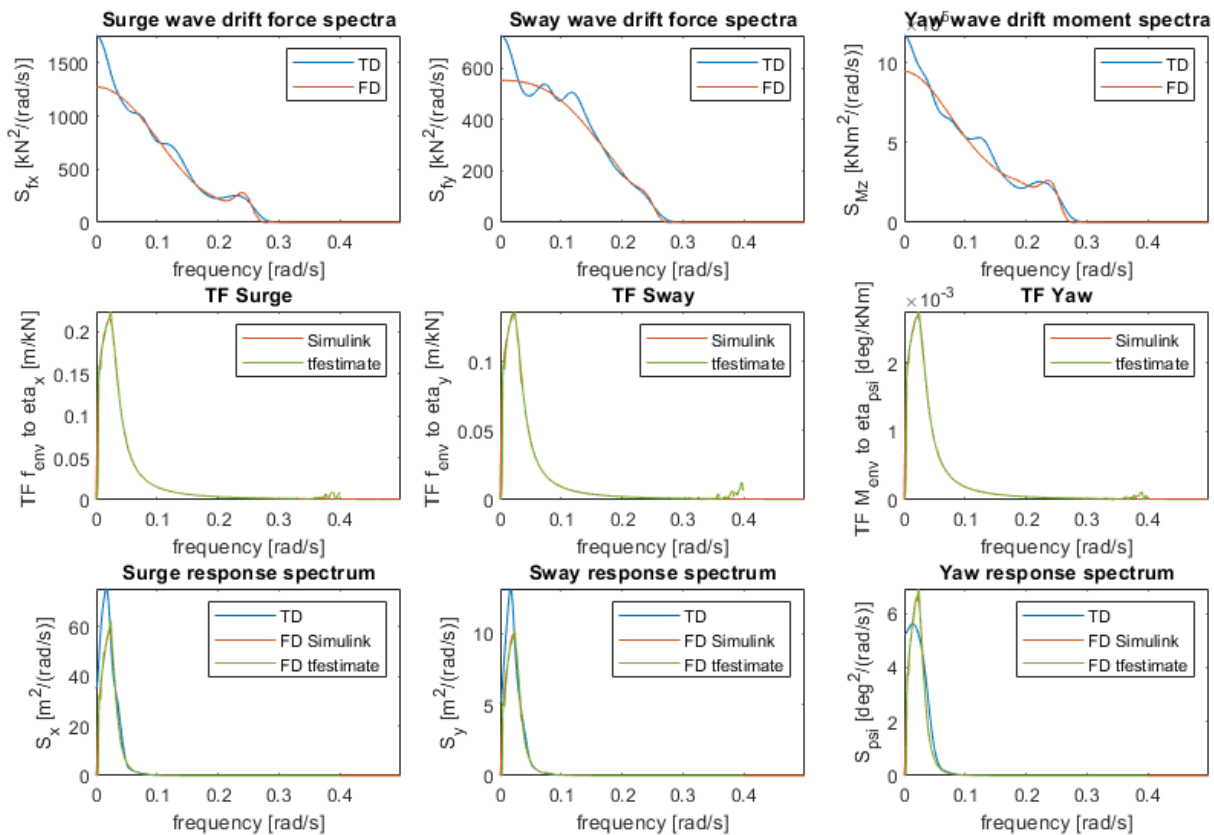
Figure 7.17: FD Benchmark model overview, including input spectra, TFs (both methods) and output spectra - Benchmark, loaded from 15°by high sea-state

Figure 7.17 is an visual overview of the different input spectra, transfer functions and output spectra. The blue spectra representing the spectra found with the *dat2spec.m* function are based on the TD model. The orange input spectrum is made using a spectral calculation, the TF is created using the Simulink method. The response spectrum is the results of Equation 2.28. The green response spectrum is determined using the same model, except with a TF created using the *tf estimate* function.

The response spectra of the FD benchmark simulation differ significantly to that of the TD simulation. For surge and sway the FD simulations are underestimated, were for yaw higher rotations are expected by the FD simulations then by the TD simulations response spectra, see Figure 7.17. This however does not mean that the frequency domain model is not working correctly. It is important to note that the found TD spectra are an representation of the time record in the frequency domain. However, during the transformation of this data information

is lost, for example phase shift. Furthermore the method of obtaining the spectrum is very sensitive, errors are easily incorporated. How well the spectra are made needs to be determined using a different analysis. For this the data is transformed back to time domain. An additional benefit from this is that the data is more easily perceived in time domain. Creating time traces from these spectra and comparing those to the original time trace from the TD model. Time domain results are presented in Figures 7.18 and 7.19.
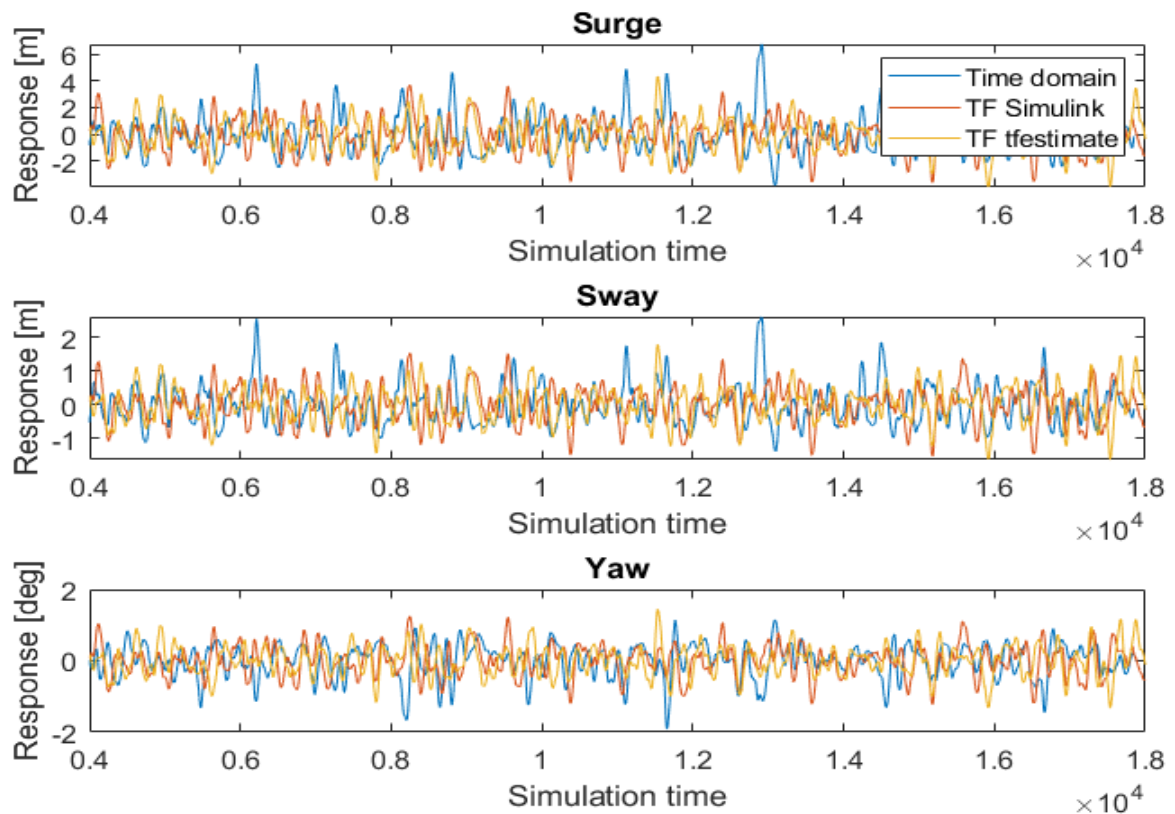
Figure 7.18: Response time trace, Benchmark, high sea-state from 15°

When analysing the results in the time domain, surge and sway display expected behaviour based on the FD analysis; The time domain simulations shows larger peaks compared to both frequency domain approaches. However, for yaw the offsets are expected to be higher for the time traces made from the FD model. The time domain results for yaw are not in agreement with the frequency domain results from Figure 7.17, as the large difference in offset is not captured.

The absence of larger peaks in both FD models compared to that of the TD model is an important finding. Larger peaks are critical for an DP operation when these offsets come close

to the operation limits. Furthermore, it can be observed that the absence of these peaks is predominantly to one direction, specifically the direction to which vessel displaced by the environmental forces acting on the vessel, see Figure 7.18. This suggest that the transfer function found for the FD model describe the DP system to be too stiff and therefore predict smaller offsets.
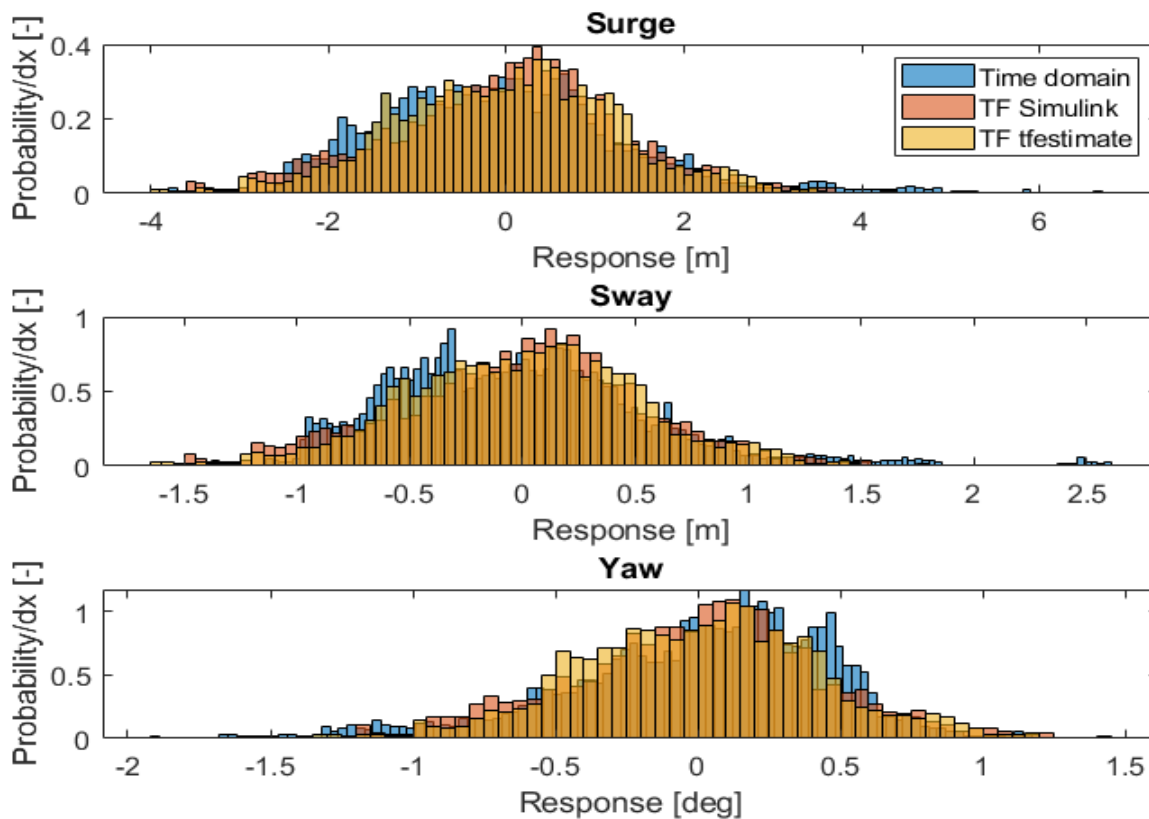
Figure 7.19: Normalized response distribution, Benchmark, high sea-state from 15°

Based on the relative differences given in Appendix F.4 & F.5, a first observation can be made. The spectra obtained with the transfer function calculated with the *tfestimate* function, has the closest match to the TD response spectra for almost all simulations. Note that some of the values found are considerably high, this would indicate that the found spectra are not similar. Keep in mind that in some simulations, no surge, sway or yaw response is present. Therefore, spectra are nearly zero. The relative difference can become very large for values that approach zero.

The first simulation, from the model containing all non-linear systems, that will be discussed in depth is; a high sea-state and loaded from 45°stern waves. Table 7.3 contains the corre-

sponding m_0 values. From this data is can be concluded that both methods of creating the TFs are performing quit well when compared to the spectra found from the TD model.

	Surge [m]	Sway [m]	Yaw [deg]
Simulink	1.09	3.46	0.58
tfestimate	1.06	3.64	0.56
Time domain	1.08	3.55	0.52
Difference TD - Simulink	1%	3%	12%
Difference TD - tfestimate	2%	3%	8%

Table 7.3: m_0 response spectra and compared to TD response spectra - Loaded from 45°by high sea-state

Results from Table 7.3 and Figure 7.20 are consistent. Notice that the response spectra for yaw rotation through both methods do not match, whereas surge and sway response show a good match.
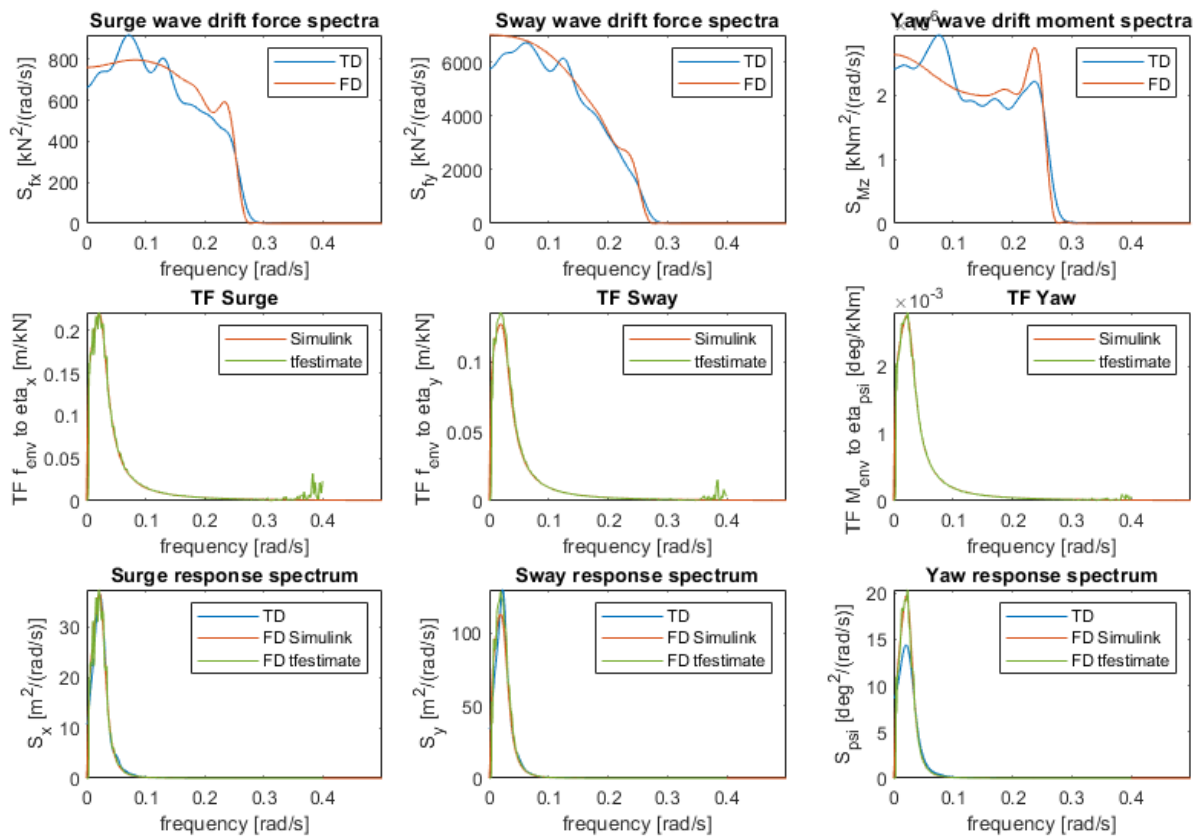
Figure 7.20: FD model overview, including input spectra, TFs and output spectra - All NLC, loaded from 45°by high sea-state

By comparing time signals created from the spectra of the FD model to signal of the TD model an understanding as to how well the model performs is created. It is expected that the time signal from the FD model shows good agreement when compared to the TD model time trace.
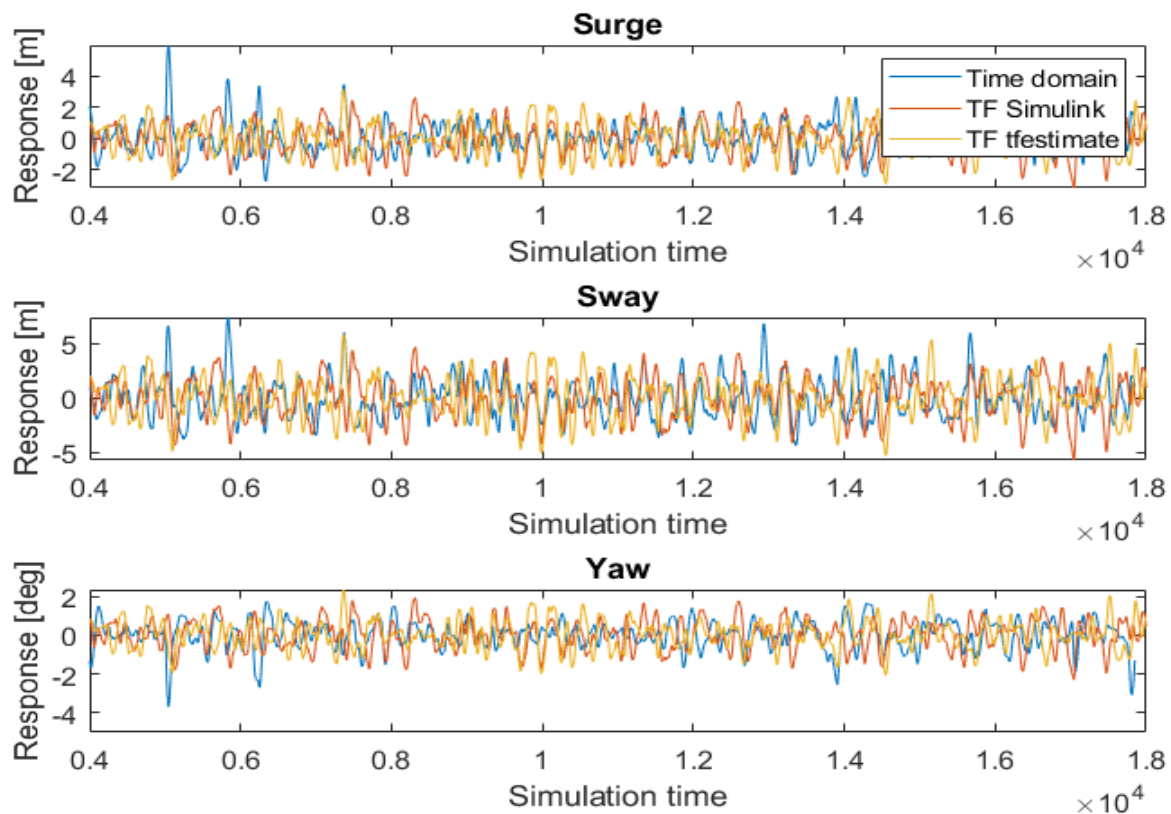
Figure 7.21: Response time trace, all NLC, high sea-state from 45°

Figure 7.21 shows that both methods perform very similar. For surge and sway the time domain signal has some larger peaks orientated in the positive direction. The yaw rotation time domain signal has slightly higher peaks in negative direction. In order to better comprehend these results the distribution of the response is plotted for each DOF and different models in Figure 7.22.
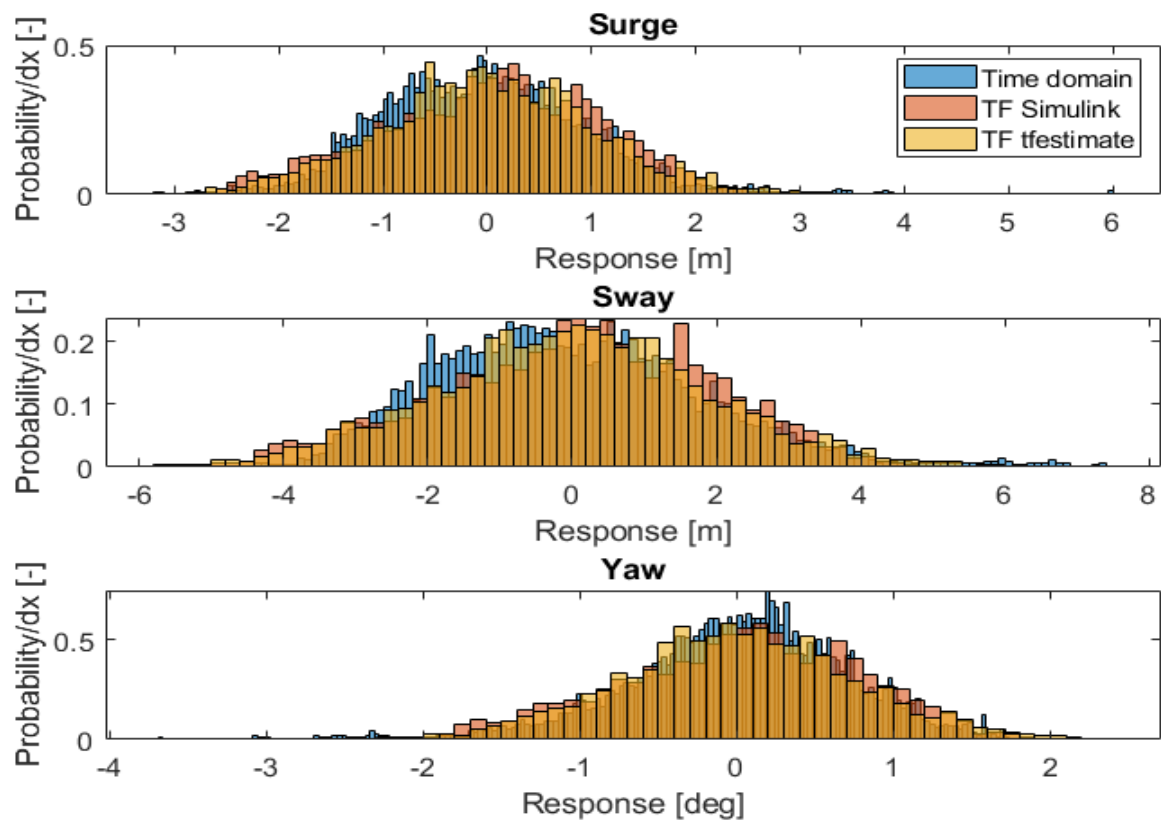
Figure 7.22: Normalized response distribution, all NLC, high sea-state from 45°

From these figures it can be observed that both methods, over all have a good fit with the time domain data. The distributions have the same shape. A point of concern rises when taking a closer look to the extreme offsets. For each DOF, both methods are not capable of capturing the most extreme offsets, in one direction. It is these offsets that are of interest for operability.

By doing the same analysis on a simulation that did not perform well on the comparison with m_0, insight is gained in how correct the TD spectra are. It is expected that the time signals and distributions from the FD model are not well fitted to that of the TD model. Table 7.4 shows the numerical analysis for the specific simulation, Appendix F.5 contains the results for all simulations.

	Surge [m]	Sway [m]	Yaw [deg]
Simulink	0.08	1.21	0.01
tfestimate	0.08	1.13	0.01
Time domain	0.04	0.58	0.00
difference TD - Simulink	95%	111%	49%
Difference TD - tfestimate	84%	96%	43%

Table 7.4: m_0 response spectra and compared to TD response spectra - Loaded from 135°by low sea-state

When comparing the results from Table 7.4 both methods of determining TFs perform very low. This can also be seen in Figure 7.23, were both methods perform very similar, as the TFs are very similar. When comparing response to that of the time domain simulation, a large difference is noted. The shape of the spectra are still very much alike, the difference is mainly in the energy present in the spectra. The expected response calculated through a frequency domain approach are overvalued.
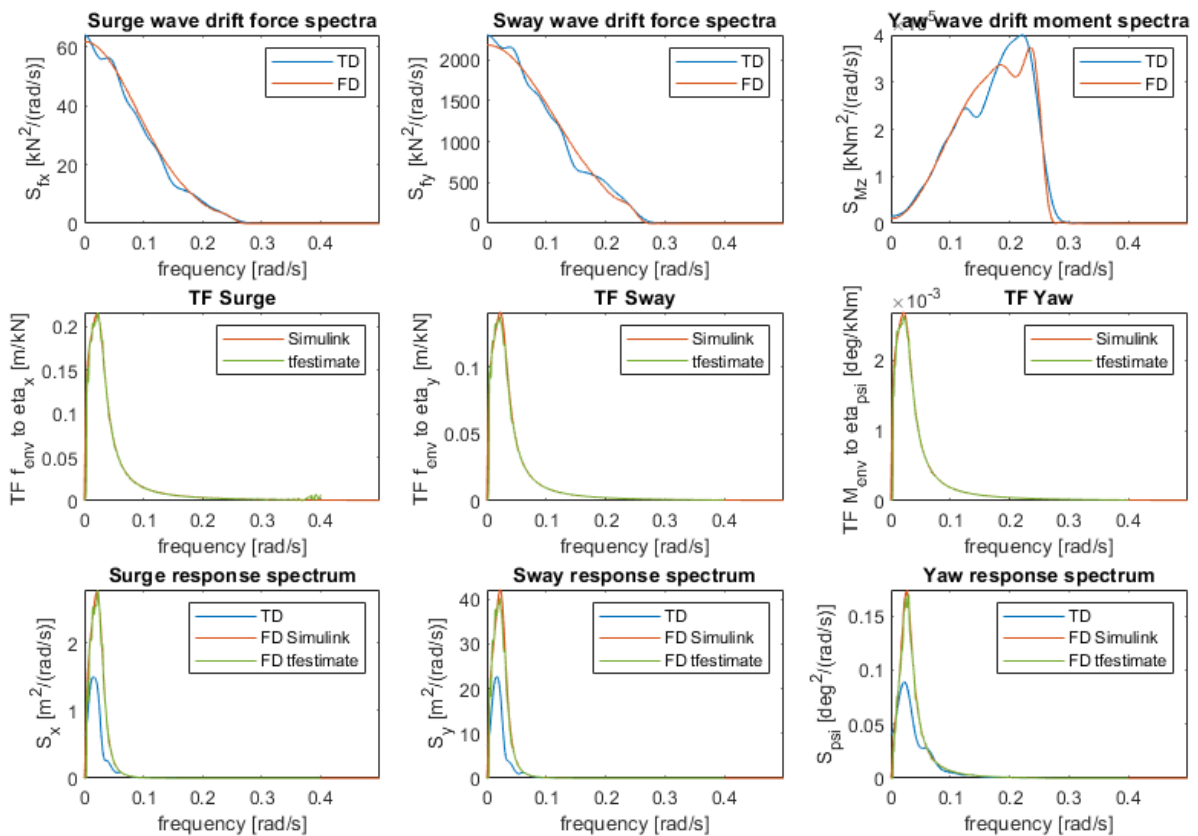

Figure 7.23: FD model overview, including input spectra, TFs and output spectra - All NLC, loaded from 135°by low sea-state

When analysing the results in time domain a different outcome is noted. The time traces in Figure 7.24 are very similar to that of Figure 7.21. Both FD models in general are similar to that of the time domain and again both models fail to capture the most extreme offsets present in the time domain simulation.
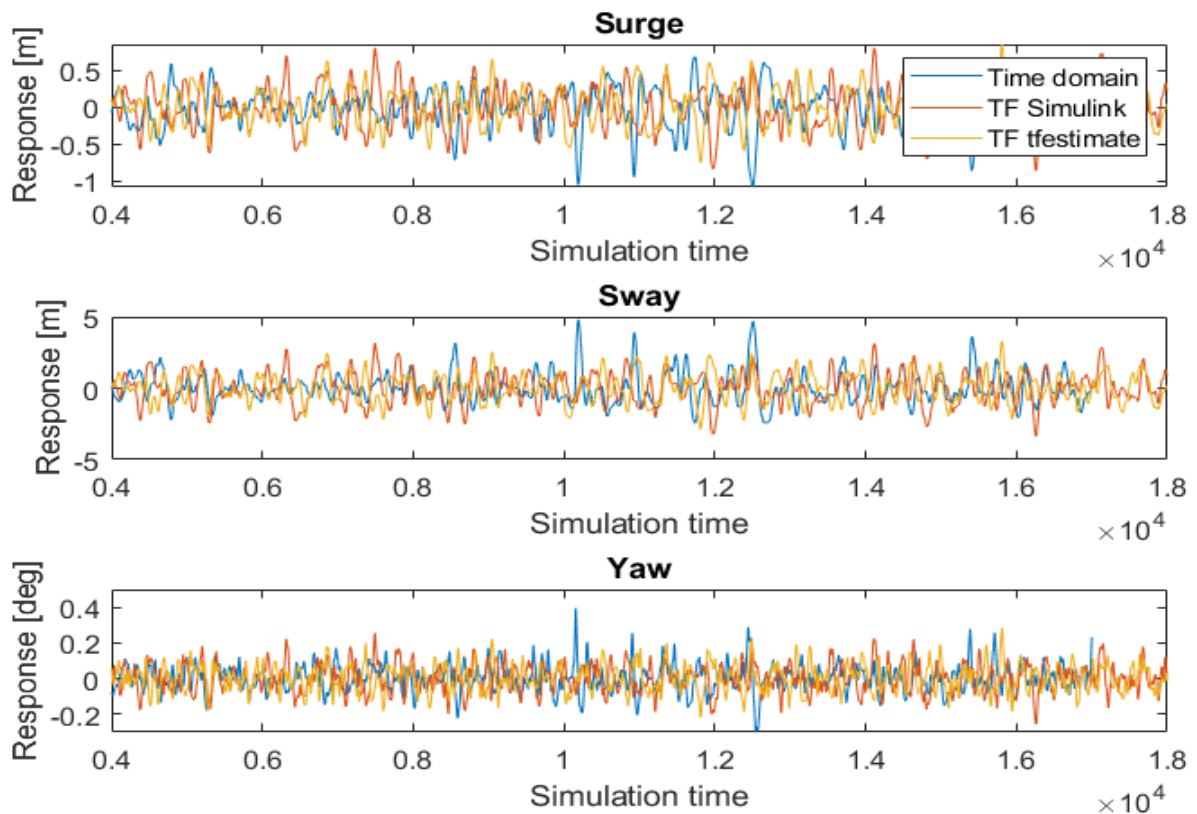
Figure 7.24: Response time trace, all NLC, low sea-state from 135°

Although the distributions from the frequency domain models do not match as close to the time domain as the previous example. Specifically the lower displacements are not captured very well and the time domain distribution is steeper. The error in the results are a lot less than was expected based on the numerical analysis given in Table 7.4. This leads to the belief that the TD DP offset spectra created with the $dat2spec.m$ function, respectively the blue spectra found in the bottom three plots in Figure 7.23, is not representative for the actual DP offset experienced by the vessel.
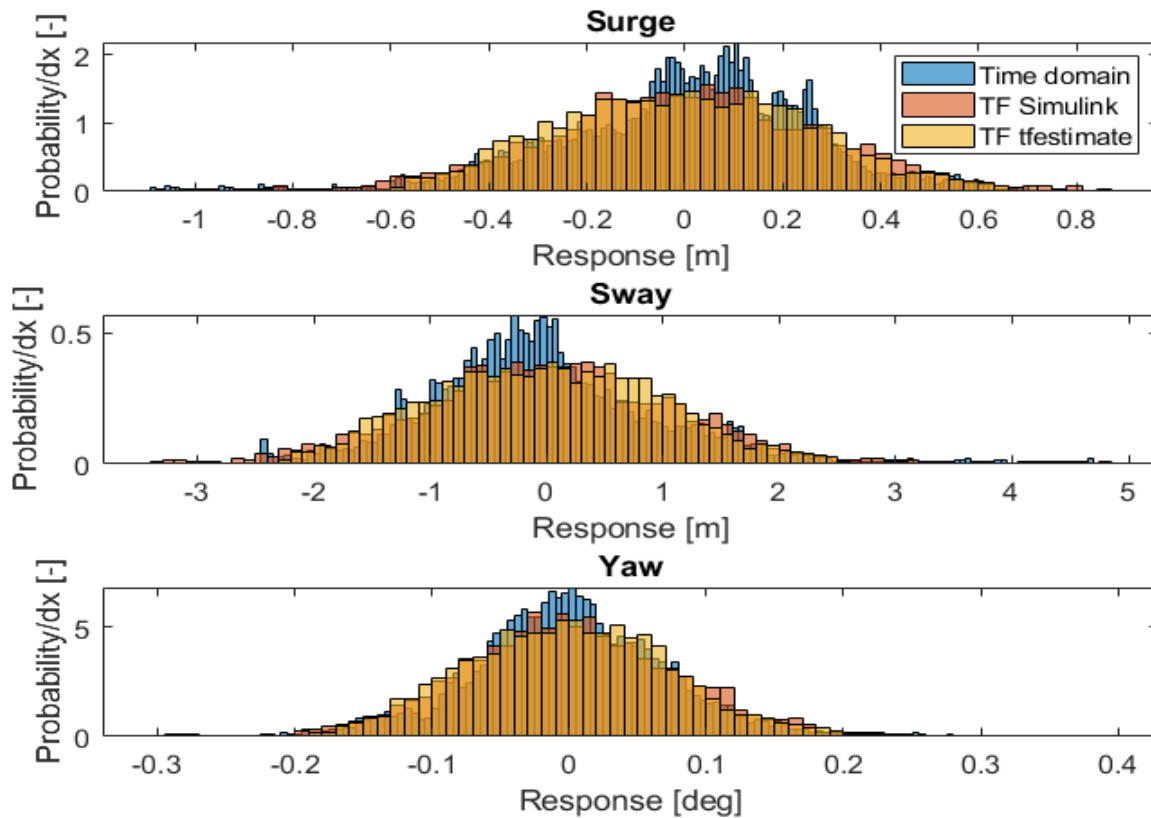
Figure 7.25: Normalized response distribution, all NLC, low sea-state from 135°

Appendix F.6 & F.7 provides an overview of the standard deviation of each response spectrum for each simulation. This overview also includes the relative difference for each response spectrum to that of the standard deviation from the time domain simulation. Based on average difference between the frequency domain and time domain results, the performance of each transfer function method is determined. The first method, based on Simulink linearization at a operating point, has an accuracy of 93%. Whereas the second method, that calculates the transfer function with MATLAB function *tfestimate* has an average accuracy of 94%. Both methods have difficulty capturing low frequent, high offset motions.

7.3.1. Cumulative distribution function

The Cumulative Distribution Function (CDF) can be derived from the normalized distribution. The CDF can be used to determine the probability of a specific offset occurring during an operation. Inversely proportional, the offset corresponding to a specific probability of occurrence can be determined.
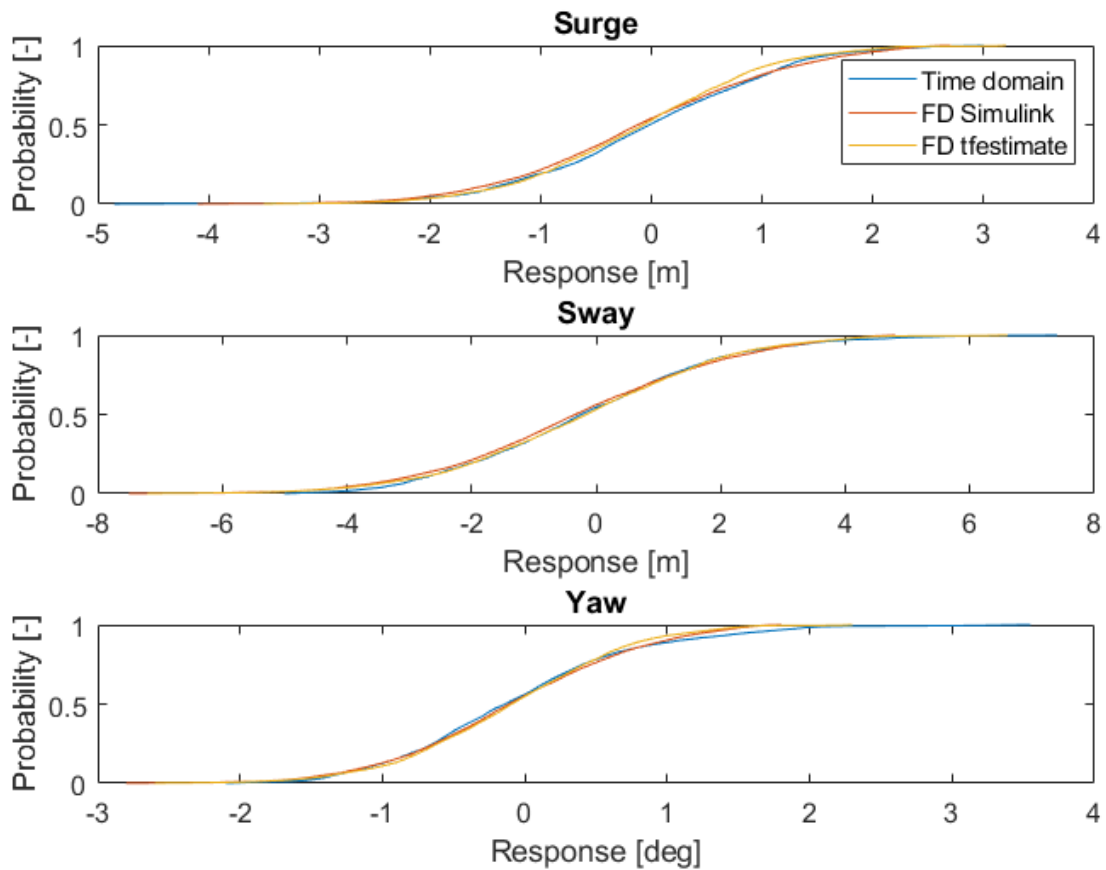
Figure 7.26: Cumulative distribution function, all NLCs, high sea-state from 135°

DOF	Dir	TD	Simulink	tfestimate	ϵ Simulink	ϵ tfestimate
Surge [m]	+	1.70	1.89	1.63	11%	4%
Sway [m]	+	3.45	3.40	3.28	1%	5%
Yaw [deg]	+	1.56	1.26	1.15	19%	26%
Surge [m]	-	-1.83	-2.02	-1.83	10%	0%
Sway [m]	-	-3.31	-3.87	-3.73	17%	13%
Yaw [deg]	-	-1.34	-1.42	-1.36	16%	2%

Table 7.5: DP offsets corresponding to probability of occurrence less then 5% including relative error to TD

Figure 7.26 provides the CDFs obtained from the time domain and both frequency domain variations, for the model containing all NLCs and is loaded from 135°by a high sea-state. An arbitrary simulation has been selected for this analysis. From the CDFs the offset corresponding to a probability of occurrence of less than 5% are provided in Table 7.5. Overall it is found that the CDF estimated through the frequency domain model that is based on *t f estimate* has a better correspondence with the time domain model.
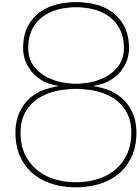
Conclusion & Recommendations

8.1. Conclusion

The main goal of this research isto determine the effects of non-linear components, present in a DP system, have on a linearised frequecny domain model of the DP system. Through research questions presented in 1 this goal is pursued. Conclusions will be presented in set order.

1. Based on literature study and discussions with experts in the field of dynamic positioning, the following Non-linear Components (NLCs) have been selected to investigated in this research.

   (a) Thruster allocation

   (b) Thruster ramp up

   (c) Thruster turning rate

   (d) Forbidden zones

   (e) Thruster saturation

   As thruster allocation is needed in order for a DP system to even be functional, this NLC is determined to serve as the benchmark model. To which all other models are compared. All tested models consist of the benchmark model with one additional of the aforementioned NLCs. Except for one, this model is the benchmark model with all NLCs incorporated. Thruster saturation is left out of the results, as under operational conditions this effect does not occur.

2. Each non-linear component has successfully been incorporated through a combination of MATLAB code and Simulink modelling. The model is set up so that each individual

NLCs can be enabled/disabled through activating or de-activating a switch. This allows for testing of different NLC combinations within one single Simulink model.

3. The vessel DP offset as calculated using the frequency domain model has the ability to accurately capture the expected motions of a vessel excited by second order wave drift forces. The transfer functions estimated have a stiff characteristic compared to the time domain model. This results in an underestimation by not accurately capturing the low frequent, high offset motions. The motions that have significant influence on the workability of an offshore operation. The effects of this is best visualized in Figure 7.19. For the different models investigated in this research the same findings have been made. When the frequency domain model is used in practice, the systematic short coming of this method should be taken into account.

4. In Section 7.1 it was found that non of the non-linear components have a significant effect on the displacements and rotation in the horizontal plane. However, when combining all NLCs for certain directions a difference was found of 18% in standard deviation of the response time trace. This difference was present at different sea-states and thus different time signals. The fact that this effect is found only at 15°and 165°, is unaffected by increasing sea-state and is causes by thruster ramp-up only when combined with all other NLCs. Leads to the expectation that an error occurs in the control system that leads to the differences found. However, this suspicion is not proven and others causes have not been ruled out. Further research is required.

5. For this research two different methods of creating transfer functions have been analysed. for both methods the conclusions and findings are discussed here.

   (a) Linearization through Simulink. This method has a significant downside, where the linearization is performed by Simulink at a specified time in the simulation. Therefore the found transfer function is only valid for a small time window around this operation point. Not taking into account the results and performance of this method in this research. A few practical concerns arise. For rather constant simulations where the vessel is loaded from a uniform direction and experiences a consistent sea-state, the found transfer function might be representative for the entire simulation. However, when predictions need to be made for more realistic cases the linearization is only valid for a small segment of the simulation. Thereby creating unreliable results. On top of this, transfer functions found for the model that included thruster ramp up had large deviations not consistent with the results found in the time domain analysis.

   (b) Linearization though $tf estimate$. The second method takes into account the entire time signal for both input and output. Thus creating a transfer function representa-

tive for the entire simulation. However, the linearization is only based on these two signals and does not take into account the complex Simulink model of the vessel. Downside to this method is that the function is complicated and allows for variations based on the different settings. Wrong implementation of this function can thus lead to deviations in the found transfer functions.

The standard deviation of the response spectra found with method 1, has an accuracy of 93% when compared to the standard deviation found in with the time domain model. Whereas method 2 has an accuracy of 94%. Although both methods differ strong in the approach of determining a transfer function, the transfer functions found are very much the same for most simulations. Therefore, the conclusion can be made that the found transfer functions are reliable. Depending on the application of the model, a method should be selected taking into account the aforementioned characteristics.

8.2. Recommendations

For further development of a frequency domain model of a dynamic positioned vessel, the following recommendations are made:

1. Identify natural frequencies of non-linear components analytically. The conclusion of this research based on experimental data from computer models is that natural frequencies of the investigated NLCs exist outside the low frequent excitation range. Analytical prove of this hypothesis would significantly strengthen the case around a frequency domain approach to offset prediction.

2. Determine effect of realistic conditions. Offshore conditions are hardly unidirectional. By introducing two dimensional spectra based on 4D QTFs, a more realistic simulation can be run. It is expected that short comings regarding underestimation of low frequent, high offset could be effected by this. Forces that are more spread out over direction will lead to smaller standard deviation of the time signal. This could have influence on the large offset peaks found in the time domain simulations and absent in the frequency domain simulations.

3. During this research, theoretical DP controller settings are used. Furthermore, PID controllers present in the model have been tuned using Simulink software. This approach results in a stable TD DP model. In practise offshore vessels have different DP settings. It is advised that the model is tested with actual settings as it is expected to influence the performance of the model.

4. Compare model tests to actual vessel data. In this research the data obtained from the time domain model is assumed to be the 'truth' and is used to compare against. Deviations from the real vessel, in the model are therefore always present. This could lead to deviations in the behaviour of the model compared to that of the actual vessel.

5. Determine practical safety factors that compensate for underestimation of low frequent, high offset motions from frequency domain model.

B

Appendix
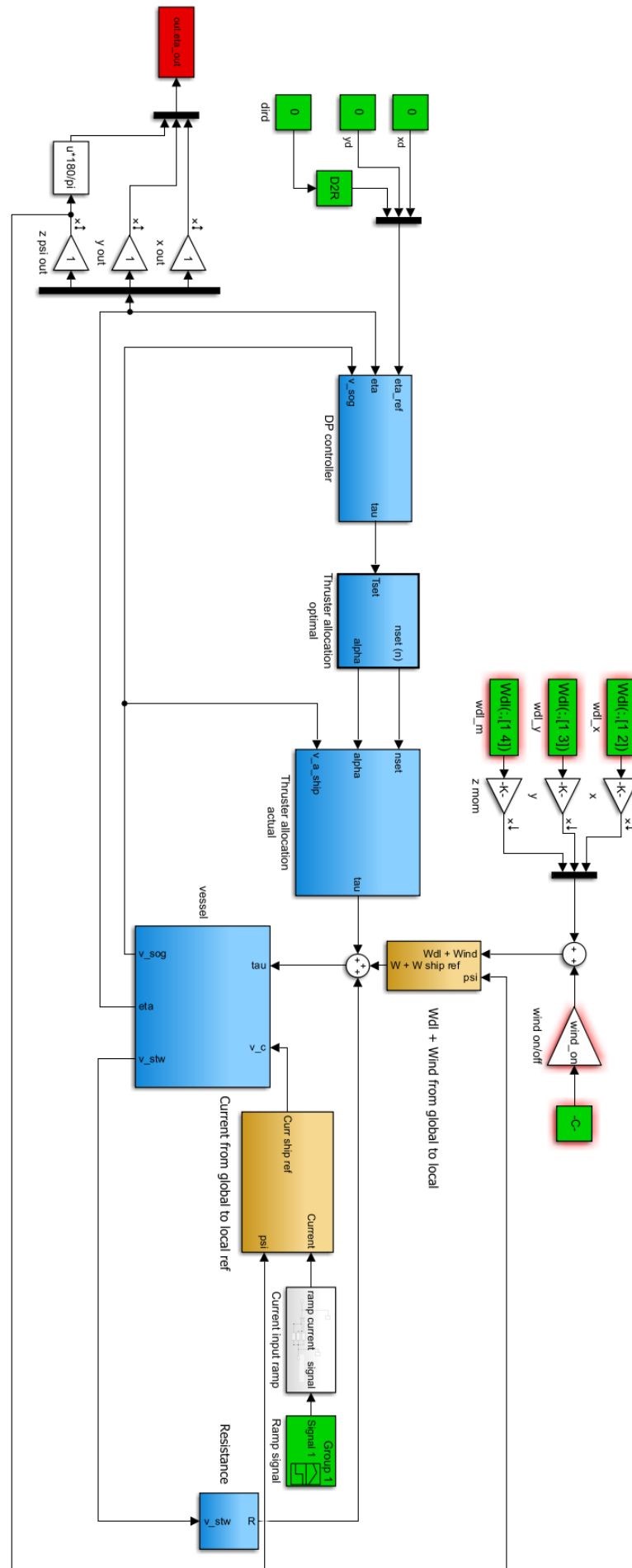
Figure B.1: Schematic overview Simulink model

C

Appendix

$$P = \begin{bmatrix} 0.2 & 0 & 0 & 0 & 0 & 0 & 0 & 0 & 0 & 0 \\ 0 & 0.2 & 0 & 0 & 0 & 0 & 0 & 0 & 0 & 0 \\ 0 & 0 & 0.2 & 0 & 0 & 0 & 0 & 0 & 0 & 0 \\ 0 & 0 & 0 & 0.2 & 0 & 0 & 0 & 0 & 0 & 0 \\ 0 & 0 & 0 & 0 & 0.2 & 0 & 0 & 0 & 0 & 0 \\ 0 & 0 & 0 & 0 & 0 & 0.2 & 0 & 0 & 0 & 0 \\ 0 & 0 & 0 & 0 & 0 & 0 & 0.2 & 0 & 0 & 0 \\ 0 & 0 & 0 & 0 & 0 & 0 & 0 & 0.2 & 0 & 0 \\ 0 & 0 & 0 & 0 & 0 & 0 & 0 & 0 & 0.2 & 0 \\ 0 & 0 & 0 & 0 & 0 & 0 & 0 & 0 & 0 & 0.2 \end{bmatrix} \tag{C.1}$$

$$q = \begin{bmatrix} 0 & 0 & 0 & 0 & 0 & 0 & 0 & 0 & 0 & 0 \end{bmatrix}^T \tag{C.2}$$

D
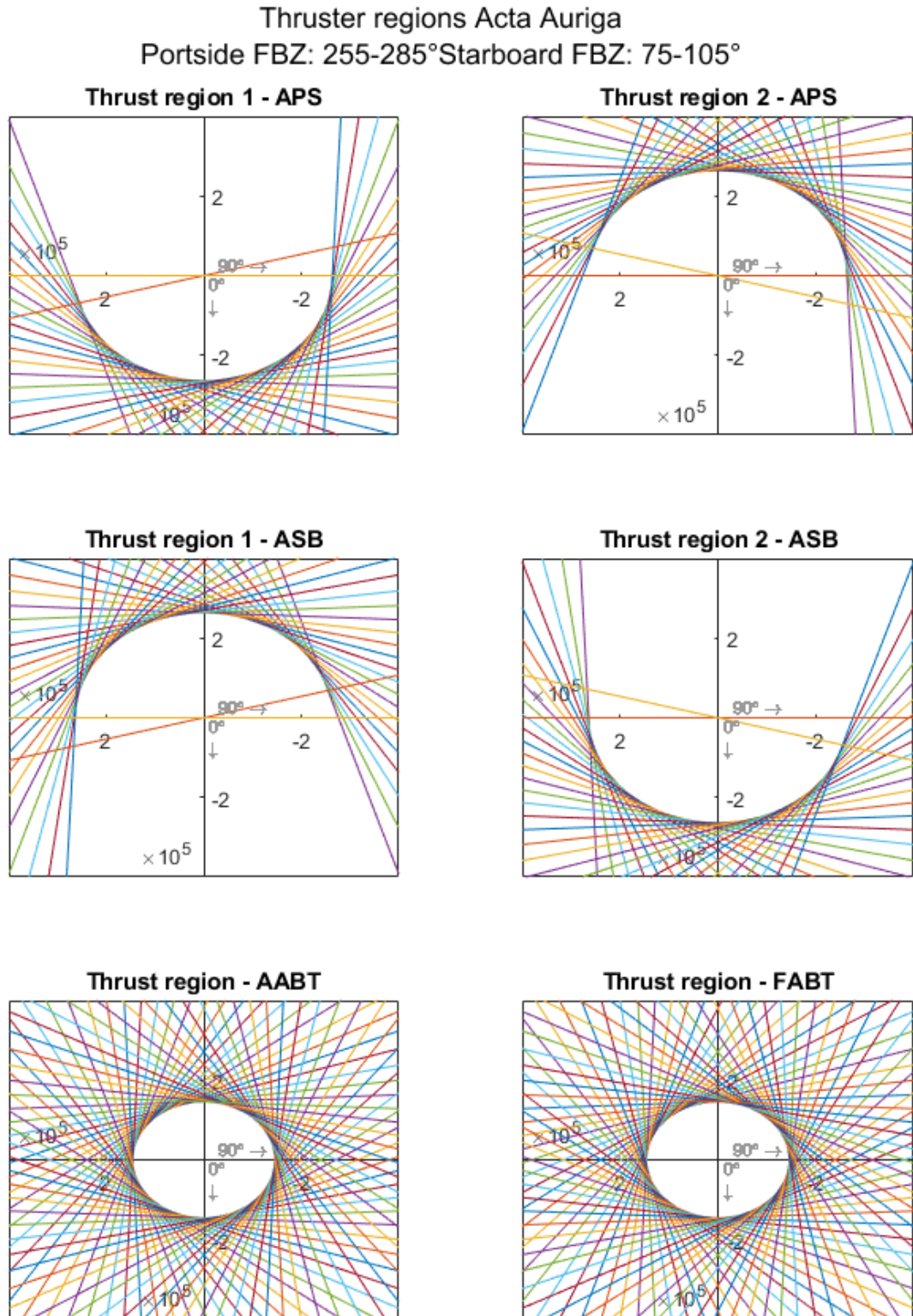
Appendix

Figure D.1: Thrust regions Acta Auriga including split regions due to FBZ
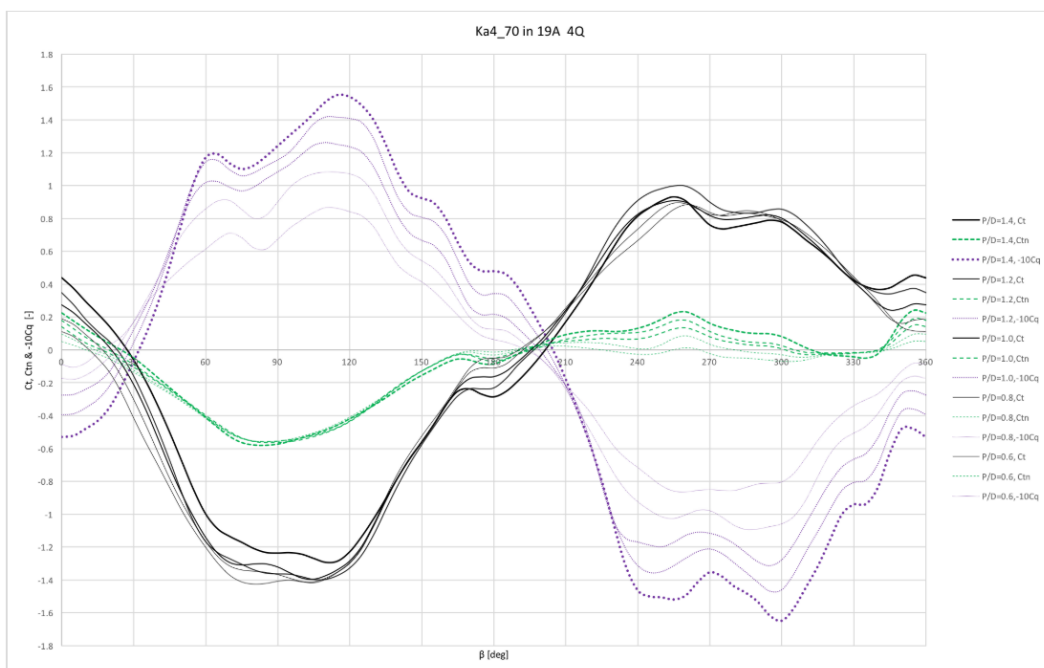
Figure D.2: 4Q diagram Ka4-70 in 19A duct

E
Appendix

Direction [deg]		LOW			MEDIUM			HIGH		
		Surge [kN]	Sway [kN]	Yaw [kN]	Surge [kN]	Sway [kN]	Yaw [kN]	Surge [kN]	Sway [kN]	Yaw [kN]
0	TD	5,1049	2,80E-06	-0,00052	22,3219	-1,60E-07	-0,0013	22,3219	-1,86E-05	-0,002
	FD	5,0345	2,86E-06	-5,07E-04	22,4108	7,37E-07	-0,0013	22,4108	-1,81E-05	-0,002
	diff	1%	2%	2%	0%	122%	0%	0%	3%	0%
15	TD	5,1341	4,254	-66,6902	21,9721	10,9733	-218,565	21,9721	15,4539	-466,914
	FD	5,1835	4,293	-67,3508	21,963	11,0904	-222,078	21,963	15,4311	-470,102
	diff	1%	1%	1%	0%	1%	2%	0%	0%	1%
45	TD	4,2889	23,9817	-120,166	16,9741	42,1458	-484,574	16,9741	59,0314	-859,319
	FD	4,3022	24,0696	-120,028	17,0501	42,1461	-491,629	17,0501	59,2562	-857,955
	diff	0%	0%	0%	0%	0%	1%	0%	0%	0%
90	TD	-2,0991	45,9019	-19,67	-4,5871	88,4434	33,2736	-4,5871	122,3636	34,0287
	FD	-2,1498	46,9013	-20,5607	-4,6332	88,7367	33,0797	-4,6332	123,3202	33,1432
	diff	2%	2%	4%	1%	0%	1%	1%	1%	3%
135	TD	-4,6861	27,8067	65,6077	-19,1284	46,5797	472,7029	-19,1284	65,7466	838,4806
	FD	-4,6585	27,6285	64,625	-19,2123	47,0705	483,0724	-19,2123	66,0135	840,4045
	diff	1%	1%	2%	0%	1%	2%	0%	0%	0%
165	TD	-3,5269	6,0283	30,5912	-20,1009	14,1584	163,5457	-20,1009	19,5731	382,3681
	FD	-3,5443	6,044	30,768	-20,3211	14,1056	162,3903	-20,3211	19,7729	384,2457
	diff	0%	0%	1%	1%	0%	1%	1%	1%	0%
180	TD	-3,1759	4,78E-06	-2,61E-04	-19,6349	2,60E-07	-9,37E-04	-19,6349	-3,46E-05	-0,0016
	FD	-3,1812	4,86E-06	-2,58E-04	-19,9493	-4,63E-07	-9,59E-04	-19,9493	-3,54E-05	-0,0016
	diff	0%	2%	1%	2%	156%	2%	2%	2%	0%

Table E.1: Overview error between time domain and frequency domain calculation mean wave drift force
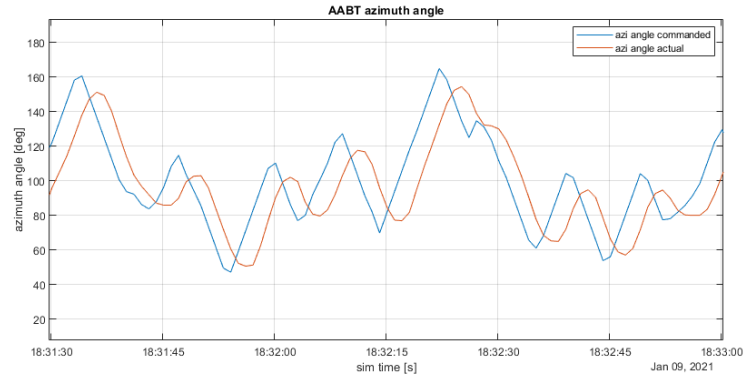
(a) vessel data turning rate - AABT
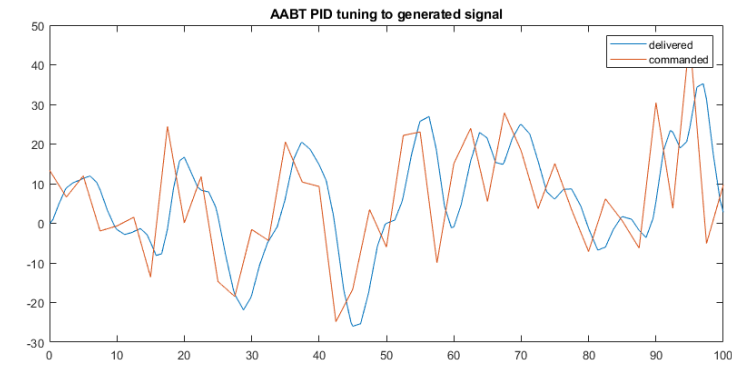
(b) model data turning rate - AABT
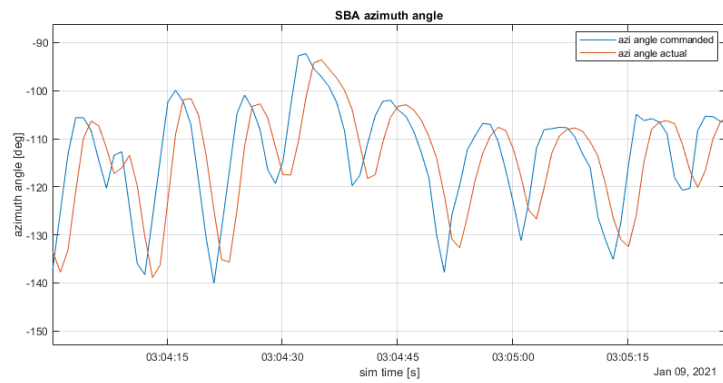
(c) vessel data turning rate - SBA

(d) model data turning rate - SBA

Figure E.1: Validation: comparison model and vessel data of turning rate of different azimuth types
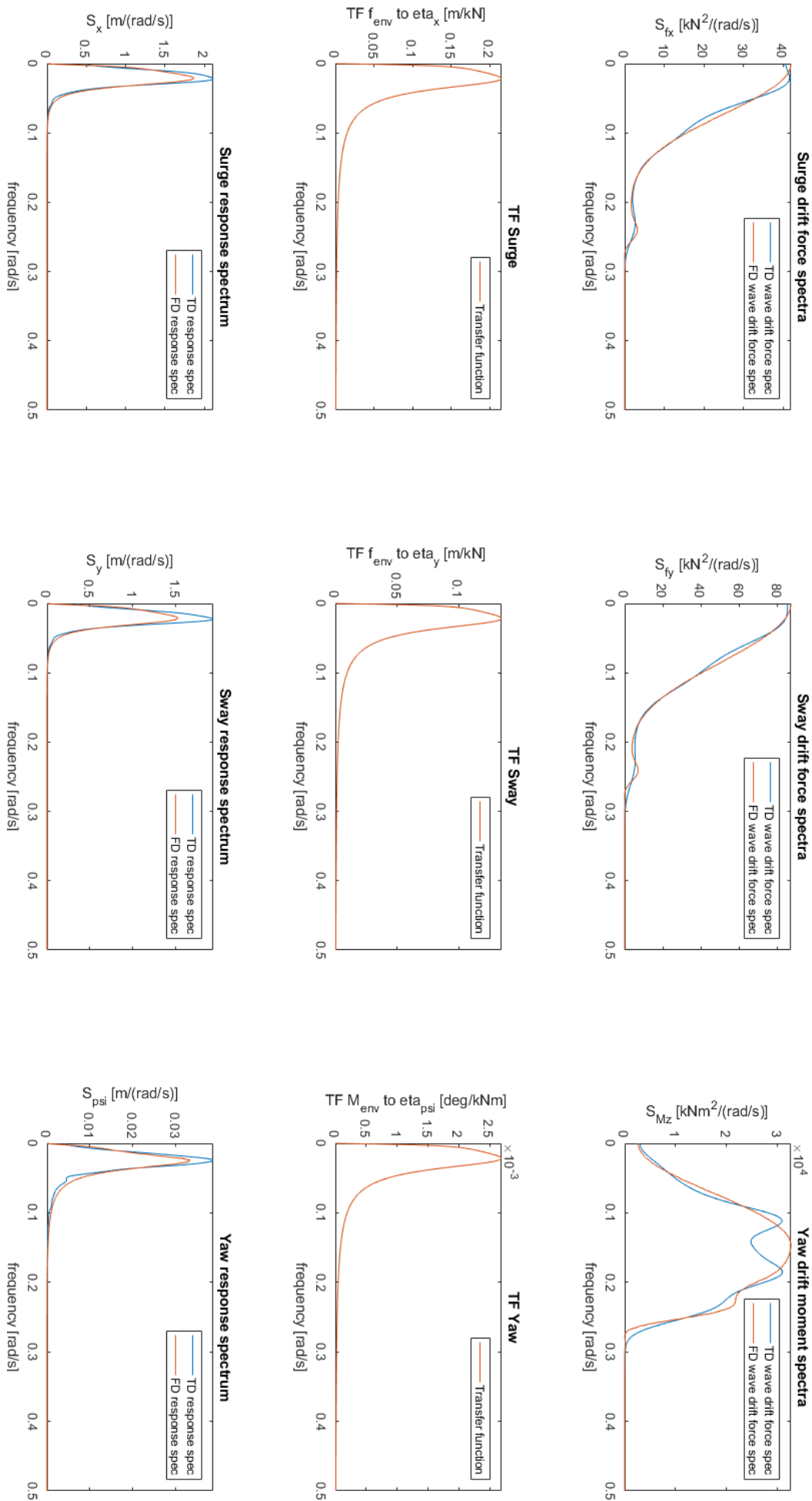
Figure E.2: Verification of frequency domain model

F

Appendix

Direction [deg]		LOW			MEDIUM			HIGH		
		Surge [m]	Sway[m]	Yaw [deg]	Surge [m]	Sway[m]	Yaw [deg]	Surge [m]	Sway[m]	Yaw [deg]
0	Simulink	0.11	0.00	0.00	0.88	0.00	0.00	1.81	0.00	0.00
	tfestimate	0.10	0.00	0.00	0.86	0.00	0.00	1.75	0.00	0.00
	TD	0.09	0.00	0.00	0.83	0.00	0.00	1.81	0.00	0.00
	ϵ S - TD	15%	6%	9%	6%	9%	7%	0%	10%	1%
	ϵ tf - TD	11%	3%	14%	3%	10%	11%	3%	10%	4%
15	Simulink	0.12	0.02	0.00	0.86	0.19	0.04	1.70	0.30	0.19
	tfestimate	0.11	0.02	0.00	0.84	0.18	0.04	1.68	0.28	0.19
	TD	0.11	0.02	0.00	0.86	0.19	0.04	2.21	0.36	0.22
	ϵ S - TD	10%	11%	9%	0%	0%	3%	23%	18%	13%
	ϵ tf - TD	5%	5%	4%	3%	3%	1%	24%	22%	16%
45	Simulink	0.07	0.86	0.01	0.70	2.01	0.20	1.06	3.51	0.55
	tfestimate	0.07	0.84	0.01	0.69	1.90	0.19	1.05	3.73	0.55
	TD	0.08	0.94	0.01	0.64	1.87	0.15	1.04	3.63	0.51
	ϵ S - TD	13%	8%	15%	9%	8%	35%	2%	3%	9%
	ϵ tf - TD	14%	11%	17%	8%	2%	29%	0%	3%	8%
90	Simulink	0.02	3.34	0.00	0.04	9.17	0.01	0.09	16.13	0.02
	tfestimate	0.02	3.32	0.00	0.03	10.02	0.01	0.07	19.49	0.01
	TD	0.02	3.06	0.00	0.04	11.22	0.01	0.08	22.93	0.01
	ϵ S - TD	16%	9%	16%	7%	18%	17%	6%	30%	46%
	ϵ tf - TD	8%	8%	1%	6%	11%	25%	10%	15%	11%

Table F.1: Area under response spectra (m_0) Benchmark model, spectra obtained from Simulink TF and $tfestimate$ TF and compared to spectra [DEEL 1]

Direction [deg]		LOW			MEDIUM			HIGH		
		Surge [m]	Sway[m]	Yaw [deg]	Surge [m]	Sway[m]	Yaw [deg]	Surge [m]	Sway[m]	Yaw [deg]
135	Simulink	0.08	1.16	0.01	0.83	2.40	0.25	1.33	4.56	0.62
	tfestimate	0.08	1.13	0.01	0.78	2.44	0.24	1.15	4.69	0.60
	TD	0.07	1.15	0.01	0.65	2.42	0.19	1.23	4.21	0.73
	ϵ S - TD	10%	1%	4%	28%	1%	29%	8%	14%	14%
	ϵ tf - TD	3%	2%	1%	19%	1%	26%	7%	12%	17%
165	Simulink	0.05	0.04	0.00	0.95	0.27	0.03	1.77	0.44	0.18
	tfestimate	0.05	0.04	0.00	0.89	0.26	0.03	1.66	0.43	0.17
	TD	0.06	0.05	0.00	1.12	0.31	0.04	1.75	0.44	0.18
	ϵ S - TD	5%	11%	7%	15%	14%	13%	1%	0%	2%
	ϵ tf - TD	8%	13%	9%	20%	18%	15%	5%	1%	2%
180	Simulink	0.04	0.00	0.00	0.93	0.00	0.00	1.79	0.00	0.00
	tfestimate	0.04	0.00	0.00	0.90	0.00	0.00	1.75	0.00	0.00
	TD	0.05	0.00	0.00	1.00	0.00	0.00	1.62	0.00	0.00
	ϵ S - TD	8%	3%	7%	7%	24%	4%	10%	2%	3%
	ϵ tf - TD	12%	1%	8%	10%	25%	7%	8%	3%	1%

Table F.2: Area under response spectra (m_0) Benchmark model, spectra obtained from Simulink TF and *tf estimate* TF and compared to spectra [DEEL 2]

Direction [deg]		LOW Surge [kN]	LOW Sway [kN]	LOW Yaw [kN]	MEDIUM Surge [kN]	MEDIUM Sway [kN]	MEDIUM Yaw [kN]	HIGH Surge [kN]	HIGH Sway [kN]	HIGH Yaw [kN]
0	TD	9.05	0.00	0.00	76.02	0.00	0.00	183.89	0.00	0.00
	FD	9.65	0.00	0.00	76.56	0.00	0.00	176.47	0.00	0.00
	ϵ	6%	0%	3%	1%	3%	7%	4%	6%	3%
15	TD	8.75	3.92	2942.27	73.66	47.85	28781.47	182.55	99.67	133822.05
	FD	9.95	4.58	3398.33	74.85	49.51	29625.62	169.64	95.06	127659.23
	ϵ	12%	14%	13%	2%	3%	3%	8%	5%	5%
45	TD	6.82	213.83	43384.19	77.39	659.01	247801.83	174.80	1259.17	583800.93
	FD	6.69	211.96	42792.72	77.08	641.76	236727.97	181.15	1335.45	581583.68
	ϵ	2%	1%	1%	0%	3%	5%	4%	6%	0%
90	TD	2.52	1082.68	1802.21	5.42	4588.98	20252.58	12.26	9720.14	38024.42
	FD	2.72	1145.35	1825.26	5.39	4671.93	20254.28	12.65	10063.78	40102.87
	ϵ	7%	5%	1%	1%	2%	0%	3%	3%	5%
135	TD	7.04	298.48	57873.07	95.85	922.28	253768.37	227.84	1881.00	647140.52
	FD	7.21	297.67	55341.40	101.31	901.51	277351.69	234.81	1897.11	670291.89
	ϵ	2%	0%	5%	5%	2%	9%	3%	1%	3%
165	TD	3.82	8.70	5062.70	102.20	93.21	41238.93	189.15	147.27	146950.11
	FD	3.89	8.92	5409.66	83.92	75.50	39086.20	188.16	148.38	147641.03
	ϵ	2%	2%	6%	22%	23%	6%	1%	1%	0%
180	TD	3.01	0.00	0.00	78.14	0.00	0.00	185.92	0.00	0.00
	FD	3.18	0.00	0.00	80.37	0.00	0.00	182.07	0.00	0.00
	ϵ	5%	1%	2%	3%	2%	2%	2%	0%	5%

Table F.3: Area under wave drift force spectra (m_0) All NLC model, spectra obtained from time and frequency domain

Direction [deg]		LOW Surge [m]	Sway [m]	Yaw [deg]	MEDIUM Surge [m]	Sway [m]	Yaw [deg]	HIGH Surge [m]	Sway [m]	Yaw [deg]
0	Simulink	0.11	0.00	0.00	0.87	0.00	0.00	1.78	0.00	0.00
	tfestimate	0.10	0.00	0.00	0.84	0.00	0.00	1.71	0.00	0.00
	TD	0.09	0.00	0.00	0.82	0.00	0.00	1.77	0.00	0.00
	ε S - TD	14%	37%	40%	6%	5%	36%	0%	26%	27%
	ε tf - TD	11%	1%	19%	3%	12%	42%	4%	3%	46%
15	Simulink	0.12	0.02	0.00	0.88	0.19	0.04	1.99	0.31	0.20
	tfestimate	0.11	0.02	0.00	0.80	0.18	0.04	2.53	0.44	0.24
	TD	0.10	0.02	0.00	0.84	0.18	0.04	2.32	0.46	0.22
	ε S - TD	11%	13%	11%	4%	3%	7%	15%	34%	7%
	ε tf - TD	5%	6%	4%	5%	3%	1%	9%	5%	13%
45	Simulink	0.07	0.84	0.01	0.70	1.99	0.21	3.46	0.58	0.58
	tfestimate	0.07	0.82	0.01	0.68	1.87	0.20	3.64	0.56	0.56
	TD	0.08	0.93	0.01	0.63	1.84	0.15	3.55	0.52	0.52
	ε S - TD	13%	9%	17%	10%	8%	36%	1%	3%	12%
	ε tf - TD	5%	6%	4%	8%	2%	29%	2%	3%	8%
90	Simulink	0.02	3.29	0.00	0.04	8.96	0.01	0.09	15.53	0.02
	tfestimate	0.02	3.24	0.00	0.03	9.75	0.01	0.07	18.87	0.01
	TD	0.02	2.98	0.00	0.04	10.95	0.01	0.08	22.11	0.01
	ε S - TD	19%	10%	27%	10%	18%	12%	10%	30%	51%
	ε tf - TD	8%	9%	1%	6%	11%	27%	10%	15%	14%

Table F.4: Area under response spectra (m_0) All NLC model, spectra obtained from Simulink TF and $tf\,estimate$ TF and compared to spectra [DEEL.1]

Direction [deg]		LOW Surge [m]	Sway [m]	Yaw [deg]	MEDIUM Surge [m]	Sway [m]	Yaw [deg]	HIGH Surge [m]	Sway [m]	Yaw [deg]
135	Simulink	0.08	1.21	0.01	0.83	2.26	0.25	1.33	4.60	0.62
	tfestimate	0.08	1.13	0.01	0.78	2.44	0.24	1.16	4.75	0.60
	TD	0.04	0.58	0.00	0.72	2.31	0.22	1.08	3.81	0.60
	ε S - TD	95%	111%	49%	16%	2%	11%	24%	21%	5%
	ε tf - TD	84%	96%	43%	8%	5%	10%	8%	25%	1%
165	Simulink	0.06	0.05	0.00	1.30	0.36	0.04	1.80	0.42	0.18
	tfestimate	0.06	0.05	0.00	1.21	0.35	0.04	2.32	0.64	0.24
	TD	0.06	0.05	0.00	1.30	0.38	0.04	2.75	0.70	0.26
	ε S - TD	5%	6%	18%	0%	4%	8%	34%	40%	33%
	ε tf - TD	2%	4%	2%	7%	6%	16%	16%	8%	8%
180	Simulink	0.04	0.00	0.00	1.12	0.00	0.00	1.78	0.00	0.00
	tfestimate	0.04	0.00	0.00	1.16	0.00	0.00	1.71	0.00	0.00
	TD	0.05	0.00	0.00	1.39	0.00	0.00	1.69	0.00	0.00
	ε S - TD	7%	40%	17%	20%	100%	100%	5%	22%	8%
	ε tf - TD	12%	5%	23%	17%	100%	100%	1%	17%	32%

Table F.5: Area under response spectra (m_0), spectra obtained from Simulink TF and $tfestimate$ TF and compared to spectra [DEEL 2]

Direction [deg]		LOW			MEDIUM			HIGH		
		Surge [m]	Sway [m]	Yaw [deg]	Surge [m]	Sway [m]	Yaw [deg]	Surge [m]	Sway [m]	Yaw [deg]
0	Simulink	0.33	0.00	0.00	0.93	0.00	0.00	1.33	0.00	0.00
	tfestimate	0.32	0.00	0.00	0.92	0.00	0.00	1.31	0.00	0.00
	spectrum	0.31	0.00	0.00	0.91	0.00	0.00	1.33	0.00	0.00
	TD time trace	0.33	0.00	0.00	0.89	0.00	0.00	1.32	0.00	0.00
	ϵ S - TD TT	1%	0%	0%	4%	0%	0%	1%	0%	0%
	ϵ tf - TD TT	3%	0%	0%	3%	0%	0%	1%	0%	0%
	ϵ spec & TT	7%	0%	0%	1%	0%	0%	1%	0%	0%
15	Simulink	0.34	0.15	0.05	0.94	0.44	0.19	1.41	0.55	0.45
	tfestimate	0.33	0.15	0.05	0.90	0.42	0.19	1.59	0.66	0.49
	spectrum	0.32	0.14	0.05	0.92	0.43	0.19	1.52	0.68	0.46
	TD time trace	0.31	0.13	0.05	0.94	0.44	0.20	1.75	0.71	0.51
	ϵ S - TD TT	12%	15%	11%	0%	0%	2%	20%	23%	12%
	ϵ tf - TD TT	9%	11%	8%	5%	3%	5%	9%	7%	3%
	ϵ spec & TT	6%	8%	5%	2%	2%	5%	13%	5%	9%
45	Simulink	0.26	0.92	0.09	0.84	1.41	0.46	1.04	1.86	0.76
	tfestimate	0.26	0.91	0.09	0.83	1.37	0.44	1.03	1.91	0.75
	spectrum	0.28	0.96	0.10	0.80	1.36	0.39	1.04	1.88	0.72
	TD time trace	0.27	0.93	0.10	0.80	1.36	0.39	1.05	1.87	0.78
	ϵ S - TD TT	4%	1%	5%	4%	4%	16%	0%	0%	3%
	ϵ tf - TD TT	5%	2%	4%	3%	1%	13%	2%	2%	4%
	ϵ spec & TT	2%	4%	5%	1%	0%	1%	1%	1%	8%
90	Simulink	0.15	1.81	0.03	0.20	2.99	0.10	0.30	3.94	0.13
	tfestimate	0.14	1.80	0.04	0.18	3.12	0.09	0.27	4.34	0.09
	spectrum	0.14	1.73	0.04	0.19	3.31	0.10	0.28	4.70	0.10
	TD time trace	0.14	1.71	0.04	0.20	3.45	0.10	0.30	4.84	0.10
	ϵ S - TD TT	4%	5%	9%	3%	13%	7%	1%	19%	27%
	ϵ tf - TD TT	10%	6%	9%	9%	9%	16%	10%	10%	4%
	ϵ spec & TT	1%	1%	9%	7%	4%	2%	5%	3%	3%

Table F.6: Standard deviation response spectra (Simulink, tfestimate, TD) and relative error to TD time signal [DEEL 1]

Direction [deg]		LOW			MEDIUM			HIGH		
		Surge [m]	Sway[m]	Yaw [deg]	Surge [m]	Sway[m]	Yaw [deg]	Surge [m]	Sway[m]	Yaw [deg]
135	Simulink	0.28	1.10	0.08	0.91	1.50	0.50	1.15	2.14	0.79
	tfestimate	0.28	1.06	0.08	0.88	1.56	0.49	1.08	2.18	0.78
	spectrum	0.20	0.76	0.06	0.85	1.52	0.47	1.04	1.95	0.77
	TD time trace	0.27	1.07	0.07	0.81	1.57	0.42	1.12	2.06	0.86
	ϵ S - TD TT	6%	3%	5%	13%	4%	17%	3%	4%	8%
	ϵ tf - TD TT	3%	0%	3%	9%	1%	16%	4%	6%	10%
	ϵ spec & TT	24%	29%	14%	5%	3%	11%	7%	5%	10%
165	Simulink	0.24	0.22	0.04	1.14	0.60	0.20	1.34	0.65	0.42
	tfestimate	0.25	0.23	0.04	1.10	0.60	0.21	1.52	0.80	0.49
	spectrum	0.25	0.23	0.04	1.14	0.61	0.19	1.66	0.84	0.51
	TD time trace	0.28	0.26	0.04	1.34	0.73	0.23	1.64	0.87	0.48
	ϵ S - TD TT	12%	14%	20%	15%	18%	13%	18%	26%	12%
	ϵ tf - TD TT	11%	13%	13%	18%	19%	10%	7%	8%	3%
	ϵ spec & TT	10%	11%	12%	15%	16%	16%	1%	4%	7%
180	Simulink	0.21	0.00	0.00	1.06	0.00	0.00	1.34	0.00	0.00
	tfestimate	0.21	0.00	0.00	1.08	0.00	0.00	1.31	0.00	0.00
	spectrum	0.22	0.00	0.00	1.18	0.02	0.00	1.30	0.00	0.00
	TD time trace	0.22	0.00	0.00	1.12	0.01	0.00	1.16	0.00	0.00
	ϵ S - TD TT	2%	0%	0%	6%	0%	0%	15%	0%	0%
	ϵ tf - TD TT	5%	0%	0%	4%	0%	0%	13%	0%	0%
	ϵ spec & TT	2%	0%	0%	5%	84%	91%	12%	0%	0%

Table F.7: Standard deviation response spectra (Simulink, tfestimate, TD) and relative error to TD time signal [DEEL 2]

Bibliography

[1] Adrian Wills. Qpip. URL `https://gitlab.inria.fr/alta/alta/-/commit/abbc0209527c5929458c1f5719c68ce48e0b3645`.

[2] Werner Blendermann. *Schiffsform und Windlast- Korrelations- und Regressionsanalyse von Windkanalmessungen am Modell.* Technische Universität Hamburg-Harburg, Hambrug, 1993. ISBN 3892205337.

[3] VERITEC Marine Technology Consultants. *Vibration Control in Ships.* VERITEC, Hovik, 1985.

[4] R. G. De Jong. 3DP, 2018.

[5] Christiaan De Wit. Optimal thrust allocation methods for dynamic positioning of ships. *Delft University of Technology, Netherlands*, (July):56, 2009.

[6] Nitilaksh Desai. Dynamic Positioning: Method for Disaster Prevention and Risk Management. *Procedia Earth and Planetary Science*, 11:216–223, 2015. ISSN 18785220. doi: 10.1016/j.proeps.2015.06.028.

[7] DNV. Environmental conditions and environmental testing. *RECOMMENDED PRACTICE DNV-RP-C205*, 2(October):92–99, 2010. ISSN 02750473. doi: 10.1109/INTLEC. 1993.388591.

[8] O. M. Faltinsen. *Sea Loads on Ships and Offshore.* Cambridge University Press, Cambridge, 1990. ISBN 0521458706.

[9] Oil Companies International Marine Forum. Prediction of Wind and Current Loads on VLCCs. 2, 1994.

[10] L. H. Holthuijsen. *Waves in Oceanic and Coastal Waters.* Cambridge University Press, Cambrigde, 2e edition, 2008. ISBN 9780521129954.

[11] IRENA. Future of Wind: Deployment, investment, technology, grid integration and socio-economic aspects, 2019. URL `https://www.irena.org/documentdownloads/publications/re{_}technologies{_}cost{_}analysis-hydropower.pdf`.

[12] J M J Journée, W W Massie, and R H M Huijsmans. *OFFSHORE HYDROMECHAN-ICS Third Edition (2015) Based on Original Lecture Notes (2000)*. Delft University of Technology, Delft, third edit edition, 2015.

[13] E. Bouws H. Carlson D. Cartwright K. Eake et al. K.F. Hasselman, T. Barnett. *Ergänzungsheft zur Deutschen Hydrographischen Zeitschrift, title = Measurements of wind-wave growth and swell decay during the joint North Sea wave project (JONSWAP), volume = 12, year = 1967.*

[14] R. S. Langley. Second order frequency domain analysis of moored vessels. *Applied Ocean Research*, 9(1):7–18, 1987. ISSN 01411187. doi: 10.1016/0141-1187(87)90027-7.

[15] Kongsberg Maritime. Us type azimuthing thruster. URL `https://www.kongsberg.com/maritime/products/propulsors-and-propulsion-systems/thrusters/azimuth-thrusters/us-type-azimuthing-thruster/#technicalInformation`.

[16] H.E. Saunders. *Hydrodynamics in Ship Design*. SNAME, 1957.

[17] K.E. Schoenherr. Formulation of propeller blade strength. 3, 1963.

[18] Peter Schorn and Frederick Fisher. Testing the convexity of a polygon. In *Graphics Gems*, pages 7–15. Elsevier, 1 1994.

[19] K. Suyehiro. On the drift of ships caused by rolling among waves. *Trans. Inst. Naval Arch*, 66, 1924.

[20] J. M. Finger T. H. Naylor. Verification of Computer Simulation Models. *Management Science*, 2(October):92–101, 1967.

[21] WAFO-group. *WAFO - A Matlab Toolbox for Analysis of Random Waves and Loads - A Tutorial*. Math. Stat., Center for Math. Sci., Lund Univ., Lund, Sweden, 2017.

[22] Peter Wellens. Cfd impact forces. University Lecture, 2020.

[23] P. F. De Wet. A Frequency Domain Approach to Estimate DP Footprint, 2019.

[24] Willemijn Pauw, Remco Hageman, Andries Nap. Offshore Support Vessel ACTA AURIGA. Technical Report November, 2019.

[25] C.A. Willemse, H.T. Grimmelius, and A.R. Tjallema. *Dynamic Positioning*. Delft University of Technology, Delft, 2008.